Ocean ventilation and anthropogenic carbon based on evaluated transient tracer applications

DISSERTATION

zur Erlangung des Titels
DOKTOR DER NATURWISSENSCHAFTEN

der
Mathematisch-Naturwissenschaftlichen Fakultät

an der
Christian-Albrechts-Universität zu Kiel

vorgelegt von

Tim Stöven
Kiel 2015

Erstgutachter: Prof. Dr. Arne Körtzinger

Zweitgutachter: Prof. Dr. Darryn Waugh

Tag der mündlichen Prüfung: Kiel, den 15.07.2015

Zum Druck genehmigt: Kiel, den 15.07.2015

Prof. Dr. Wolfgang J. Duschl

- Dekan -

Contents

Abbrevations

CO_2	carbon dioxide
CFC	chlorofluorocarbon
CFC-12	chlorofluorocarbon-12
DIC	dissolved inorganic carbon
EMT	Estern Mediterranean Transient
IG-TTD	Inverse Gaussian - Transit Time Distribution
SF_6	sulfur hexafluoride
TTD	Transit Time Distribution

Zusammenfassung

Diese Dissertation war Teil des Projekts "Carbon and transient tracer dynamics: A bi-polar view on Southern Ocean eddies and the changing Arctic Ocean", welches von der Deutschen Forschungsgemeinschaft (DFG) im Rahmen des Schwerpunktprogramms 1035 "Antarctic Research with comparative investigations in Arctic ice areas" gefördert wurde. Das Ziel dieser Arbeit war es Ventilations- und Transportprozesse von bestimmten Meeresgebieten zu untersuchen und die verschiedenen Anwendungsmöglichkeiten von Spurengasen und des Transit Time Distribution (TTD) Modells zu evaluieren. Die Ergebnisse sind in drei Manuskripte unterteilt.

Das erste Manuskript beschreibt die Ventilation des Mittelmeeres in 2011 und stellt Methoden vor, welche genutzt werden können, um die Inverse Gaussian - Transit Time Distribution (IG-TTD) und weitere Linearkombinationen des Modells zu definieren bzw. einzuschränken. Es konnte gezeigt werden, dass die Ventilation im östlichen Mittelmeer durch zwei unterschiedliche Mechanismen geprägt ist. Wassermassen welche während der extremen Tiefenwasserbildung der 1990er Jahre gebildet wurden, sind gekennzeichnet durch advektive Charakteristiken und können mit dem einfachen IG-TTD Modell beschrieben werden. Wassermassen, die im Adriatischen Meer gebildet wurden, zeigen einen deutlich diffusiveren Anteil und können durch eine Linearkombination zweier IG-TTDs beschrieben werden. Diese unterschiedlichen Charakteristiken führen dazu, dass das aktuell gebildete Tiefenwasser aus dem Adriatischem Meer ein höheres mittleres Alter aufweist als das Tiefenwasser welches weitaus früher gebildet wurde und seinen Ursprung im Kretischen Meer hat. Die umfangreiche Tiefenwasserbildung im westlichen Mittelmeer in 2004-2005 kann ebenfalls durch eine Linearkombination beschrieben werden. Das Modell zeigt, dass die erhöhte Spurengaskonzentration im Tiefenwasser nur zu einem ähnlichen mittleren Alter wie die darüber liegenden Wasserschichten führt, welche geringere Spurengaskonzentrationen aufweisen.

Das zweite Manuskript verdeutlicht die besonderen Eigenschaften und Merkmale von derzeitig angewandten Spurengasen und erörtert anhand von Felddaten aus

dem südlichen Atlantik und des Südlichen Ozeans die unterschiedlichen Anwendungsgrenzen des IG-TTD Modells. Das Verhältnis zwischen relativer Spurengaskonzentration (in %) und dem Spurengasalter ermöglicht eine Einteilung der verschiedenen Anwendungsbereiche und zeigt, welche Spurengaskombinationen genutzt werden können, um das IG-TTD Modell zu definieren und einzuschränken. Es wird gezeigt, dass Abweichungen in der Spurengassättigung einen signifikanten Einfluss auf diese Einschränkungen haben kann (Fehlerbereich von mehr $>$ 100 % für 15 % Sättigungsabweichung). Die neue Methode der Gültigkeitsbereiche, welche eine einfache Möglichkeit zur Überprüfung der Anwendbarkeit des IG-TTD Modells bietet, wird anhand von Felddaten diverser Spurengasmessungen vorgestellt. Des Weiteren konnte anhand dieser Methode gezeigt werden, dass das IG-TTD Modell südlich der Subantarktischen Front die Ventilation der dortigen Wassermassen nicht beschreiben kann. Das Modell ist darüberhinaus durch gewisse Sensitivitätsbereiche der Spurengase beschränkt.

Das dritte Manuskript beschreibt Transportmengenabschätzungen von gelöstem anorganischen Kohlenstoff und dem dazugehörigen anthropogenem Anteil durch die Framstraße in 2012. Hierfür wurde angenommen, dass die Standardparameter des IG-TTD Modells die vorherrschenden Ventilationsmuster beschreiben. Darauf basierend wurde der Überschussanteil von Schwefelhexafluorid (SF_6) und der anthropogene Kohlenstoffgehalt in diesem Gebiet berechnet. Die Transportmengen der hydrographischen Daten wurden durch ein Geschwindigkeitfeld abgeschätzt, welches auf Daten der Verankerungskette entlang der Sektion beruht. Der große Fehlerbereich der Transportvolumen verhindert signifikante Aussagen über die vorherrschenden Transportverhältnisse. Die Daten deuten aber an, dass die nord- und südwärts transportierte Menge an anthropogenem Kohlenstoff relativ ausgeglichen ist.

Summary

This PhD thesis was part of the project "Carbon and transient tracer dynamics: A bi-polar view on Southern Ocean eddies and the changing Arctic Ocean" and was funded by the Deutsche Forschungsgemeinschaft (DFG) in the framework of the priority programme 1035 "Antarctic Research with comparative investigations in Arctic ice areas". The aim of the project was to examine ventilation and transport processes of specific ocean areas as well as to evaluate various aspects of transient tracer and Transit Time Distribution (TTD) model applications. The results are subdivided into three paper manuscripts.

The first manuscript describes the ventilation of the Mediterranean Sea in 2011 and, furthermore, demonstrates methods to constrain single and combined Inverse Gaussian - Transit Time Distributions (IG-TTDs). Measurements of multiple transient tracers were used to numerically constrain the IG-TTD model and to analyze the different ventilation pattern and water mass characteristics. It was shown that the ventilation in the Eastern Mediterranean Sea was characterized by two different formation types. Water masses belonging to the Eastern Mediterranean Transient (EMT) event showed a relatively advective-like behavior and could be described by a single IG-TTD. Water masses of Adriatic origin showed a more diffusive behavior and could be described by a linear combination of two IG-TTDs, known as 2IG-TTD. This led to contrary results between the mean age of the water and the chronological sequence of the deep water formations. The mean age of recently formed Eastern Mediterranean Deep Water of Adriatic source was higher than deep water originating from the EMT event in the 1990s. The extensive deep water formation in the Western Mediterranean Sea could be described by the 2IG-TTD. The model output showed that the elevated transient tracer concentrations of the deep water yielded a similar mean age of $\approx$ 200 years as the mid water depth with lower tracer concentration.

The second manuscript highlights specific characteristics of commonly used transient tracers and points out the different limits of the IG-TTD model based on field data applications in the South Atlantic and Southern Ocean. The relation-

ship between the relative transient tracer concentration (in %) and the tracer age highlighted the specific application ranges of the tracers and indicated possible tracer combinations which can be used to constrain the IG-TTD. It was shown that deviations in tracer saturation have a significant impact on the constraints of the IG-TTD ($>$ 100 % uncert. for 15 % deviation in saturation). The new method of validity areas was demonstrated using field data of several tracer surveys. This provided an easy-to-use approach for validating the applicability of the IG-TTD. Furthermore, this method showed that the application of the IG-TTD is limited by water mass characteristics south of the Subantarctic Front and specific sensitivity limits of the transient tracers.

The third manuscript describes flux estimates of dissolved inorganic carbon (DIC) and anthropogenic carbon through the Fram Strait in 2012. The excess of SF_6 and the anthropogenic carbon content in this area was estimated assuming a standard parameterisation of the IG-TTD. Hydrographic data was obtained along a mooring array at 78°50′N which allowed for flux estimates based on a mean velocity field. High uncertainties in the flux data inhibited significant statements about the transport budget. However, the results indicated that the north- and southward transport of anthropogenic carbon is balanced in the Fram Strait.

Introduction

The global climate has been changing throughout the Earth's history. A primary question is how human behavior influences this change and what can be done to counteract negative effects and to support positive ones. Hence, the understanding and predictability of natural processes provides the basis for future strategies. However, the prediction of changes of individual natural processes is complicated and inhibits constraints on climate prognosis. All natural processes are part of an extremely complex interacting system or, symbolically described, a large changing box of jigsaw pieces.

One important jigsaw piece is ocean ventilation which is, in simple terms, a naturally driven process where surface water propagates into the ocean's interior. The boundary condition of the surface water depends on the interaction between the ocean and the atmosphere, i.e. it is based on the pursuit of an equilibrium state at the air-sea interface. This means that the initial physical and chemical properties of a water parcel, e.g. temperature, salinity and dissolved gases, originate from the specific boundary condition. Thus, ocean ventilation describes not only the transport of water masses but also the transport of boundary conditions into the ocean's interior. Accordingly, several key processes related to climate change are based on ventilation processes such as the global heat distribution and the storage of carbon dioxide (CO_2) in the ocean. Furthermore, ocean ventilation is important for several mesoscale processes, e.g. the ventilation of oxygen minimum zones [Brandt et al., 2010], which has a limited influence on climate change, but a large impact on local fishing industries. Investigations of ocean ventilation are found in various fields of research which indicates the high importance of this topic.

One possible method to analyze local and global ventilation processes are transient tracer measurements. Transient tracers are compounds which provide time information on a discrete part of the geosphere. The time information of hydrographic samples is either based on radioactive decay (radioactive transient tracers) or a changing concentration of the boundary condition, commonly known as input function (chronological transient tracers). Ventilation processes can then

be quantified by applying a theoretical ventilation model to the transient tracer data. However, the modeling of ocean ventilation is very challenging due to complex interactions of various changing variables and only the basic structure of the ventilation pattern can be estimated. A commonly used model is the Transit Time Distribution (TTD), which was developed to describe atmospheric transport processes [Hall and Plumb, 1994] but can also be applied to the ocean [e.g. Klatt et al., 2002]. An empirical applicable solution of the TTD model is provided by Waugh et al. [2003], known as the Inverse-Gaussian Transit Time Distribution (IG-TTD).

The framework of transient tracer data and the IG-TTD provides a powerful tool to investigate ocean ventilation. The IG-TTD determines the mean age of a water parcel based on the carried time information of the transient tracer concentration and the shape of the IG-TTD. The different time information of transient tracers can be used to numerically constrain the IG-TTD model, i.e. the shape of the resulting distribution. A constrained model can then describe a significant mean age and additional ventilation characteristics such as the ratio between advection and diffusion. A transient tracer survey thus yields a momentary state of the prevailing ventilation pattern. Time series of transient tracer measurements additionally provide information about changes in ventilation and ventilation rates [e.g Schneider et al., 2014]. Another possible application is related to the offset of human made CO_2 which has a major impact on the global environmental system [e.g. Solomon et al., 2009]. The anthropogenic part of dissolved inorganic carbon in the ocean cannot directly be measured but can be estimated using the IG-TTD framework [Waugh et al., 2006].

Detailed introductions to the different transient tracers, the definitions of "age", the IG-TTD model and the corresponding applications are presented in the following manuscripts. The used data sets include new dichlorodifluoromethane (CFC-12) and SF_6 measurements which were conducted during three expeditions. The first data set was obtained during the M84/3 cruise in the Mediterranean Sea in April 2011 [Tanhua et al., 2013], the second during the ANT-XXVIII/3 cruise in the Southern Ocean in January-March 2012 [Wolf-Gladrow, 2013] and the third during the ARK-XXVII/1 cruise in the Fram Strait in June-July 2012 [Beszczynska-Möller, 2013]. The methodologies, e.g. the sampling procedure, the measurement systems, calibration routines, etc., are similar for all cruises and are discussed in detail in Stöven [2011]. Specific data information and statistics are presented in the corresponding manuscripts.

Manuscript I

Ocean Sci., 10, 439–457, 2014
www.ocean-sci.net/10/439/2014/
doi:10.5194/os-10-439-2014

Ocean Science Open Access

Ventilation of the Mediterranean Sea constrained by multiple transient tracer measurements

T. Stöven and T. Tanhua

Helmholtz Centre for Ocean Research Kiel, GEOMAR, Kiel, Germany

Correspondence to: T. Stöven (tstoeven@geomar.de)

Received: 9 September 2013 – Published in Ocean Sci. Discuss.: 10 October 2013
Revised: 14 February 2014 – Accepted: 14 April 2014 – Published: 5 June 2014

Abstract. Ventilation is the primary pathway for atmosphere–ocean boundary perturbations, such as temperature anomalies, to be relayed to the ocean interior. It is also a conduit for gas exchange between the interface of atmosphere and ocean. Thus it is a mechanism whereby, for instance, the ocean interior is oxygenated and enriched in anthropogenic carbon. The ventilation of the Mediterranean Sea is fast in comparison to the world ocean and has large temporal variability. Here we present transient tracer data from a field campaign in April 2011 that sampled a unique suite of transient tracers (SF_6, CFC-12, ^3H and ^3He) in all major basins of the Mediterranean. We apply the transit time distribution (TTD) model to the data in order to constrain the mean age, the ratio of the advective / diffusive transport and the number of water masses significant for ventilation.

We found that the eastern part of the eastern Mediterranean can be reasonably described with a one-dimensional inverse Gaussian TTD (IG-TTD), and thus constrained with two independent tracers. The ventilation of the Ionian Sea and the western Mediterranean can only be constrained by a linear combination of IG-TTDs. We approximate the ventilation with a one-dimensional, two inverse Gaussian TTD (2IG-TTD) for these areas and demonstrate a possibility of constraining a 2IG-TTD from the available transient tracer data. The deep water in the Ionian Sea has a mean age between 120 and 160 years and is therefore substantially older than the mean age of the Levantine Basin deep water (60–80 years). These results are in contrast to those expected by the higher transient tracer concentrations in the Ionian Sea deep water. This is partly due to deep water of Adriatic origin having more diffusive properties in transport and formation (i.e., a high ratio of diffusion over advection), compared to the deep water of Aegean Sea origin that still dominates the deep Levantine Basin deep water after the Eastern Mediterranean Transient (EMT) in the early 1990s. The tracer minimum zone (TMZ) in the intermediate of the Levantine Basin is the oldest water mass with a mean age up to 290 years. We also show that the deep western Mediterranean has contributed approximately 40 % of recently ventilated deep water from the Western Mediterranean Transition (WMT) event of the mid-2000s. The deep water has higher transient tracer concentrations than the mid-depth water, but the mean age is similar with values between 180 and 220 years.

1 Introduction

The Mediterranean Sea is a marginal sea, where the observational record shows significant changes in ventilation (Schneider et al., 2014). The most prominent transient event in the eastern Mediterranean Sea (EMed) is the transfer of the deep water source from the Adriatic Sea to the Aegean Sea and Sea of Crete and vice versa. The observed massive dense water input from the Aegean Sea and Sea of Crete in the early 1990s is known as the Eastern Mediterranean Transient (EMT) event (Roether et al., 1996; Klein et al., 1999; Lascaratos et al., 1999). The extensive deep water formation in the western Mediterranean Sea (WMed) between 2004 and 2006, known as the Western Mediterranean Transition (WMT) event (Schroeder et al., 2008, 2010), is thought to have been triggered by the EMT event (Schroeder et al., 2006). Nevertheless, both events are part of a general circulation pattern which can be observed in the Mediterranean Sea. The surface water in the WMed is supplied by less dense Atlantic water (AW) through the Strait of Gibraltar. The AW flows eastwards at depths < 200 m into the Tyrrhenian Sea

and into the EMed via the Strait of Sicily. The salinity of the AW increases along the pathway from 36.5 to > 38 due to net evaporation and is then described as modified Atlantic water (MAW) (Wuest, 1961). The heat loss during winter time in the MAW in the EMed leads to a sufficient increase of density to form the Levantine intermediate water (LIW) at depths between 200 and 600 m (Brasseur et al., 1996; Wuest, 1961). The exact area of the LIW formation process is poorly constrained and possibly variable, but it is expected to be in the eastern part of the EMed near Rhodes (Malanotte-Rizzoli and Hecht, 1988; Lascaratos et al., 1993; Roether et al., 1998). The main volume of the LIW flows back westwards over the shallow sill between Sicily and Tunisia entering the Tyrrhenian Sea along the continental slope of Italy (Wuest, 1961). Parts of the LIW enter the Adriatic Sea via the Strait of Otranto, where it serves as an initial source of the Adriatic Sea overflow water (ASOW). The formation of ASOW in the southern Adriatic pit is based on interactions between the LIW and water masses coming from the northern Adriatic Sea as well as the natural preconditioning factors, for example, wind stress and heat loss (Artegiani et al., 1996a, b). The ASOW flows over the sill of Otranto into the Ionian Sea intruding into the bottom layer and thus representing a source of eastern Mediterranean deep water (EMDW) (Schlitzer et al., 1991; Roether and Schlitzer, 1991). Furthermore, the Ionian Sea is connected with the Levantine Sea via the Cretan Passage, where portions of newly formed EMDW reach the deep water of the Levantine Sea. In 1992–1993, the water-mass conditions in the well-ventilated Aegean Sea and Sea of Crete changed into a more salty and cold state, sufficient enough to initialize the massive dense water input of Cretan deep water (CDW) into the abyssal basins of the EMed (Klein et al., 1999). This EMT event resulted in a disruption of the usual formation pattern of the EMDW. The Adriatic Sea as a major deep water source was thereby replaced by the Aegean Sea and Sea of Crete with the consequence that the bottom layer of the Ionian Sea was now supplied with dense water via the Antikythera Strait and the Levantine Sea via the Kasos Strait. The simultaneous dense water input into both basins, in conjunction with the large amount of the outflow, caused an uplift of the intermediate water layers in the Ionian and Levantine seas. One consequence of the EMT event seemed to be the preconditioning of the WMT event in 2004–2006 by uplifted water masses entering the WMed via the Strait of Sicily. However, the major triggering factor was the heat loss due to the mistral in the Gulf of Lion and the Balearic Sea, which resulted in the extensive deep water formation in the WMed. Although the total magnitude of the WMT event was smaller than the EMT event it was still sufficient to cause a near-complete renewal of the western Mediterranean deep water (WMDW). Recent water-mass analyses indicate, that the EMed is returning to a pre-EMT state with the Adriatic Sea as a major deep water source (Hainbucher et al., 2006; Rubino and Hainbucher, 2007).

The analysis of ventilation processes and their periodicity is an important issue in the understanding of their climate impact. Such analyses are not trivial, however, given the range of methods, views and concepts involved in understanding ventilation processes. For example, transient tracer distributions were used in the EMed by Roether et al. (1996, 2007) and in the WMed by Rhein et al. (1999) to quantify ventilation timescales. The time dependence of the transient tracers were used for first-age estimates based on simple approaches which provided an estimate of an apparent age or tracer age (Roether et al., 1998; Roether and Lupton, 2011). More complex age models, for example, the transit time distribution (TTD) model, account for the influence of mixing processes leading to a more realistic mean age estimate. A TTD related approach of age spectra modeling was carried out by Steinfeldt (2004) for the EMed in 1987, providing one of the first competing age estimates to the tracer age approach. The TTD model was, more recently, used for a time-series analysis of the entire Mediterranean Sea by Schneider et al. (2014). Such concepts of age and timescales in the ocean can also contain commonly used parameters like volume fluxes (changes) per time unit, normally stated as ventilation rate as well as residence time, influence time, tracer age, apparent age and mean age. Some of these parameters are occasionally presented in different contexts and meanings, leading to controversial discussions (Delhez et al., 2013). However, this paper does not include quantitative statements about ventilation rates or residence times. This study was focused on providing methods to constrain the mean age of the Mediterranean Sea within the framework of TTD models, which were then used to describe ventilation in terms of "age" structure and further qualitative characteristics, such as the advective and diffusive behavior of the different water masses. To this end, measurements of the transient tracers dichlorodifluoromethane (CFC-12) and sulfur hexafluoride (SF_6) as well as helium isotopes (^{3}He, ^{4}He) and tritium (^{3}H) were carried out during the *Meteor* expedition M84/3 in 2011 yielding a comprehensive data set of time dependent tracers (Fig. 1). The insights gained in this TTD model application method should also provide possible improvements for continuative estimates of ventilation rates, defined by Primeau and Holzer (2006); Hall et al. (2007) and anthropogenic carbon contents (Tanhua et al., 2008).

2 Materials and method

2.1 Transient tracers

2.1.1 Chronological transient tracers

The uses of chronological transient tracers, such as chlorofluorocarbons (CFCs) and SF_6 to estimate the age of a water mass are based on an increasing tracer concentration in the atmosphere. Concentrations of trace gases in the atmosphere are, for example, measured continuously by the world-wide

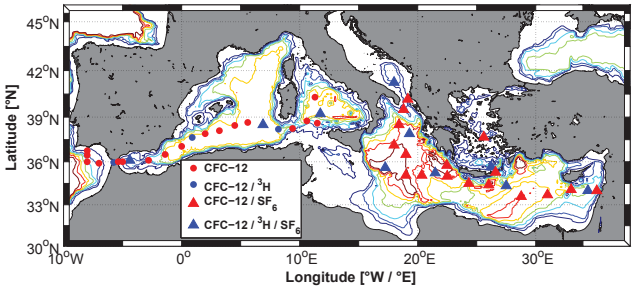

Figure 1. Transient tracer sample stations of the M84/3 cruise from Istanbul to Vigo. Triangles indicate stations including SF_6 measurements and a blue color coding indicates tritium measurements. CFC-12 was measured at all stations on this map. The depth contours are 500 : 500 : 3500.

AGAGE network, so that the emission history and atmospheric variations over time are well known (Walker et al., 2000; Bullister, 2011), which then provide the tracer's input functions. The production of CFCs, and ultimately their emissions, were decreased in the late 1980s and then finally stopped in the 1990s as a result of the Montreal Protocol. This has resulted in a steady decrease of atmospheric CFC-12 concentrations such that in 2011 the concentration was 532 ppt (Bullister, 2011). Because the concentrations of CFC-12 in the atmosphere were increasing prior to the 1990s and then decreased up until 2011, CFC-12 concentrations in seawater that are higher than the 2011 atmospheric concentration could therefore represent one of two dates (i.e., before the 1990s or after the 1990s, Fig. 2). To this end, CFC-12 concentrations are inconclusive for tracer age determination between 1994 and 2011. SF_6 concentrations are still increasing approximately linearly but the emission rate is relatively low so that the concentration in the atmosphere is reportedly below 8 ppt. Some local restrictions are in place for the production and use of SF_6, but an international agreement has yet to be reached, despite its global warming potential of 22 000 (Houghton et al., 1996). Tracers enter the ocean's surface layer via gas exchange and the solubility is a function of temperature, salinity and the physical nature of the molecule. Solubility functions are available for most of the CFCs and SF_6 (Warner and Weiss, 1985; Bullister et al., 2002) and are used to convert the measured gravimetric units (e.g., pmol kg^{-1} for CFC-12 and fmol kg^{-1} for SF_6), into the partial pressure (ppt) of the tracer. The partial pressure is the preferred choice since it is independent of pressure, salinity and temperature and thus directly comparable within the complete water column and atmosphere.

Chronological tracers are conserved tracers with no significant sources or sinks in the ocean interior. The concentration in the water column depends on the last time the water parcel was in contact with the atmosphere and on the influence of mixing and diffusion.

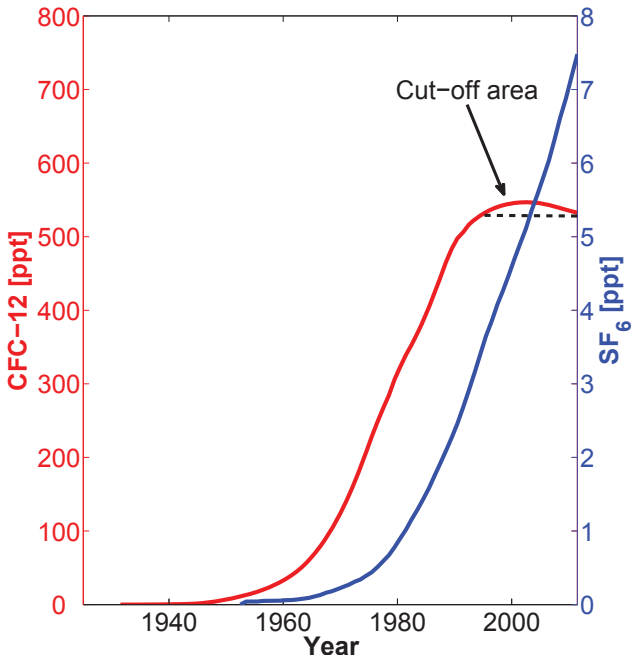

Figure 2. Atmospheric histories of CFC-12 (red) and of SF_6 (blue). The decreasing trend of CFC-12 produces a cut-off area between 1994 and 2011, which means that any CFC-12 concentration above 532 ppt provides only inconclusive information about ventilation.

2.1.2 Radioactive transient tracers

The radioactive tracers such as tritium and its decay product helium-3 (^3He) form the second class of transient tracers. Tritium has a natural background concentration of ≈ 0.3 tritium units (TU) in the atmosphere, where 1 TU equals the number of one tritium atom per 10^{18} hydrogen atoms (Ferronsky and Polyakov, 1982). Due to nuclear bomb tests in the late 1950s and 1960s, the tritium concentration increased up to 100 TU in the atmosphere and declined afterwards to a current concentration of 1–1.2 TU in 2011 (Roether et al., 2013). The input of tritium into the ocean surface layer is a function of radioactive decay in the atmosphere, vapor pressure, the variance of location and magnitude of precipitation and fresh water flux by riverine input. Tritium decays to helium-3, known as tritiugenic helium-3 ($^3He_{trit}$) which equilibrates with the atmosphere as long as the water parcel remains in the boundary layer of gas exchange. Once the water reaches the oceans interior, radioactive decay serves as time varying sink. However, the total concentration of helium-3 ($^3He_{tot}$) in sea water consists of several shares of different sources. The determination of the $^3He_{trit}$ share requires the knowledge of excess helium-3 ($^3He_{ex}$), that is, the surface saturation and the terrigenic share ($^3He_{terr}$) from the earth crust and mantle (i.e., the sea floor as source of ^3He).

The Mediterranean is characterized by higher tritium concentrations than the Atlantic due to continental influences in terms of weather conditions and fresh water input. A

commonly used tritium input function (TIF) for the North Atlantic was obtained by Dreisigacker and Roether (1978) and further developed for the EMed by Roether et al. (1992). Based on this data set, another TIF for the EMed was created by R. Steinfeldt (unpublished data) where the data after 1974 was extrapolated by using the decay function of tritium. In the WMed the surface layer is mainly influenced by the inflow of Atlantic water (AW), so that the input function needs to be corrected for the degree of dilution. The difference between the mean surface tritium concentration of the M84/3 cruise and the concentration value of the TIF by R. Steinfeldt (unpublished data) of the same year can be used to determine correction factors for the eastern and western Mediterranean. Under the assumption that the determined offset is constant over years, both factors can be used as an offset correction to create two alternative input functions (Fig. 3) which can be applied to a TTD mixing model (see below). The corrected TIFs have a surface (input) concentration which is 15 % lower in the EMed and 35 % lower in the WMed than suggested in the original input function. Figure 3 shows the recent TIF of the Mediterranean Sea by Roether et al. (2013), which also relies on the data set of Dreisigacker and Roether (1978). This TIF was recalculated for the EMed by using a dilution factor and mean surface tritium concentrations obtained during several cruises between 1974 and 2011. Comparing both recent TIFs of the EMed shows that the shape of both curves is relatively similar. This indicates that both input functions seem to be useful approaches for the EMed despite the different methods used in their estimation. However, by using an interpolated form of the input function of Roether et al. (2013), a higher mean age is yielded compared to the input function we obtained. The main deviation from the decay-based input function is the data point of 1978, following that the interpolated tritium concentrations were significantly elevated between 1975 and 1987, producing differences in mean age. The mean deviation between the different TIFs and the original TIF of the North Atlantic are 86 % and 61 %, respectively (Roether et al., 2013), for the EMed and 43 % for the WMed.

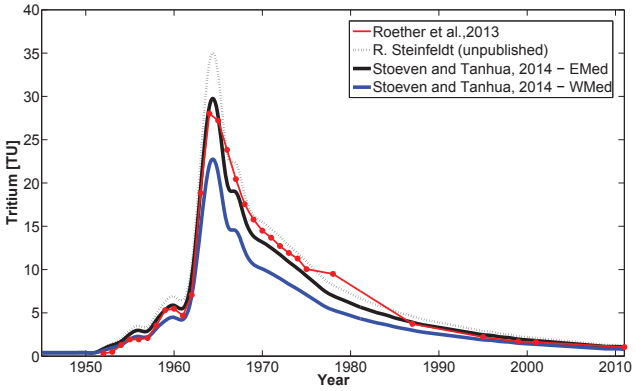

Figure 3. Input functions of tritium. The dotted black curve shows the decay based input function of the Mediterranean Sea by R. Steinfeldt (unpublished data). The black and blue curves describe the off set corrected input functions for the eastern and western Mediterranean Sea. The red curve shows the suggested input function by Roether et al. (2013) of the eastern Mediterranean Sea.

2.2 Tracer age and the transit time distribution

The age of a water parcel can be described in different ways. For chronological transient tracers, the measured concentration of sample c in year t_s (year of sampling) can be set in relation to the same concentration c_0 with the relevant year t_{hist} of the atmospheric history of the tracer (Eq. 1).

$$c(t_s) = c_0(t_{hist}) \tag{1}$$

The difference between the year of sampling t_s and the obtained year t_{hist} defines the tracer age τ (Eq. 2).

$$\tau = t_s - t_{hist} \tag{2}$$

The tracer age of radioactive tracers depends on first order kinetics shown in Eq. (3). The initial concentration c_i, the in situ concentration c and the decay constant λ are the required parameters to calculate the elapsed time of a tracer in a water parcel.

$$\tau = \frac{1}{\lambda} \cdot \ln\left(\frac{c_i}{c}\right) \tag{3}$$

As mentioned above, tritium has, in addition to the radioactive decay, a relevant input function and thus an unknown part for c_i. Therefore, the share of $^3He_{trit}$ needs to be determined which replaces the initial concentration of tritium and Eq. (3) can be rewritten as Eq. (4). A generally accepted value for the decay constant of tritium is $\lambda = 0.05576/a$ (Unterweger et al., 1980; Taylor and Roether, 1982).

$$\tau = \frac{1}{\lambda} \cdot \ln\left(1 + \frac{\left[^3He_{trit}\right]}{\left[^3H\right]}\right) \tag{4}$$

The informative value of a tracer age is relatively low because it is based on the assumption of a complete advective behavior neglecting any diffusive mixing process. However, there are also methods such as dilution models (Roether et al., 2013) and the tracer age of CFC-12 and SF_6 with a $\approx$ 14 year time lag (Tanhua et al., 2013c; Schneider et al., 2014) that allow an estimation of changes in ventilation.

The TTD model is based on the Green's function and was invented to describe atmospheric ventilation processes (Hall and Plumb, 1994). However, the basic idea that a parcel of molecules changes its location under the influence of advection and diffusion can also be applied to ventilation processes of the ocean. Equation (5) is an analytical expression of the Green's function which provides access to use field data within the TTD model (Waugh et al., 2003). It is based on a one-dimensional flow model with constant advective velocity and diffusivity and is therefore known as

the one-dimensional inverse Gaussian transit time distribution (IG-TTD).

$$G(t) = \sqrt{\frac{\Gamma^3}{4\pi\,\Delta^2 t^3}} \cdot \exp\left(\frac{-\Gamma(t-\Gamma)^2}{4\Delta^2 t}\right) \quad (5)$$

The key variables in this equation are Γ for the mean age and Δ for the width of the distribution. The age spectra t is defined by the initial year t_i of the atmospheric history or the input function of the tracer and the year of sampling t_s. To give a statement on the share of advection and diffusion, the Δ/Γ ratio can be used. A low ratio, such as 0.4–0.8, indicates a high advective part (e.g., extensive deep water formations), whereas a high ratio like $1.2-1.8$ indicates a more diffusive character of the water parcel. The definite integral of Eq. (6) contains the link between the measured concentration of a sample $c(t_\mathrm{s})$ and the mean age of the TTD. The parameter r describes the location of the water parcel, t – the time range of the tracer and $e^{-\lambda t}$ – the decay correction for radioactive transient tracers.

$$c(t_\mathrm{s}, r) = \int_0^\infty c_0(t_\mathrm{s}-t)e^{-\lambda t} \cdot G(t,r)\mathrm{d}t \quad (6)$$

A further approach to determine a mean age is the linear combination of two distributions which is shown in Eq. (7). Hereby, α describes the percentage ratio between the two G-functions. Such a two inverse Gaussian TTD (2IG-TTD) can be envisioned for two water masses with different histories (age), but with similar density, that mixes in the ocean interior. This model has been explored by, for instance, Waugh et al. (2002).

$$c(t_\mathrm{s}, r) = \int_0^\infty c_0(t_\mathrm{s}-t)e^{-\lambda t}\cdot \left[\alpha\, G(\Gamma_1, \Delta_1, t, r) + (1-\alpha)\, G(\Gamma_2, \Delta_2, t, r)\right]\mathrm{d}t \quad (7)$$

The number of possible combinations of distributions and parameters provides a comprehensive concept of age modeling in the ocean. The main complexity consists of finding accurate and reasonable solutions related to the field data. The mean age is then determined by Eq. (8), whereas Γ_1 and Γ_2 are the partial mean age results of each G-function.

$$\Gamma = \alpha \cdot \Gamma_1 + (1-\alpha)\cdot\Gamma_2 \quad (8)$$

2.3 Practical application of the TTD model

A common procedure described in several published articles (e.g., Schneider et al., 2010; Waugh et al., 2006, 2004) is to apply the IG-TTD with a ratio of $\Delta/\Gamma = 1.0$ to the tracer data to calculate a water-mass mean age. The Δ/Γ ratio has been demonstrated to be close to 1 in large parts of the world ocean (i.e., established as standard ratio). This standard ratio can be used to analyze transient tracer time series in terms of changes in ventilation, where the rate of age growth yr^{-1} is more in focus than a precise mean age (Huhn et al., 2013). The recently published work by Schneider et al. (2014) is also based on the standard ratio of $\Delta/\Gamma = 1.0$, which allows a comparison to be made between all data sets and thus an analysis of changes during the period of interest. In the case of a time series, it is rarely possible to apply similar constraints to different data sets. The standard ratio should also be used within tracer surveys with only few sample points because local outliers of constrained data points can produce significant flaws in interpolation. For a comprehensive data set, consisting of more than one transient tracer, a constrained TTD model provides an alternative. The determined Δ/Γ ratios provide a first insight into the water-mass structure concerning the advective and dispersive behavior. The further analysis of ventilation processes, rates and recent changes in water masses as well as the estimation of the anthropogenic carbon column inventory is based on the determined mean age and thus dependent on the exact Δ/Γ ratio. However, it is an important principle to identify in which manner a TTD method was applied before comparing different studies.

2.3.1 Constraining the IG-TTD model

There have been several approaches made to constrain a TTD model. For instance, Waugh et al. (2002) uses the lower and upper mean age limit of the transient tracers and plot them against the standard deviation (σ) of the TTD. In the case of an IG-TTD it can be approximated as $\Delta = \sigma/\sqrt{2}$. The area which is spanned by all tracers then constrain the TTD. Other methods are based on property–property plots. For example are tracer concentrations plotted against each other including predicted concentration curves by the TTD for different Δ/Γ ratios, whereas the best fit of a predicted curve to the bunch of data provides a single overall constraint of the TTD (Waugh et al., 2004). A similar method is used by Schneider et al. (2012) where the CFC-12 mean age is plotted vs. the SF_6 mean age for different Δ/Γ ratios. Hereby, a good correlation between the data points and the bisecting line (slope = 1) denotes the ideal ratio. However, each method to constrain a TTD requires a transient tracer couple. The tracers of the couple need to have sufficiently different input functions to constrain the Δ/Γ ratio. Tracer couples with similar atmospheric histories (e.g., CFC-12 and CFC-11) will yield a wide range of possible outcomes and will result in a poorly constrained TTD. Useful couples are CFC-12–SF_6 and tritium–SF_6.

Our approach is based on constraining single data points instead of determining an overall Δ/Γ ratio. Therefore, the first step of data processing includes the calculation of the mean age for Δ/Γ ratios between 0.0 and 1.8 for every data point and tracer, always taking into account the correct input function of the source region. The determined data points of mean age vs. Δ/Γ ratio are used to obtain second-order

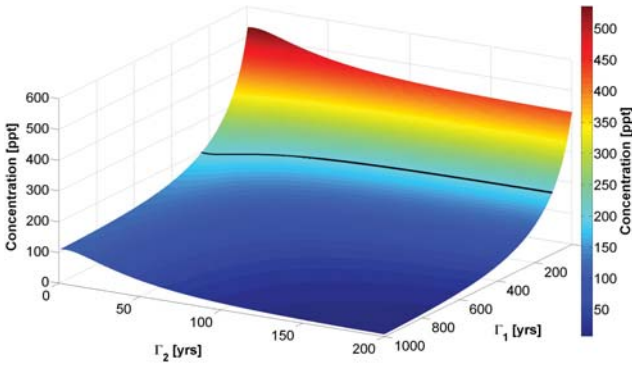

Figure 4. Example mean age matrix of CFC-12 with $^{\Delta_1}/_{\Gamma_1} = 1.4$, $^{\Delta_2}/_{\Gamma_2} = 0.6$ and $\alpha = 80$. The color-coding denotes the concentration of CFC-12 (in ppt, also on the z axis) with a black concentration contour line at 200 ppt; x and y axis denotes the mean age of the 2IG distributions that make up the TTD. The combination of all three-dimensional tracer matrices provides the needed information to constrain a 2IG-TTD, see text.

polynomial regressions. Following this, every sample point of every tracer can be expressed by a mean age function (Eq. 9).

$$\Gamma = a\left(^{\Delta}/_{\Gamma}\right)^2 + b\left(^{\Delta}/_{\Gamma}\right) + c \tag{9}$$

The intersection between two mean age functions denotes the constrained Δ/Γ ratio and mean age. In some cases where no exact intersection can be found it is useful to determine the local minimum of a combined mean age function in the range of Δ/Γ. A local minimum indicates the point of the smallest difference in mean age, which should be used to a maximum difference of 5 years to ensure also the consideration of a mean analytical error of $\approx 4\,\%$ (see below). To obtain the mean age of such a minimum function, the average of both mean age values needs to be calculated. However, in some cases it is more meaningful to use one of the tracer's mean age rather than the average mean age. For example, the SF_6 mean age for recently ventilated waters is more significant than the CFC-12 mean age due to the recent non-transient input function of CFC-12. In contrast, the CFC-12 mean age should be used in older water layers where SF_6 concentrations are close to the detection limit (Tanhua et al., 2008).

A further aspect of the IG-TTD model is the validity area of each tracer couple, which defines the possible range of IG-TTD solutions. A rough classification of the specific validity area of a couple can be done by determining the tracer age differences. For example, if the difference of the tracer age between SF_6 and CFC-12 is large (10 years for the sampling year of 2011), it indicates that an IG distribution cannot explain the tracer distribution, and more refined models of the TTD are needed, for instance the linear combination of two IG-TTDs.

2.3.2 Constraining the 2IG-TTD model

Due to the five free parameters α, Γ_1, Γ_2, Δ_1 and Δ_2, the system of equations is under-determined for any tracer survey with less than five measured transient tracers. Most surveys include two or three transient tracers with sufficiently different atmospheric histories. Here we introduce one way to use an under-determined 2IG-TTD model. Based on oceanographic water-mass analysis one can estimate the composition of the current state of the water masses and roughly the underlying mixing processes. As described earlier, the western and eastern Mediterranean are both affected by an extensive deep water formation with recently ventilated and salty water from the surface and intermediate layers, respectively. The null hypothesis is that an old and more stationary water mass can be described by an IG-TTD which has been intruded by a younger water parcel described by another IG-TTD. Hereby the younger water parcel might be characterized by a more advective behavior with a low ratio (e.g., $\Delta/\Gamma = 0.6$). The ratio of the more stationary water mass is set to $\Delta/\Gamma = 1.4$, describing a typical ratio of a more diffusive/dispersive behavior. By making assumptions about the Δ/Γ ratio of both IG-TTDs one can calculate mean age matrices for different α's with $x = \Gamma_1$, $y = \Gamma_2$ and $z = C_{\text{tracer}}$. The concentration of a measured sample generates different concentration curves for each α in the x–y plane (Fig. 4). The predefined 2IG-TTD is constrained if there is an intersection area of the concentration curves of different tracers describing one mean age (Eq. 8).

2.4 Sampling and measurements

The expedition M84/3 from Istanbul (Turkey) to Vigo (Spain) took place from the 5 to 28 April in 2011 on the German research vessel *FS Meteor* (Tanhua et al., 2013a, b). Figure 1 shows an overview of the sample stations with different symbols denoting which tracers were measured. The transient tracers CFC-12 and SF_6 were sampled at nearly all stations in the EMed, whereas only three stations of SF_6 exist in the WMed. Tritium was sampled at 7 stations in the EMed and 6 stations in the WMed. The sampling depths were chosen to cover the most important water layers in a sufficient resolution. Starting with an minimum sampling depth increment of 25 m in the surface and mixed layer and ending with a maximum increment of 500 m in the deep water layers (see Table 1).

2.4.1 CFC-12 and SF_6

The measurements of CFC-12 and SF_6 were mainly performed on board. The water samples were taken with 250 mL glass syringes or 300 mL glass ampules, under exclusion of atmosphere, from the Niskin bottles. The syringes and ampules were stored in a cooling box filled with water of $\approx 0\,^{\circ}\text{C}$ to prevent outgasing of the tracers. The measurements were

Table 1. Standard sampling depths of the M84/3 cruise in 2011.

Increment [m]	Depth range [m]
25	0–100
50	100–300
100	300–600
200	600–1000
250	1000–2500
500	2500–bottom

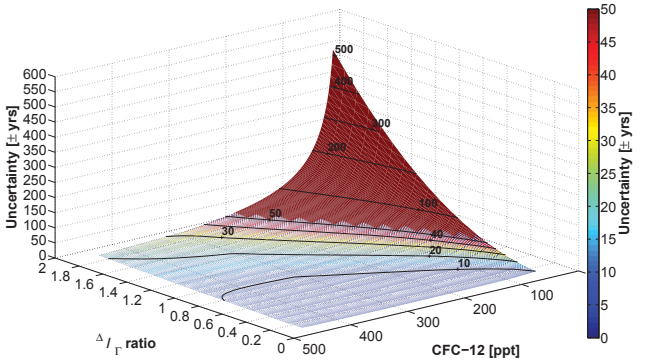

Figure 5. Absolute error of mean age calculations depending on CFC-12 concentrations and $^{\Delta}/_{\Gamma}$ ratios. The color coding is restricted to a maximum of 50 years for an improved error resolution of the main area.

carried out with similar analytical systems as described by Bullister and Wisegarver (2008) and Law et al. (1994). The first measurement system named VS1 consisted of a Shimadzu GC14a gas chromatograph equipped with an electron capture detector (ECD), stainless steel tubing system and Valco valves. An evacuated vacuum sparge tower (VST) was used to transfer the water sample out of the glass ampule into the measurement system. Due to the low pressure in the VST, most of the dissolved gases pass over into the head space during the filling process. The residual was purged out with nitrogen (ECD-quality). The analytes were trapped on a 1/16″ column packed with 70 cm *Heysep D* and then separated with a 1/8″ precolumn, packed with 30 cm *Porasil C* and a 1/8″ main column consisting of 180 cm *Carbograph 1AC* and a 20 cm *Molsieve 5 Å* tail end. The trap was installed in a Dewar filled with a bottom layer of liquid nitrogen. The distance between trap and cooling medium was regulated by a Lab Boy to hold a temperature range between −70 and −60 °C during the purge process. Due to some problems with the VS1 system and a sudden break down of the ECD several samples from key stations have been flame sealed in glass ampules for a later onshore measurement. The sealed ampules were measured during summer 2011 at the IfM-GEOMAR in Kiel with the repaired VS1 instrument and an installed ampule cracker system similar to Vollmer and Weiss (2002).

The second measurement system PT3 consisted of a Shimadzu GC2014 gas chromatograph with a similar basic setup like the VS1 system but with a different column composition, sample chamber and trap system. The 1/8″ precolumn consisted of 60 cm *Porasil C* and 10 cm *Molsieve 5 Å*, the 1/8″ main column of 180 cm *Carbograph 1AC* and 30 cm *Molsieve 5 Å*. Insufficient base line separation prevented a quantitative analysis of SF_6 with this column setup. For each measurement, an aliquot of ≈ 200 mL was injected into the sample chamber with a sampling syringe and then purged with high purified nitrogen. A pressure regulated ethanol bath was used for keeping the trap cold. The ethanol was cooled by a Julabo cooling finger to a minimum temperature of −68 °C. For the purge and trap process the fill level is raised until the trap dips into the ethanol and is lowered again for the heating process (Bullister and Wisegarver, 2008). The traps of both measurement systems were heated to 90 °C by an electrical current flow, which was automatically regulated by a proportional–integral–derivative controller (PID). A detailed description of the data set, the sampling, the calibration and measuring procedure including chromatograms and the specific retention times as well as a precise technical overview can be found in the published diploma thesis by Stöven (2011).

2.4.2 Tritium

Water samples for tritium measurements were taken in 1 L plastic bottles and sent to the Institute of Environmental Physics at the University of Bremen where the samples were degassed and stored for several weeks to accumulate $^3He_{trit}$. The measurements of the tritiugenic helium isotopes were then carried out with a sector field mass spectrometer. Details of the measuring procedure and statistical evaluations can be found in Sültenfuß et al. (2009) and the results are described in Roether et al. (2013).

2.4.3 Uncertainties

The precisions of CFC-12 and SF_6 measurements from both instruments can be found in Table 2. The error of calibration routines, that is, standard gas, standard loops, temperature and pressure, is ≈ 1 %. The uncertainty of the purge efficiency of CFC-12 is estimated to be 2 % and negligible low for SF_6 so that the accuracy of CFC-12 is approximately 3 % and 1 % for SF_6. The uncertainty of the atmospheric history is < 1 % for SF_6 and CFC-12, whereas for low concentrations of CFC-12 an error of ≤ 4 % should be assumed due to the time period prior reliable CFC measurements (Tanhua et al., 2008; Walker et al., 2000). The input functions depend on the degree of saturation during a water-mass formation which is influenced by wind speed, mixed layer depth, convection velocity, pressure and temperature drops as well as the atmospheric emission increase of a tracer, resulting in an approximate 10 % propagation of uncertainty (Haine

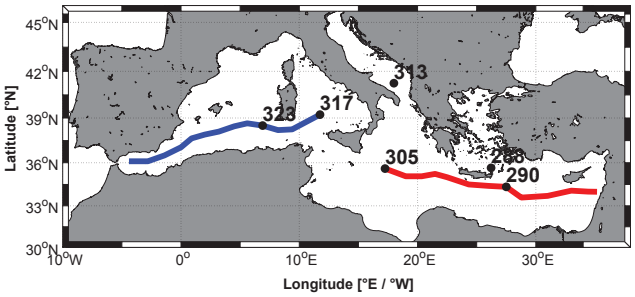

Figure 6. Sections and key stations of the transient tracer analysis. The red line shows the EMed section, the blue line the WMed section and the black dots the key stations.

and Richards, 1995; DeGrandpre et al., 2006; Tanhua et al., 2008). Furthermore, there are some regions were SF_6 has been used for release experiments (e.g., 1996 in the Greenland Sea gyre; Watson et al., 1999), which could produce an offset in concentrations. Since 2006 it is recommended to use an alternative tracer for release experiments to avoid such interferences with SF_6 of atmospheric origin. However, there was a release experiment using 1.327 mole of SF_6 in the Gulf of Lion in 2007 within the Lagrangian transport experiment (LATEX) (Hu et al., 2009). The SF_6 was released at shallow depths and it can be assumed that most of the SF_6 will be ventilated to the atmosphere, but nonetheless it is a possible error source with an unknown impact on further SF_6 surveys in this region. Assuming the worst case scenario of a deep water formation within this SF_6 patch, for example, the WMT event with a water renewal volume of $\approx 1.5 \times 10^{14}\,m^3$ (Schroeder et al., 2008), the interior concentration of SF_6 would be elevated by $0.009\,fmol\,kg^{-1}$ which is negligible.

The error of tritium measurements is given as $\pm 3\,\%$ and ± 0.02 TU whichever is greater (Roether et al., 2013). The input functions of tritium are in contrast to the atmospheric histories of CFC-12 and SF_6 not well documented and have several regional influencing factors as already mentioned above. An uncertainty of up to 15 % might be a realistic estimate of the used input functions.

The uncertainties in mean age is a function of errors in transient tracer concentrations and the Δ/Γ ratio. Figure 5 shows an example for absolute errors in mean age calculations based on CFC-12. The mean age becomes more uncertain for low tracer concentrations and high Δ/Γ ratios. The error functions for SF_6 and tritium are similar to the one of CFC-12.

Table 2. Precision of CFC-12 and SF_6 measurements.

	Precision	
System	SF_6	CFC-12
VS1	$\pm 1.4\,\%$ / ± 0.05 ppt	$\pm 0.6\,\%$ / ± 2 ppt
PT3	–	$\pm 0.3\,\%$ / ± 1 ppt
Cracker	$\pm 4.3\,\%$ / ± 0.07 ppt	$\pm 1.9\,\%$ / ± 5 ppt

3 Results and discussion

3.1 General ventilation pattern

3.1.1 Eastern Mediterranean Sea

The zonal sections of the transient tracer concentrations of the Ionian and Levantine seas show some significant characteristics of their ventilation (Figs. 6, 7). Between 27° E and the coast of Lebanon, a clear tracer minimum zone (TMZ) can be identified by all three tracers which vertically spreads from approximately 700 to 1600 m depths. The core concentration of the TMZ is 106 ppt for CFC-12, 0.3 ppt for SF_6 and 0.3 TU for tritium, whereas the lowest values are not visible in the gridded fields shown in Fig. 7. Beneath this TMZ, the tracer concentrations are elevated in the deep water due to the deep water formation in the eastern Mediterranean Sea that led to a high volume input of tracer rich and dense water masses. The bottom concentration of the tracers are ≈ 200 ppt for CFC-12, ≈ 1.1 ppt for SF_6 and ≈ 0.6 TU for tritium. In the westerly parts of the section (i.e., the deep Ionian Sea), the tracer concentration is higher in the deep and bottom layer than in the east. This water-mass characteristic belongs to recent intrusions of ASOW coming from the deep water source in the Adriatic Sea. Station 313 in the southern Adriatic pit can be used as representative example for the source region of the ASOW. The concentration profiles show, that the southern Adriatic pit is a well-mixed and ventilated basin with minimum tracer concentrations of CFC-12 > 429 ppt, $SF_6 > 5$ ppt and tritium > 0.9 TU (Fig. 8a). The high concentrations of CFC-12 and tritium throughout the entire water column at station 288 in the Sea of Crete can be related to the time range from the 1990s until the present day (Fig. 8b). The concentration gradient of SF_6, however, indicates a recent return to a more layered structure in the Sea of Crete, so that the high concentrations of CFC-12 and tritium in the intermediate and deep water have to be formed before this layering process, probably during the 1990s. This would imply that the EMT source region was a completely mixed basin during the outflow event. This difference in tracer structures is related to the increasing input function of SF_6 and the weak input functions of CFCs since the early 1990s (i.e., the onset of the EMT). CFC-12 and tritium concentrations cannot be used to identify the recent change in ventilation of the Sea of Crete. A further

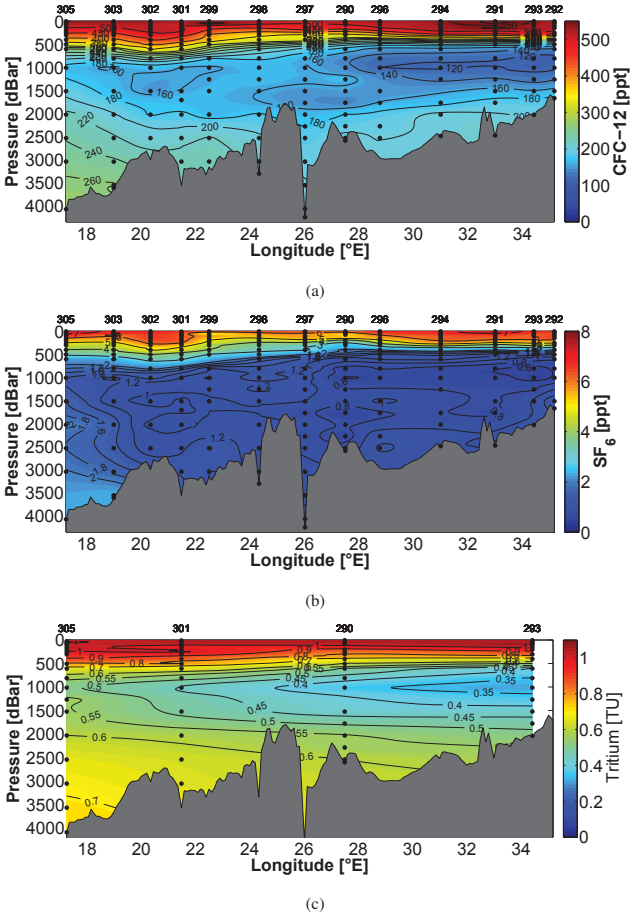

Figure 7. Transient tracer concentrations in the EMed during April 2011 (cruise M84/3), red line in Fig. 6. **(a)** CFC-12 in ppt, **(b)** SF_6 in ppt and (**c**) tritium in TU.

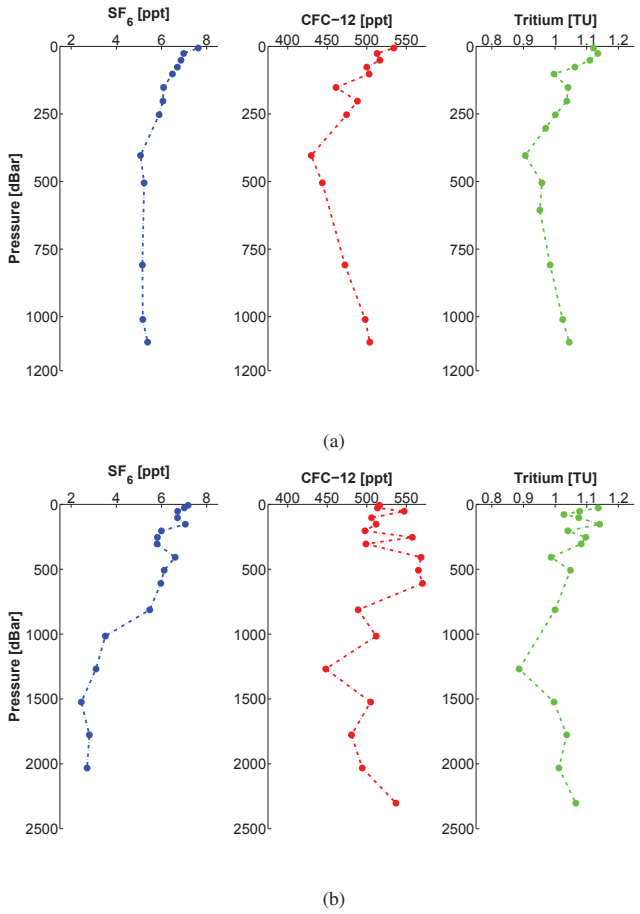

Figure 8. Profiles of transient tracers **(a)** in the Adriatic Sea at station 313 and **(b)** in the Sea of Crete at station 288 during April 2011. All three transient tracer show high concentrations throughout the entire water column of the Adriatic Sea. The Sea of Crete profiles show a clear concentration gradient for SF_6, whereas the CFC-12 and tritium concentrations scatter around their maximum values.

aspect is the distribution of SF_6 in the Ionian and Levantine seas which looks more homogeneous in the intermediate and deep water compared to CFC-12. This is based on the relatively young atmospheric history of SF_6, leading to deep water masses which are only less affected by this tracer. Accurate measurements between 1 ppt and the detection limit are needed to have a useful resolution. As mentioned above, CFC-12 has a long atmospheric history with a rapid concentration increase over several decades. Thus, CFC-12 has a large dynamic scale within the measurement range, so that CFC-12 is an important tracer for intermediately old water masses.

3.1.2 Western Mediterranean Sea

The CFC-12 and tritium section from the Tyrrhenian Sea through the western basin into the Alboran Sea show, that the western Mediterranean deep water (WMDW) is completely intruded by recently ventilated water masses coming from the extensive deep water formation during 2004–2006 (Figs. 6, 9) (Schroeder et al., 2008, 2010). The CFC-12 concentrations are > 260 ppt (Fig. 9a) and the tritium concentrations are > 0.5 TU (Fig. 9b) throughout the entire bottom layer of the western basin reaching the channel between Sardinia and Sicily. Figure 10 shows in detail that newly formed WMDW starts to enter the Tyrrhenian Sea along this bottom contour without reaching the interior water masses in 2011. The Tyrrhenian Sea is characterized by CFC-12 concentrations below 180 ppt and tritium concentrations < 0.5 TU suggesting that this basin was not affected by input of the 2004–2006 deep water formation into the deep and bottom water layers by 2011. These relatively low tracer concentrations from the Tyrrhenian Basin rudimentary extends as tongue into the intermediate layer between 700 and 1300 m of the western basin which correlates with the results of Rhein et al. (1999).

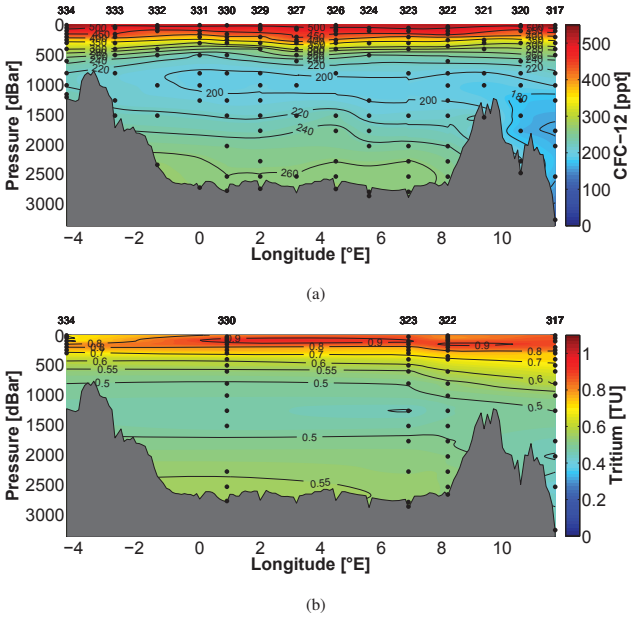

Figure 9. (a) CFC-12 concentration in ppt and **(b)** Tritium concentration in TU of the western basin and the Tyrrhenian Sea, blue line in Fig. 6.

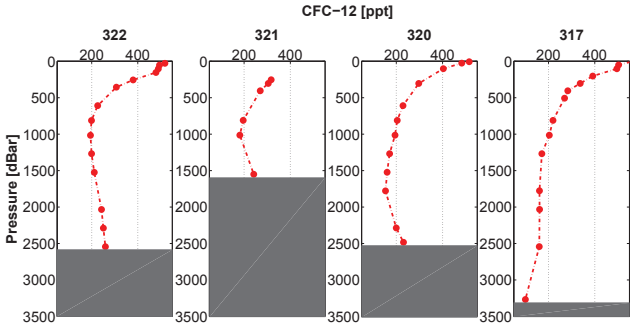

Figure 10. CFC-12 concentration in ppt along the shallow sill between Sardinia and Sicily. The elevated CFC-12 concentration of the bottom layer indicates the overflow of WMDW into the Tyrrhenian Sea. The depth of each station is indicated by the gray patch in each panel.

3.2 Transit time distributions

3.2.1 IG-TTD

The first approach of a mean age is based on the obtained Δ/Γ ratios for the IG-TTD model which also provide further information on water-mass characteristics. The major share of Δ/Γ ratios was determinable for the CFC-12/SF_6 tracer couple in a reasonable range for samples of the EMed. Figure 11a shows the section of Δ/Γ ratios as interpolated macrostructure in the EMed based on CFC-12 and SF_6 and the IG-TTD model. The sectional interpolation quality is reduced due to few constrainable data points. Figure 11a indicates that the TMZ spreading is more affected by the EMT event than the tracer concentrations suggest. The water below 1200 m in the Levantine Basin has Δ/Γ ratios between 0.4 and 0.6 indicating a high advective behavior of the EMT event. The TMZ has ratios between 1 and 1.3 as expected for a stable water mass where diffusion predominates. The low Δ/Γ ratios of the EMT water masses are also observed in the easterly deep waters of the Ionian Sea, whereas the deep waters further west formed by ASOW have ratios between 1.2 and 1.4. Combining the second tracer couple consisting of SF_6 and tritium yields a similar trend of Δ/Γ ratios in the EMed (Fig. 11b). However, there are only four stations with tritium measurements available within the section of the EMed (290, 292, 301, 305) and thus the sectional interpolation is restricted to 34 data points which does not allow a resolution of local phenomena but only provides a rough overview.

Comparing the Δ/Γ ratios in the intermediate and deep water layers of the Sea of Crete (Fig. 12a) with the EMT water masses in the Ionian and Levantine seas (Fig. 11a), one can see that the formation of the Cretan Sea overflow water (CSOW) as well as the EMT event itself were based on distinctly advective processes with an expected mean age approaching the tracer age. In contrast, water masses coming from Adriatic deep water (AdDW) seems to be formed by water masses with a more dispersive character belonging to slower formed water layers indicated by significant high Δ/Γ ratios between 1.1 and 1.6 (Fig. 12b). The red dots in Fig. 12b indicate non-constrained data points. It can be supposed that the formation of ASOW is based on slower dispersive processes of different water masses. The westerly bottom water of the Ionian Sea show the same dispersive characteristics as the ASOW (Fig. 11a). This indicates that both states of Δ/Γ ratios were mainly defined by the formation process of ASOW–CSOW source water and only in minor share by mixing processes along the current pathway from source region into the interior of the Levantine and Ionian seas. Therefore, the transient tracer concentrations of both deep water masses are not necessarily simply indicators of their ventilation.

Figure 13 show the determined mean age constrained by either CFC-12 and SF_6 or tritium and SF_6. The tritium-/SF_6-based maximum mean age of the TMZ in the Levantine Sea is 260 years and the deep and bottom water have a mean age between 70 and 80 years. In contrast, the CFC-12/SF_6 based maximum mean age of the TMZ is 230 years with a further high mean age in the Ionian Sea between 120 and 180 years. The deep and bottom water from the EMT event is the youngest water with a mean age between 50 and 80 years reaching up to the intermediate layers at station 290 which is near the overflow area of the CSOW. Table 3 shows the mean age related to the results by Schneider et al. (2014) which were obtained by using the standard Δ/Γ ratio of 1.0. The comparison shows clearly the significant influence

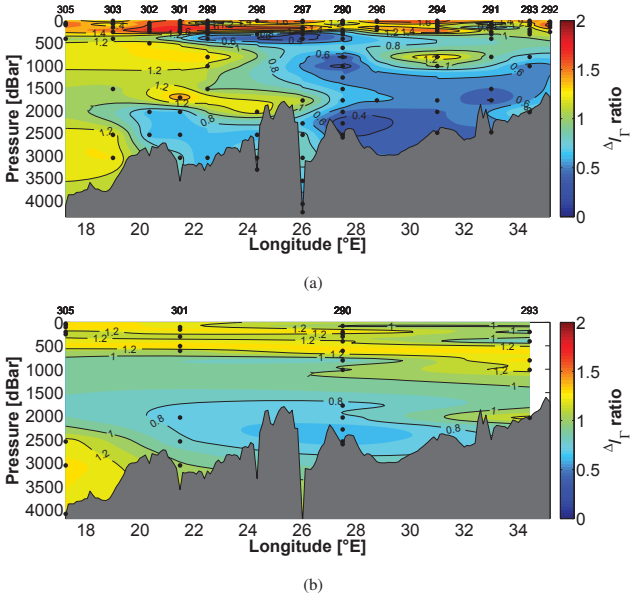

Figure 11. Determined $^{\Delta}/_{\Gamma}$ ratios in the EMed based on **(a)** the transient tracer couple CFC-12 and SF_6 and **(b)** tritium and SF_6. The black points indicate the constrained data points of the section.

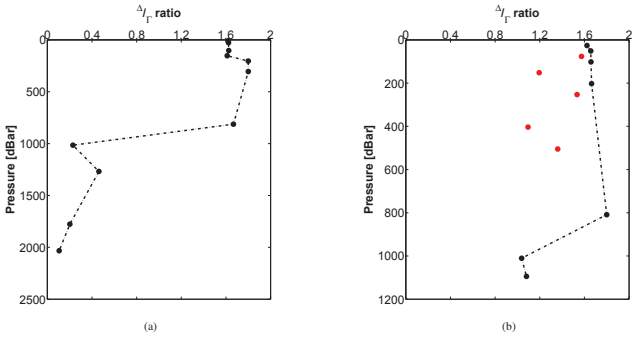

Figure 12. Determined $^{\Delta}/_{\Gamma}$ ratios **(a)** in the Sea of Crete at station 288 and **(b)** in the Adriatic Sea at station 313 obtained by the transient tracer couple CFC-12 and SF_6. The red dots in **(b)** indicate ratios with a mean age difference > 5 years and thus defined as non-constrained within the IG-TTD model.

of the Δ/Γ ratio leading to a mean age difference between both TTD approaches of almost 80 years at 800 m depth in the TMZ. It should be pointed out that the TTD method presented by Schneider et al. (2014) was used in another context (i.e., the analysis of a time series), with the aim of detecting temporal variations of ventilation.

The deep water in the Ionian Basin has a mean age of 100 years which underlines the difference of both deep water formations. Although the Adriatic deep water formation is contemporary and the EMT event replenished large parts of the deep waters in the early 1990s, the deep water layer formed by water masses from the Sea of Crete is much younger than the one from the Adriatic Sea. The mean age of both source regions is quite young with a maximum mean age in the deep water of $\approx$ 20 years in the Aegean Sea (Fig. 14a), which highly correlates with the timing of the EMT event in the early 1990s, and $\approx$ 10–17 years in the Adriatic Sea (Fig. 14b). The mean age gradient with depth is much steeper in the Adriatic Sea than in the Sea of Crete which also shows that the ventilation processes of both basins are significantly different. However, the SF_6 mean age indicated by red dots in Fig. 14b at station 313 in the Adriatic Sea fit into the mean age gradient, even though these results are based on minimum functions with a difference of more than 5 years. Such data points are defined as non-constrained, due to the uncertainty by using different transient tracers with the same "approached" constraints (even if there are a number of possible true solutions for one transient tracer). Figure 15 shows the mean age functions of CFC-12 and SF_6 including the analytical error range of 4 %. Figure 15a shows an example of the CDW and Fig. 15b of the ASDW. Both plots show the differences in water-mass structure, in terms of advective / diffusive ratios, despite uncertainties in the mean age calculations.

Neglecting any systematic errors in sampling and measurements, the TTD mean age is strongly influenced by the input function of a transient tracer (see Sect. 2.4.3). The TIF by Dreisigacker and Roether (1978) and Roether et al. (1992) is a rough estimate of the complex regional impact factors and provides a mean input of tritium into the surface layer of the ocean. Nevertheless, this input function is the best existing approach and the results of the offset corrected input function clearly show that the shape of the curve tends to be correct. The corrected input function of the EMed generates similar but still a slightly higher mean age results compared to the ones obtained by CFC-12 and SF_6 (Fig. 13). This indicates that the corrected input function probably still overestimates the mean input of tritium in the eastern Mediterranean Sea. The IG-TTD provides significant results for the EMed using the tracer couple of CFC-12 and SF_6, whereas SF_6 and tritium should be used with some caution.

The analysis of Δ/Γ ratios in the WMed is restricted to only three stations (317, 323, 334) for which the concentration ratios between the two transient tracer couples were not applicable to the IG-TTD model. The simple approach of water-mass analysis concerning the advective / diffusive ratio and the calculation of a mean age is not possible. Another distribution model is needed to estimate a mean age of non-constrainable data points of both tracer couples in the western Mediterranean Sea.

In this context, it is useful to determine the validity area of a tracer couple, to decide whether the IG or 2IG-TTD model should be applied. Figure 16 shows the validity area of the IG- and 2IG-TTD models by using the tracer age differences of SF_6 and CFC-12 in the EMed. The young and advective EMT water mass can be described by the IG-TTD, whereas the mean age of the intermediate water and parts of the deep

Table 3. Comparison of mean age results between a TTD model with constrained Δ / Γ ratios and a TTD model with standard ratio $\Delta / \Gamma = 1.0$ (Schneider et al., 2014).

	Constrained ratios		Standard ratio		
Pressure [dBar]	Mean age [yr]	Δ / Γ ratio	Mean age [yr]	Δ / Γ ratio	Difference [yr]
200	27	0.80	29	1.0	2
250	30	0.63	38	1.0	8
300	38	0.71	47	1.0	9
400	47	0.61	69	1.0	22
600	83	0.76	105	1.0	22
800	44	0.21	123	1.0	79
1000	43	0.21	120	1.0	77
1250	57	0.47	105	1.0	48
1500	67	0.63	115	1.0	48
1750	77	0.59	135	1.0	58
2000	48	0.43	99	1.0	51
2250	41	0.19	99	1.0	58
2500	41	0.25	80	1.0	39
2600	52	0.53	94	1.0	42

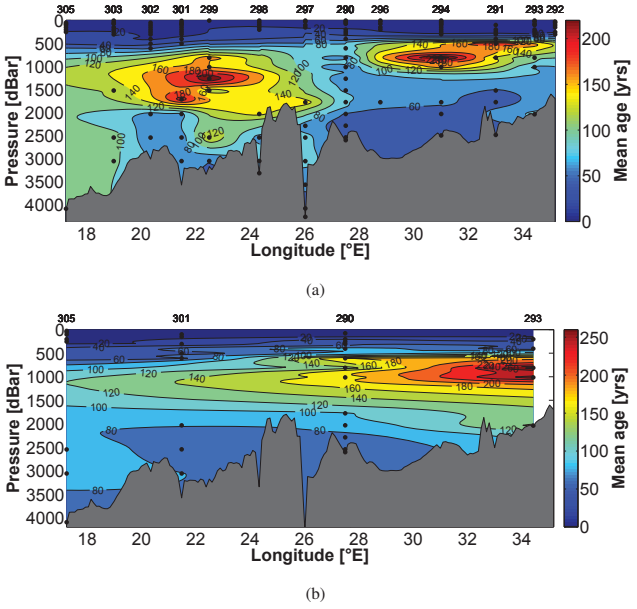

Figure 13. Mean age of the EMed based on an IG-TTD constrained by **(a)** the transient tracer couple CFC-12 and SF_6 and **(b)** tritium and SF_6.

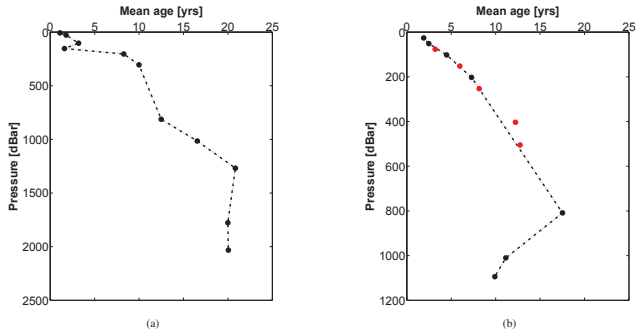

Figure 14. Determined mean age **(a)** in the Sea of Crete at station 288 and **(b)** in the Adriatic Sea at station 313 based on SF_6 and an IG-TTD constrained by the transient tracer couple CFC-12 and SF_6. The red dots show SF_6 mean age results with a difference of more than 5 years compared to the CFC-12 mean age (i.e., non-constrained mean age).

water in the EMed as well as the complete WMed might be better evaluated by a 2IG-TTD. The limiting difference also depends on the tracer concentration to some extend, so that the mixed layer and parts of the pycnocline can also be described by the IG model, although the tracer age difference is larger than 10 years. Development of a clear mathematical definition of validity areas of different tracer couples and distribution models will be part of future work.

3.2.2 2IG-TTD

The predefined 2IG-TTD was applied to several key stations in the EMed and WMed (290, 305, 317, 323) shown in Fig. 6. As mentioned above we assumed fixed Δ / Γ ratios for both TTDs so that $\Delta_1 / \Gamma_1 = 1.4$ and $\Delta_2 / \Gamma_2 = 0.6$, respectively and that the mean age $\Gamma_2 < \Gamma_1$ under the assumption that Γ_2 describes the younger water parcel. The concentration curve (Fig. 4) of each transient tracer were combined in one matrix to determine the intersections. The weighting factor α was separated in 10 % steps and thus we yielded eleven concentration matrices for each sample point. The determination of the intersections was carried out numerically to obtain a first overview of possible 2IG-TTD results which are shown in Table 4, where the mean age is based on the concentrations

Table 4. Suggested mean age based on a 2IG-TTD at **(a)** station 290, **(b)** station 305, **(c)** station 317 and **(d)** station 323, where n.c. stands for non-constrained data points. The most prominent water layers are labeled according to the OMP of Hainbucher et al. (2013) including modified Atlantic water (MAW), Levantine surface water (LSW), Levantine intermediate water (LIW), eastern Mediterranean deep water (EMDW), western Mediterranean deep water (WMDW), Tyrrhenian deep water (TDW) and Adriatic deep water (AdDW).

(a)	Pressure [dBar]	α [%]	Γ_1 [yr]	Γ_2 [yr]	Mean age [yr]	Water layer
	51	0	0	12	12	LSW
	75	0	0	15	15	transition
	202	0	0	25	25	LIW
	254	0	0	30	30	LIW
	304	0	0	38	38	LIW
	404	0	0	46	46	transition
	607	0	0	60	60	transition
	810	n.c.	n.c.	n.c.	n.c.	transition
	1013	n.c.	n.c.	n.c.	n.c.	EMDW
	1267	n.c.	n.c.	n.c.	n.c.	EMDW
	1522	0	0	67	67	EMDW
	1775	0	0	77	77	EMDW
	2031	n.c.	n.c.	n.c.	n.c.	EMDW
	2286	n.c.	n.c.	n.c.	n.c.	EMDW
	2540	n.c.	n.c.	n.c.	n.c.	EMDW
	2600	0	0	60	60	EMDW
(b)	Pressure [dBar]	α [%]	Γ_1 [yr]	Γ_2 [yr]	Mean age [yr]	Water layer
	26	n.c.	n.c.	n.c.	n.c.	MAW
	52	n.c.	n.c.	n.c.	n.c.	MAW
	77	n.c.	n.c.	n.c.	n.c.	transition
	102	10	59	1	7	transition
	152	40	23	1	10	LIW
	203	50	28	1	15	LIW
	254	60	33	2	20	LIW
	304	50	63	2	33	LIW
	405	60	81	2	50	transition
	506	70	125	2	88	transition
	608	70	207	7	147	transition
	1013	80	320	8	258	AdDW
	1522	80	246	5	197	AdDW
	2032	70	279	4	196	AdDW
	2543	90	138	7	125	AdDW
	3053	80	167	6	134	AdDW
	4087	90	101	4	91	AdDW

of CFC-12, SF_6 and to some extent also tritium (see discussion below).

Station 290 in the Levantine Sea can be perfectly described by the IG-TTD which is also indicated by the 2IG-TTD results. As shown in Table 4 the best fits for all samples were obtained for $\alpha = 0$ which is the lower limiting case where the 2IG-TTD turns into an IG-TTD with $\Gamma = \Gamma_2$. Hence, the mean age of the 2IG-TTD is the same as the one from the constrained IG-TTD where $\Delta / \Gamma = 0.6$. The missing data in Table 4 corresponds to the mean age of IG-TTDs with Δ / Γ ratios < 0.6. Figure 17 shows the characteristics of such a concentration curve plot. For $\alpha = 0$, the lines of CFC-12 and SF_6 are overlapping, whereas the one of tritium is slightly above, again indicating a higher mean age by this tracer. The sensitivity of changes with increasing α is of different extend for each tracer. The rate of change is highest for tritium, followed by CFC-12 and lowest for SF_6. This results in curve intersections when $\Gamma_2(\text{Tritium}) > \Gamma_2(\text{CFC-12}) > \Gamma_2(SF_6)$ at $\alpha = 0$.

Such condition can be found at station 305, which is a key station in the Ionian Sea where the IG-TTD is less constrained in the intermediate and deep water. However, CFC-12 and SF_6 intersect each other for several values of alpha, so we chose the one with the lowest difference to the tritium intersection (Fig. 18). Table 4 shows the results of the 2IG-TTD for station 305. The intermediate and deep water is characterized by high α values between 80 and 90 %, indicating a stronger influence of more stationary water masses.

Table 4. Continued.

(c)	Pressure [dBar]	α [%]	Γ_1 [yr]	Γ_2 [yr]	Mean age [yr]	Water layer
	51	n.c.	n.c.	n.c.	n.c.	MAW
	102	n.c.	n.c.	n.c.	n.c.	transition
	203	n.c.	n.c.	n.c.	n.c.	LIW
	304	n.c.	n.c.	n.c.	n.c.	LIW
	405	n.c.	n.c.	n.c.	n.c.	LIW
	507	n.c.	n.c.	n.c.	n.c.	LIW
	811	n.c.	n.c.	n.c.	n.c.	transition
	1014	n.c.	n.c.	n.c.	n.c.	TDW
	1267	70	757	3	531	TDW
	1776	80	370	6	297	TDW
	2032	90	230	18	208	TDW
	2542	90	246	4	221	TDW
	3268	n.c.	n.c.	n.c.	n.c.	TDW
(d)	Pressure [dBar]	α [%]	Γ_1 [yr]	Γ_2 [yr]	Mean age [yr]	Water layer
	52	n.c.	n.c.	n.c.	n.c.	MAW
	103	n.c.	n.c.	n.c.	n.c.	transition
	203	50	127	2	64	transition
	304	60	135	2	82	LIW
	406	70	170	3	120	LIW
	812	80	228	8	184	transition
	1523	80	222	4	178	WMDW
	2031	60	411	4	248	WMDW
	2287	60	332	1	200	WMDW
	2542	60	294	3	177	WMDW
	2798	60	364	2	219	WMDW

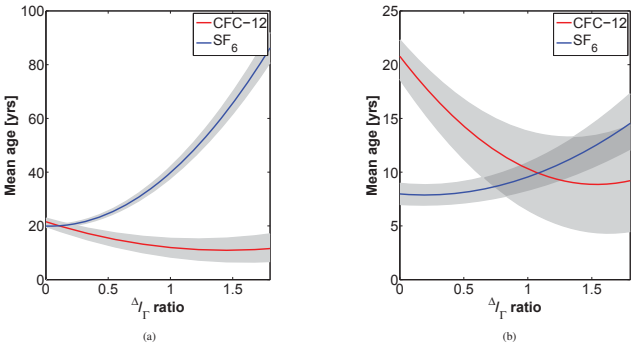

Figure 15. Mean age functions of CFC-12 and SF_6 at station 288, **(a)** in the Sea of Crete at 2030 m depth and **(b)** at station 313 in the Adriatic Sea at 1094 m depth with an error range of 4 % analytical error.

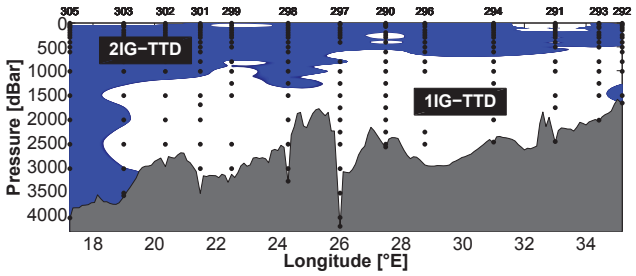

Figure 16. Differences of the tracer age between CFC-12 and SF_6. The white shading describes tracer age differences below and the blue shading above 10 years.

Looking at the single mean age results of the distribution, the total mean age is mainly influenced by Γ_1 rather than Γ_2, whereas both single results are not significant for statements about real mixing processes. They are rather part of the predefined model characteristics and provide only tendencies of the water-mass behavior. Whereas the total mean age from the constrained and exact determined TTD model describes the solved equation and thus a significant mean age result of a water parcel. The highest mean age of 260 years can be found at $\approx$ 1000 m depth, whereas the mean age decreases to 90 years at the bottom layer. This is in full compliance with the expected younger water masses belonging to the ASOW. Compared to the IG-TTD, which indicates a mean age of 100 years for most of the water column, the 2IG-TTD shows a more differentiated structure with a clear mean age maximum. This case indicates that the 2IG-TTD provides more reasonable results.

The order of the tracer mean age at station 317 in the Tyrrhenian Sea changes from the required standard condition

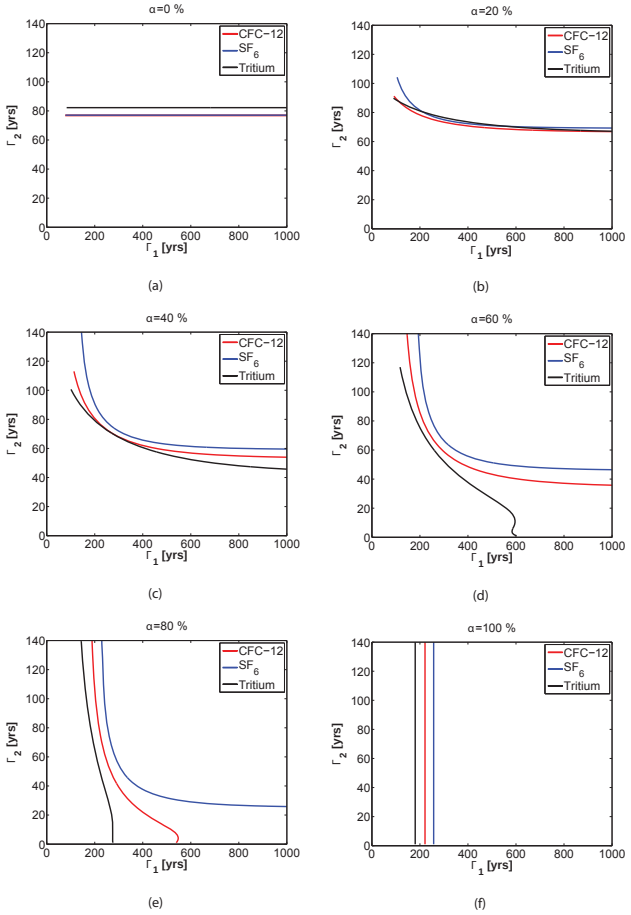

Figure 17. Example of a mean age calculation from three transient tracers (CFC-12, SF_6 and tritium) at station 290 at 1775 m depth. The six panels are for different fractions of the older water mass (α value). The Δ/Γ ratios are set to 0.6 for the younger water mass, and to 1.4 for the older water mass. Panel **(a)** shows the selected result, see text.

into $\Gamma_2(\text{CFC-12}) > \Gamma_2(\text{Tritium}) > \Gamma_2(SF_6)$ for depths shallower than 1250 m. This change in order is also the limit of the used model, so that only four samples could be determined in the Tyrrhenian Sea (Table 4). The mean age is $\approx$ 200 years in the deep water and increase up to 531 years at 1250 m. The Tyrrhenian Sea is less affected by intrusion of younger water masses and thus one would expect this high mean age in this basin. There might be several reasons why the major part of the mean age is not determinable in the Tyrrhenian Sea. The values for Γ_1 are increasing with decreasing depth up to 757 years. The used mean age matrices have a size of 1000×200, so that a maximum mean age of 1000 years can be determined for Γ_1. The shape of the curves of CFC-12 and SF_6 show the tendency to have intersections beyond this limit and thus a much higher mean age for Γ_1 than 1000 years. Another possible reason might be the assumed values of Δ/Γ ratios of the 2IG-TTD.

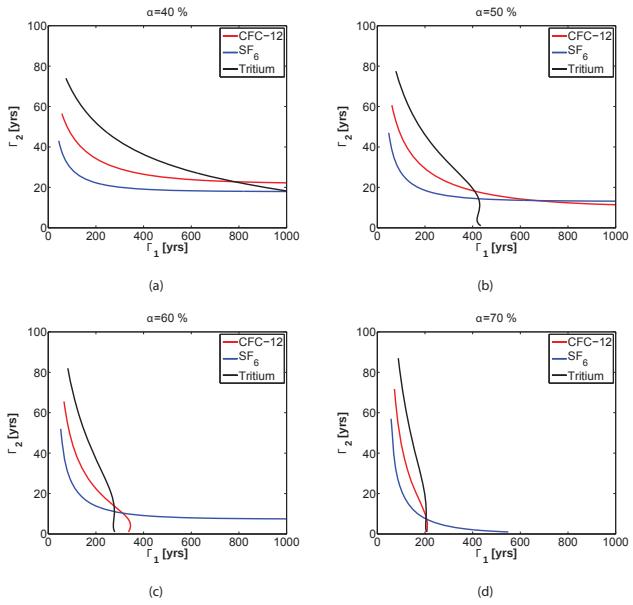

Figure 18. Example for a mean age calculation from three transient tracers (CFC-12, SF_6 and tritium) at station 305 at 608 m depth. Panel (**d**) shows a triple intersection of all three transient tracer concentrations ($\alpha = 70\,\%$) and thus a solution for the mean age at this data point of 147 years.

Station 323 in the Algero-Provençal Basin shows significant characteristics of the newly formed deep and bottom water layer with a constant α of 60 % and a mean age between 170 and 250 years (Table 4, Fig. 19). The lower values of α besides a relatively high mean age describe the extensive intrusion of young water masses into an old deep water layer. The interbasin circulation pattern between the Algero-Provençal Basin and the Tyrrhenian Sea is characterized by high α values denoting less influence of advective water mass input at depth between 1500 and 800 m. However, the mean age is relatively low at this depth range at station 323. Even though the massive inflow of recently ventilated water of 2004–2006 might have notably lowered the mean age, the oldest water masses can be still found in the deep and bottom water. So it can be suggested that these water layers of the western basin were probably less mixed over decadal to centennial timescales. The IG-TTD and tracer age concepts both indicates the oldest waters at intermediate depths (e.g., Rhein et al., 1999; Schneider et al., 2014), whereas our analysis show the highest mean age values in the deep water. This illustrates the power of the 2IG-TTD approach.

3.3 Best mean age approach

The combination of both TTD models allows for an exchange of non-constrainable data points within the IG-TTD by constrained data points of the predefined 2IG-TTD, so that in total 96 % of the data points in the EMed and 81 % in the WMed could be constrained (Table 5). This

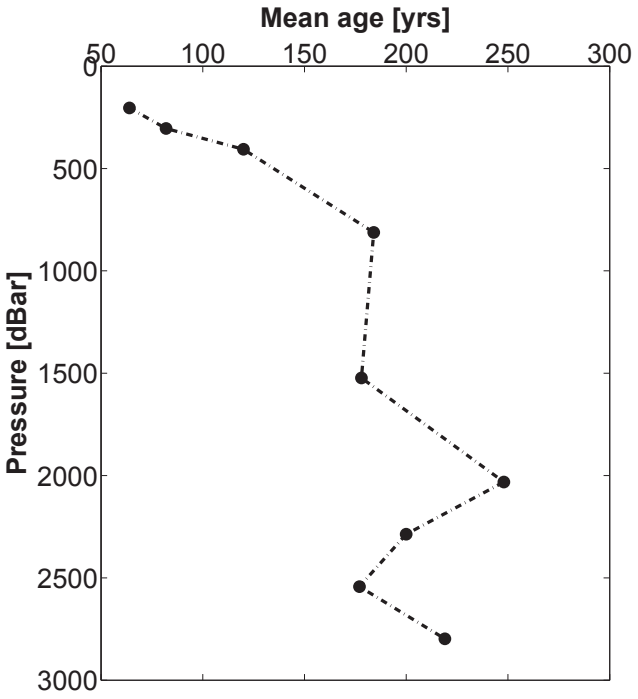

Figure 19. Mean age at station 323 in the WMed based on a 2IG-TTD constrained by the transient tracer couple CFC-12 and SF_6.

Table 5. Number of constrained data points of the IG- and 2IG-TTD using SF_6, CFC-12 and Tritium.

Tracer couple		Data points	IG	2IG
CFC-12/SF_6	Total	412	230	301
	WMed	38	14	23
	EMed	375	216	278
$^3H/SF_6$	Total	206	71	–
	WMed	86	17	–
	EMed	120	54	–

cross-interlocking of both models provides the best estimate of the mean age in the eastern part of the Mediterranean Sea (Fig. 20). The young water masses of the EMT event can be clearly seen in the deep and bottom layers of the Levantine and Ionian Basin with a mean age between 60 and 80 years as well as the newly formed deep water in the westerly parts of the Ionian Basin with a mean age between 120 and 160 years. The mean age maximum layer extends from 600 to 2000 m depth throughout the entire EMed with a mean age between 160 and 290 years. The maximum mean age of 290 years can be found in the TMZ in the Levantine Sea. This high mean age layer is disrupted by a lower mean age of $\approx$ 140 years at the outflow areas of the Sea of Crete (station 299 and 290) and the area near Rhodes (station 293).

4 Conclusions

We have described a comprehensive data set of transient tracer concentrations obtained during the *Meteor* 84/3 cruise in the Mediterranean Sea in April 2011. For the first time measurements of SF_6, CFC-12, tritium and ^{3}He were performed simultaneous on a cruise covering all major basins of the Mediterranean Sea. With this data set, we constrain ventilation characteristics using the transit time distribution (TTD) framework. In particular we constrain the TTD assuming inverse Gaussian (IG) shape of the TTD, either as a one-modal (IG) or two-modal (2IG) distribution. The shape-determining parameters of the IG distribution are the width (Δ) and mean age (Γ), the relative contribution of the two water masses of a 2IG distribution (α), as well as the ratio of Δ/Γ that is indicative of the diffusive to advective transport characteristic of a water mass.

Most regions of the EMed can be described by the IG-TTD model but with widely different Δ/Γ characteristic of the two main deep-water sources, the Cretan deep water (CDW) and the Adriatic Sea overflow water (ASOW), which have developed their Δ/Γ ratio already at their origin region rather than along the flow pathway. The Aegean Sea source water shows a more advective (i.e., a low Δ/Γ ratio) behavior than the Adriatic Sea source water. The majority of the deep water in the eastern Mediterranean of Aegean source originates from the Eastern Mediterranean Transient (EMT) event in the early 1990s. The unusually high deep-water formation rates during this event might explain the advective characteristics of this water mass, which had a mean age between 50 and 80 years. The mean age of the EMT-induced water masses in the Levantine Basin is thus still younger than the deep water in the deep Ionian Sea that has a mean age of approximately 120–160 years using the 2IG-TD model. This is, at first sight, counterintuitive considering the higher CFC-12 concentration in the deep Ionian Sea due to recent contribution from the deep water source in the Adriatic Sea. All tracers show a distinct minimum at around 1000 m depth throughout the Med, although the origin of this tracer minimum zone (TMZ) is slightly different for the eastern and western basins. For the EMed horizontal gradients in the Δ/Γ ratio lead to a mean age distribution that not directly correlated to the tracer concentrations, with lower a mean age southeast of Crete, in the outflow region of water from the Sea of Crete, and a higher age in the Levantine Basin and Ionian Sea.

Although most of the EMed ventilation can be described by an IG-TTD model, there are areas where this model of mixing cannot explain the observed tracer distributions. We found the IG-TTD approximation to be invalid for water samples with a tracer age difference exceeding $\approx$ 10 years (for the SF_6-CFC-12 couple sampled in 2011). Thus we use a 2IG model to constrain the TTD in the western part of the Ionian Sea and most of the WMed. The Western Mediterranean Transition (WMT) event with enhanced deep-water

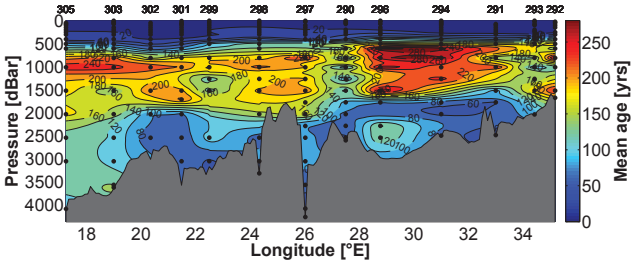

Figure 20. Best estimate of the mean age of the EMed based on the combination of an IG-TTD and a predefined 2IG-TTD constrained by the transient tracer couple CFC-12 and SF_6.

formation during the winters of 2004–2006 in the western basin can be characterized by the 2IG-TTD model, where the recently ventilated deep-water with advective properties mixes with more stationary water of more diffusive character. The contemporaneous deep water in WMed has approximately 40 % contribution of recently ventilated waters from the WMT, leading to a mean age of about 200 years, which is similar or higher than the mean age higher up in the water column that have lower CFC-12 and SF_6 concentrations. This highlights the need to constrain the TTD in order to understand the "age" of a water mass based on transient tracer concentrations. The recently ventilated deep water was observed as elevated concentrations of CFC-12 in excess of 200 ppt along the bottom in the Sardinia Channel towards, but not yet within, the Tyrrhenian Sea. The horizontally relatively homogeneous CFC-12 concentration of the western basin suggest that the TTD structure determined at station 323, SW of Sardinia, can be extrapolated to large parts of the WMed.

The results presented here point to the need to consider alternatives to the commonly applied IG-TTD model, particularly in regions with variable ventilation or where more water masses mix with each other. For observational constraints of more complex TTDs, a suite of transient tracers needs to be measured and interpreted. For such regions in the ocean, we show that a predefined 2IG-TTD provides a useful tool.

Acknowledgements. The authors want to thank the captain and crew on the research vessel *Meteor* for the excellent cooperation during the campaign. The *Meteor* cruise M84/3 and the transient tracer measurements were supported by a grant from the Deutsche Forschungsgemeinschaft Senatskommission für Ozenographie (DFG), and from a grant from the DFG; TA 317/3-1. Furthermore we would like to thank Wolfgang Roether for his support, help and inspiring discussions on particular matters of helium and tritium. Our special thanks goes to Damian Grundle and Martha Gledhill for linguistic improvements of the manuscript.

The service charges for this open access publication have been covered by a Research Centre of the Helmholtz Association.

Edited by: S. Sparnocchia

References

Artegiani, A., Bregant, D., Paschini, E., Pinardi, N., Raicich, F., and Russo, A.: The Adriatic Sea General Circulation. Part I: Air-Sea Interactions and Water Mass Structure, J. Phys. Oceanogr., 27, 1492–1514, 1996a.

Artegiani, A., Bregant, D., Paschini, E., Pinardi, N., Raicich, F., and Russo, A.: The Adriatic Sea General Circulation. Part II: Baroclinic Circulation Structure, J. Phys. Oceanogr., 27, 1515–1532, 1996b.

Brasseur, P., Beckers, J., Brankart, J., and Schoenauen, R.: Seasonal temperature and salinity fields in the Mediterranean Sea: Climatological analyses of a historical data set, Deep Sea Res.-Pt. I, 43, 159–192, 1996.

Bullister, J. L.: Atmospheric CFC-11, CFC-12, CFC-113, CCl_4 and SF_6 Histories (1910–2011), Carbon Dioxide Information Analysis Center, available at: http://cdiac.ornl.gov/oceans/new_atmCFC.html (last access: 1 June 2014), 2011.

Bullister, J. L. and Wisegarver, D.: The shipboard analysis of trace levels of sulfur hexafluoride, chlorofluorocarbon-11 and chlorofluorocarbon-12 in seawater, Deep Sea Res.-Pt. I, 55, 1063–1074, 2008.

Bullister, J., Wisegarver, D., and Menzia, F.: The solubility of sulfur hexafluoride in water and seawater, Deep Sea Res.-Pt. I, 49, 175–187, 2002.

DeGrandpre, M. D., Koertzinger, A., Send, U., Wallace, D. W. R., and Bellerby, R. G. J.: Uptake and sequestration of atmospheric CO_2 in the Labrador Sea deep convection region, Geophys. Res. Lett., 33, doi:10.1029/2006GL026881, 2006.

Delhez, E., de Brye, B., de Brauwere, A., and Deleersnijder, E.: Residence time vs influence time, J. Marine Syst., 132, 185–195, doi:10.1016/j.jmarsys.2013.12.005, 2013.

Dreisigacker, E. and Roether, W.: Tritium and ^{90}Sr in North Atlantic surface water, Earth Planet. Sci. Lett., 38, 301–312, 1978.

Ferronsky, V. and Polyakov, V.: Environmental isotopes in the hydrosphere, John Wiley & Sons, Chichester, New York, 1982.

Hainbucher, D., Rubino, A., and Klein, B.: Water mass characteristics in the deep layers of the western Ionian Basin observed during May 2003, Geophys. Res. Lett., 33, L05608, doi:10.1029/2005GL025318, 2006.

Hainbucher, D., Rubino, A., Cardin, V., Tanhua, T., Schroeder, K., and Bensi, M.: Hydrographic situation during cruise M84/3 and P414 (spring 2011) in the Mediterranean Sea, Ocean Sci. Discuss., 10, 2399–2432, doi:10.5194/osd-10-2399-2013, 2013.

Haine, T. W. N. and Richards, K. J.: The influence of the seasonal mixed layer on oceanic uptake of CFCs, J. Geophys. Res.-Oceans, 100, 10727–10744, doi:10.1029/95JC00629, 1995.

Hall, T. and Plumb, R.: Age as a diagnostic of stratospheric transport, J. Geophys. Res., 99, 1059–1070, 1994.

Hall, T., Haine, T., Waugh, D., Holzer, M., Terenzi, F., and LeBel, D.: Ventilation rates Estimated from Tracers in the Presence of Mixing, J. Phys. Oceanogr., 37, 2599–2611, doi:10.1175/2006JPO3471.1, 2007.

Houghton, J., Meira Filho, L., Callander, B., Harris, N., Kattenberg, A., and Maskell, K.: Climate Change 1995, The Science of Climate Change, Cambridge University Press, 1996.

Hu, Z., Doglioli, A., Petrenko, A., Marsaleix, P., and Dekeyser, I.: Numerical simulations of eddies in the Gulf of Lion, Ocean Model., 28, 203–208, doi:10.1016/j.ocemod.2009.02.004, 2009.

Huhn, O., Rhein, M., Hoppema, M., and van Heuven, S.: Decline of deep and bottom water ventilation and slowing down of anthropogenic carbon storage in the Weddell Sea, 1984-2011, Deep Sea Res.-Pt. I, 76, 66–84, doi:10.1016/j.dsr.2013.01.005, 2013.

Klein, B., Roether, W., Manca, B., Bregant, D., Beitzel, V., Kovacevic, V., and Luchetta, A.: The large deep water transient in the Eastern Mediterranean, Deep Sea Res.-Pt. I, 46, 371–414, doi:10.1016/S0967-0637(98)00075-2, 1999.

Lascaratos, A., Williams, R., and Tragou, E.: A Mixed-Layer Study of the Formation of Levantine Intermediate Water, J. Geophys. Res., 98, 14739–14749, 1993.

Lascaratos, A., Roether, W., Nittis, K., and Klein, B.: Recent changes in deep water formation and spreading in the eastern Mediterranean Sea: a review, Prog. Oceanogr., 44, 5–36, doi:10.1016/S0079-6611(99)00019-1, 1999.

Law, C., Watson, A., and Liddicoat, M.: Automated vacuum analysis of sulphur hexafluoride in seawater: derivation of the atmospheric trend (1970–1993) and potential as a transient tracer, Mar. Chem., 48, 57–69, 1994.

Malanotte-Rizzoli, P. and Hecht, A.: Large scale properties of the eastern Mediterranean: a review, Oceanol. Acta, 11, 323–335, 1988.

Primeau, F. and Holzer, M.: The Ocean's Memory of the Atmosphere: Residence-Time and Ventilation-Rate Distribution of Water Masses, J. Phys. Oceanogr., 36, 1439–1456, doi:10.1175/JPO2919.1, 2006.

Rhein, M., Send, U., Klein, B., and Krahmann, G.: Interbasin deep water exchange in the western Mediterranean, J. Geophys. Res.-Oceans, 104, 23495–23508, doi:10.1029/1999JC900162, 1999.

Roether, W. and Lupton, J. E.: Tracers confirm downward mixing of Tyrrhenian Sea upper waters associated with the Eastern Mediterranean Transient, Ocean Sci., 7, 91–99, doi:10.5194/os-7-91-2011, 2011.

Roether, W. and Schlitzer, R.: Eastern Mediterranean deep water renewal on the basis of chlorofluoromethane and tritium data, Dynam. Atmos. Oceans, 15, 333–354, 1991.

Roether, W., Schlosser, P., Kuntz, R., and Weiss, W.: Transient-tracer studies of the thermohaline circulation of the Mediterranean, Reports in Meteorology and Oceanography, 41, 291–317, 1992.

Roether, W., Manca, B., Klein, B., Bregant, D., Georgopoulos, D., Beitzel, V., Kovacevic, V., and Luchetta, A.: Recent Changes in Eastern Mediterranean Deep Waters, Science, 271, 333–335, 1996.

Roether, W., Klein, B., Beitzel, V., and Manca, B.: Property distributions and transient-tracer ages in Levantine Intermediate Water in the Eastern Mediterranean, J. Marine Syst., 18, 71–87, 1998.

Roether, W., Klein, B., Manca, B. B., Theocharis, A., and Kioroglou, S.: Transient Eastern Mediterranean deep waters in response to the massive dense-water output of the Aegean Sea in the 1990s, Prog. Oceanogr., 74, 540–571, doi:10.1016/j.pocean.2007.03.001, 2007.

Roether, W., Jean-Baptiste, P., Fourrè, E., and Sültenfuß, J.: The transient distribution of nuclear weapon-generated tritium and its decay product ^{3}He in the Mediterranean Sea, 1952–2011, and their oceanographic potential, Ocean Sci., 9, 837–854, doi:10.5194/os-9-837-2013, 2013.

Rubino, A. and Hainbucher, D.: A large abrupt change in the abyssal water masses of the eastern Mediterranean, Geophys. Res. Lett., 34, L23607, doi:10.1029/2007GL031737, 2007.

Schlitzer, R., Roether, W., Oster, H., Junghans, H., Hausmann, M., Johannsen, H., and Michelato, A.: Chlorofluoromethane and oxygen in the Eastern Mediterranean, Deep Sea Res.-Pt. A, 38, 1531–1551, 1991.

Schneider, A., Tanhua, T., Koertzinger, A., and Wallace, D.: High anthropogenic carbon content in the eastern Mediterranean, J. Geophys. Res., 115, C12050, doi:10.1029/2010JC006171, 2010.

Schneider, A., Tanhua, T., Koertzinger, A., and Wallace, D.: An evaluation of tracer fields and anthropogenic carbon in the equatorial and the tropical North Atlantic, Deep Sea Res.-Pt. I, 67, 85–97, doi:10.1016/j.dsr.2012.05.007, 2012.

Schneider, A., Tanhua, T., Roether, W., and Steinfeldt, R.: Changes in ventilation of the Mediterranean Sea during the past 25 year, Ocean Sci., 10, 1–16, doi:10.5194/os-10-1-2014, 2014

Schroeder, K., Gasparini, G., Tangherlini, M., and Astraldi, M.: Deep and intermediate water in the western Mediterranean under the influence of the Eastern Mediterranean Transient, Geophys. Res. Lett., 33, L21607, doi:10.1029/2006GL027121, 2006.

Schroeder, K., Ribotti, A., Borghini, M., Sorgente, R., Perilli, A., and Gasparini, G.: An extensive western Mediterranean deep water renewal between 2004 and 2006, Geophys. Res. Lett., 35, L18605, doi:10.1029/2008GL035146, 2008.

Schroeder, K., Josey, S., Herrmann, M., Grignon, L., Gasparini, G., and Bryden, H.: Abrupt warming and salting of the Western Mediterranean Deep Water after 2005: Atmospheric forcings and lateral advection, J. Geophys. Res., 115, C08029, doi:10.1029/2009JC005749, 2010.

Steinfeldt, R.: Ages and age spectra of Eastern Mediterranean Deep Water, J. Marine Syst., 48, 67–81, 2004.

Stöven, T.: Ventilation processes of the Mediterranean Sea based on CFC-12 and SF_6 measurements, GEOMAR OceanRep, available at: http://oceanrep.geomar.de/id/eprint/13936 (last access: 1 June 2014), diploma thesis, Christian-Albrechts-Universität zu Kiel, 2011.

Sültenfuß, J., Roether, W., and Rhein, M.: The Bremen mass spectrometric facility for the measurement of helium isotopes, neon, and tritium in water, Isot. Environ. Health Stud., 45, 1–13, 2009.

Tanhua, T., Waugh, D., and Wallace, D.: Use of SF_6 to estimate anthropogenic CO_2 in the upper ocean, J. Geophys. Res., 113, 2156–2202, doi:10.1029/2007JC004416, 2008.

Tanhua, T., Hainbucher, D., Cardin, V., Álvarez, M., Civitarese, G., McNichol, A. P., and Key, R. M.: Repeat hydrography in the Mediterranean Sea, data from the Meteor cruise 84/3 in 2011, Earth Syst. Sci. Data, 5, 289–294, doi:10.5194/essd-5-289-2013, 2013a.

Tanhua, T., Hainbucher, D., Schroeder, K., Cardin, V., Álvarez, M., and Civitarese, G.: The Mediterranean Sea system: a review and an introduction to the special issue, Ocean Sci., 9, 789–803, doi:10.5194/os-9-789-2013, 2013b.

Tanhua, T., Waugh, D., and Bullister, J.: Estimating changes in ocean ventilation from the early 1990s CFC-12 and

late SF_6 measurements, Geophys. Res. Lett., 40, 927–932, doi:10.1002/grl.50251, 2013c.

Taylor, C. and Roether, W.: A uniform scale to report low-level tritium measurements in water, Int. J. Appl. Radiat. Is., 33, 377–382, 1982.

Unterweger, M., Coursey, B., Schima, F., and Mann, W.: Preparation and calibration of the 1987 National Bureau of Standards tritiated-water standards, Int. J. Appl. Radiat. Is., 31, 611–614, 1980.

Vollmer, M. and Weiss, R.: Simultaneous determination of sulfur hexafluoride and three chlorofluorocarbons in water and air, Mar. Chem., 78, 137–148, 2002.

Walker, S. J., Weiss, R. F., and Salameh, P. K.: Reconstructed histories of the annual mean atmospheric mole fractions for the halocarbons CFC-11 CFC-12, CFC-113, and carbon tetrachloride, J. Geophys. Res.-Oceans, 105, 14285–14296, doi:10.1029/1999JC900273, 2000.

Warner, M. and Weiss, R.: Solubilities of chlorofluorocarbons 11 and 12 in water and seawater, Deep Sea Res.-Pt. A, 32, 1485–1497, 1985.

Watson, A., Messias, M.-J., Fogelqvist, E., Van Scoy, K., Johannessen, T., Oliver, K., Stevens, D., Rey, F., Tanhua, T., Olsson, K., Carse, F., Simonsen, K., Ledwell, J., Jansen, E., Cooper, D., Kruepke, J., and Guilyardi, E.: Mixing and convection in the Greenland Sea from a tracer-release experiment, Nature, 401, 902–904, doi:10.1038/44807, 1999.

Waugh, D. W., Vollmer, M. K., Weiss, R. F., Haine, T. W. N., and Hall, T. M.: Transit time distributions in Lake Issyk-Kul, Geophys. Res. Lett., 29, 84.1–84.4, doi:10.1029/2002GL016201, 2002.

Waugh, D., Hall, T., and Haine, T.: Relationships among tracer ages, J. Geophys. Res., 108, 3138, doi:10.1029/2002JC001325, 2003.

Waugh, D., Haine, T. W., and Hall, T. M.: Transport times and anthropogenic carbon in the subpolar North Atlantic Ocean, Deep Sea Res.-Pt. I, 51, 1475–1491, 2004.

Waugh, D., Hall, T., McNeil, B., Key, R., and Matear, R.: Anthropogenic CO_2 in the oceans estimated using transit time distributions, Tellus B, 58, 376–389, 2006.

Wuest, G.: On the vertical circulation of the Mediterranean Sea, J. Geophys. Res., 66, 3261–3271, 1961.

Manuscript II

Manuscript prepared for Ocean Sci.
with version 5.0 of the LaTeX class copernicus.cls.
Date: 16 April 2015

Perspectives of transient tracer applications and limiting cases

T. Stöven[1], **T. Tanhua**[1], **M. Hoppema**[2], **and J. L. Bullister**[3]

[1]Helmholtz Centre for Ocean Research Kiel, GEOMAR, Germany
[2]Alfred Wegener Institute Helmholtz Centre for Polar and Marine Research, Bremerhaven, Germany
[3]National Oceanic and Atmospheric Administration, Pacific Marine Environmental Laboratory, 7600 Sand Point Way NE, Seattle, WA 98115, USA

Correspondence to: T. Stöven
(tstoeven@geomar.de)

Abstract. Currently available transient tracers have different application ranges which are defined by their temporal input (chronological transient tracers) or their decay rate (radioactive transient tracers). Transient tracers range from tracers for highly ventilated water masses such as sulfur hexafluoride (SF_6) through tritium (^3H) and chlorofluorocarbons (CFCs) up to tracers for less ventilated deep ocean basins such as argon-39 (^{39}Ar) and radiocarbon (^{14}C). In this context, highly ventilated water masses are defined as water masses which have been in contact with the atmosphere during the last decade. Transient tracers can be used to empirically constrain the transit time distribution (TTD), which can often be approximated with an Inverse Gaussian (IG) distribution. The IG-TTD provides information about ventilation and the advective/diffusive characteristics of a water parcel.
Here we provide an overview of commonly used transient tracer couples and the corresponding application range of the IG-TTD by using the new concept of validity areas. CFC-12, CFC-11 and SF_6 data from three different cruises in the South Atlantic Ocean and Southern Ocean as well as ^{39}Ar data from the 1980s and early 1990s in the eastern Atlantic Ocean and the Weddell Sea are used to demonstrate this method. We found that the IG-TTD can be constrained along the Greenwich Meridian south to $46°S$ which corresponds to the Subantarctic Front (SAF) denoting the application limit. The Antarctic Intermediate Water (AAIW) describes the limiting water layer in the vertical. Conspicuous high or lower ratios between the advective and diffusive components describe the transition between the validity area and the application limit of the IG-TTD model rather than describing the physical properties of the water parcel. The combination of ^{39}Ar and CFC data provides constraints on the IG-TTD in the deep water north of the SAF but not beyond this limit.

1 Introduction

Ocean ventilation plays a major role in climate. It represents transport processes from the ocean surface to the ocean's interior, carrying dissolved gases, nutrients, microorganisms but also soluble hazardous substances and other coastal and offshore pollutants (Schlosser et al., 1999). One of the most prominent processes is the accumulative uptake of anthropogenic carbon (C_{ant}) at high and mid latitudes, where large volumes of surface and intermediate waters are transported into deeper water layers (e.g. Sabine and Tanhua, 2010). The excess uptake of atmospheric carbon dioxide (CO_2) by the ocean influences the marine ecology and biology, e.g. inhibiting shell building marine organisms due to acidification (Orr et al., 2005). Oxygen supply by ventilation represents another field of interest, with focus on the economically important marine resources like fish and seafood. To this end, ocean ventilation models are an important part of describing and understanding the complex biogeochemical interactions in the ocean.
A well-established concept is the transit time distribution (TTD) model which provides information about ventilation timescales and rates (Hall and Plumb, 1994; Bolin and Rodhe, 1973). The TTD model has several solutions and intended application possibilities. For example, the one dimensional Inverse-Gaussian transit time distribution (IG-TTD) can be applied to field data of transient tracer surveys in the ocean (Waugh et al., 2003; Klatt et al., 2002). An IG-TTD can be empirically constrained with a transient tracer couple which provides reliable mean age results of water masses in the ocean (e.g. Waugh et al., 2002; Schneider et al., 2012; Sonnerup et al., 2013; Stöven and Tanhua, 2014).
Here we present an overview of some commonly used transient tracers and their current specific restrictions of use with

the IG-TTD. Section 2 highlights the power and weaknesses of each transient tracer with a focus on the analytical and natural limits as well as other features. This section also includes figures of IG-TTD based tacer time ranges and the resulting tracer order, which are shown to be indicative of the different characteristics of the transient tracers. Furthermore, a new method is proposed which allows for a fast and simple classification of the applicability of the IG-TTD to field data and which also describes the validity areas of the tracer couples. In section 4, the new method of validity areas is applied to data sets from three transient tracer surveys. The transient tracer structure and limiting factors of the IG-TTD are presented and possible solutions of the determined restrictions are shown, e.g. the use of ^{39}Ar data in deep water. This work is an extension of the work by Stöven and Tanhua (2014) with the main focus on the future scope of IG-TTD applications.

2 Transit Time Distribution

2.1 Ventilation concept

Mixing processes in the ocean are difficult to quantify due to the various combinations of possible influencing factors. Hall and Plumb (1994) introduced a Transit Time Distribution (TTD) model based on the Green's function which describes the propagation of tracer boundary conditions into the interior (Eq. 1), where $G(t)$ is the Green's function and $c(t_s, r)$ the concentration of a transient tracer at year t_s and location r. The source (boundary) concentration $c_0(t_s - t)$ is the concentration at source year $t_s - t$ related to the input function of a tracer. The exponential term accounts for the decay rate of radioactive transient tracers. Considering only the major components, like a steady and one-dimensional advective velocity and diffusion gradient, a practical model can be implemented, known as Inverse Gaussian Transit Time Distribution (IG-TTD). This particular solution of the TTD can be stated as a simplified analytical expression (Eq. 2), where Γ is the mean age, Δ the width of the distribution and t the time range (Waugh et al., 2003).

$$c(t_s, r) = \int_0^\infty c_0(t_s - t) e^{-\lambda t} \cdot G(t, r) dt \quad (1)$$

$$G(t) = \sqrt{\frac{\Gamma^3}{4\pi\Delta^2 t^3}} \cdot exp\left(\frac{-\Gamma(t-\Gamma)^2}{4\Delta^2 t}\right) \quad (2)$$

The Δ/Γ ratio of the TTD corresponds to the advective and diffusive characteristics of the fluid. Δ/Γ ratios < 1.0 describe a more advective water parcel whereas ratios > 1.0 describe a more dominant diffusive share of the mixing process. A Δ/Γ ratio higher than 1.8 leads to large uncertainties in mean age and should be avoided (see below for more details). A Δ/Γ ratio of 1.0 is considered as the standard ratio which has been applied to many tracer surveys (Schneider et al., 2014, 2010; Tanhua et al., 2008; Waugh et al., 2006, 2004; Huhn et al., 2013). However, for more complex mixing structures, several approaches have been used to constrain the Δ/Γ ratio and thus the TTD based mean age (e.g. Waugh et al., 2002; Schneider et al., 2012; Sonnerup et al., 2013; Stöven and Tanhua, 2014).

2.2 Transient Tracers

2.2.1 Sulfur hexafluoride

Sulfur hexafluoride (SF_6) is an inorganic compound which was first synthesized in the beginning of the 20th century. It has been produced since the early 1950s on an industrial-scale, mainly as insulating and quenching gas for high voltage systems. The atmospheric sources are restricted to non-natural emissions by industrial plants. It is a highly inert gas with a very low degradation rate by UV radiation leading to an atmospheric lifetime of up to 3200 years (Ravishankara et al., 1993). Significant sinks besides ocean uptake are unknown or negligible. The SF_6 concentration of oceanographic data is stated in $fmol\,kg^{-1}$ ($fmol = 10^{-15}\,mol$). Since equilibrium concentration in surface waters depends on temperature and salinity, it is more appropriate to use the partial pressure of the tracer instead. It is stated in parts per trillion (ppt), which also allows a direct comparison with the atmospheric partial pressure. The current partial pressure in the atmosphere is $\approx 8\,ppt$ in 2014 and this is increasing at a relatively constant rate (see Fig. 1). The use of SF_6 as a transient tracer in the ocean is restricted to well ventilated water masses where the partial pressure is above the detection limit of the analytical system ($\approx 0.1\,fmol\,kg^{-1}$ / $\approx 0.4\,ppt$ at salinity 35 and potential temperature 4°C). SF_6 has been used for deliberate tracer release experiments and as such there is potential for undefined offsets in concentrations in such survey areas and their surroundings (Tanhua et al., 2008, 2005).

2.2.2 Chlorofluorocarbons

Chlorofluorocarbons, e.g. dichlorodifluoromethane (CFC-12) and trichlorofluoromethane (CFC-11), were originally produced for applications as refrigerants and later also used as gas propellants. They are known as ozone depleting compounds with atmospheric lifetimes between 90 and 130 years (Minschwaner et al., 2013). Production began in the late 1920s and was phased out in the late 1980s due to the infrared mediated detrimental impact on atmospheric ozone concentrations. Hence, the observational record of the atmospheric CFC concentrations shows decreasing trends since the mid-1990s (Bullister, 2015). CFCs are only anthropogenically produced, and thus there are no sources within the ocean.

CFC-12 has no significant sinks within the ocean, whereas CFC-11 has a minor sink by degradation in anoxic regions (Tanhua et al., 2005; Krysell et al., 1994; Lee et al., 2002, 1999). 1,2,2-trifluorotrichloroethane (CFC-113) and tetrachloromethane (by definition not a CFC, but included in this context) have possible sinks in the ocean at high temperatures and low oxygen concentrations which complicate the application as transient tracers. However, carbon tetrachloride may be useful in deep cold water where degradation is expected to be slow on decadal time scales. We assume that only CFC-11 and CFC-12 are sufficiently inert compounds and usable as transient tracers in all water masses of the ocean. The concentrations are stated in $pmol\,kg^{-1}$ ($pmol = 10^{-12}\,mol$) and the partial pressure in ppt. An upcoming problem are the decreasing concentrations in the atmosphere lowering the application range as transient tracers in the ocean (Fig, 1). Values above the current atmospheric concentration describe two dates in the atmospheric histories of the CFCs which lead to undefined results within age analyses such as the tracer age and the TTD based mean age (see section 2.4 and 2.6). This atmospheric concentration limit denotes the upper limit of use of CFCs, e.g. CFC-12 concentrations of $528\,ppt$ in the northern hemisphere and $526\,ppt$ in the southern hemisphere in 2014. The lower limit of use of CFC-11 and CFC-12 is set by the detection limit of, for example, $\approx 0.01\,pmol\,kg^{-1}$ / $\approx 7.7\,ppt$ at salinity 35 and potential temperature 4°C.

2.2.3 Tritium

Tritium (^{3}H or T) is a radioactive isotope of hydrogen with a half-life of $12.32\,yrs$. It has a natural background concentration due to radiative induced formation processes in the stratosphere and is usually oxidized to tritiated water (HTO). The extremely low concentration is commonly stated in Tritium Units (TU) where $1TU$ is equivalent to 1 tritium atom per 10^{18} hydrogen atoms. The natural mean concentration in water vapor in air is $5.14TU$ / $1.66 \cdot 10^{-2}\,pCi\,mL^{-1}$ ($1\,pCi = 0.037$ decays per second) and $0.49TU$ /$1.6{\cdot}10^{-3}\,pCi\,mL^{-1}$ in the ocean surface (Cossairt, 2012). The anthropogenic sources are nuclear facilities and the nuclear bomb tests during the 1940s, 1950s and mainly the 1960s where large amounts of tritium were released into the atmosphere with an estimated total activity of $2.4 \cdot 10^2\,Bq$ (CNSC, 2009). The tritium input into the ocean depends on precipitation, river input and water vapor pressure at the air-sea interface. Mean tritium input functions, e.g. the tritium input function of the Atlantic Ocean by Dreisigacker and Roether (1978) and Roether et al. (1992), imply uncertainties based on local differences of the net input. Thus it is difficult to obtain a generally valid tritium input function without neglecting prominent regional factors. For example, distinct local influences on the surface tritium concentration can be found in the Mediterranean Sea which is characterized by a high net evaporation, large river runoff, dilution by Atlantic water and an intricate ventilation pattern (Roether et al., 2013; Stöven and Tanhua, 2014). Due to the possible uncertainties it is recommended to use the tritium input function independent isotope ratio of tritium and the decay product helium-3 ($^3He_{trit}$) for TTD applications. The isotopic ratio is given in percent of the tritium decay and stated as δ^3H in the following (Eq. 3-4).

$$R = \frac{^3H}{^3He_{trit}} = \left(e^{\lambda t} - 1\right)^{-1} \tag{3}$$

$$\delta^3 H = \frac{R}{1+R} \cdot 100 \tag{4}$$

This method requires additional measurements of helium and neon to separate the tritiugenic share of the total ^3He concentration (Eq. 5). In this equation $^3He_{tot}$ denotes the measured ^3He concentration in seawater, $^3He_{ex}$ the excess ^3He, which can be determined with neon data and $^3He_{ter}$ as the terrigenic part, released by the earth crust and mantle. The separation method is described by Roether et al. (2013). The terrigenic share has most influence on the uncertainty because it cannot be directly determined. Possible estimates are graphical methods (Aeschbach-Hertig, 1994) and kinematic models (Roether, 1989) which have been developed for the helium-tritium-dating method (Jenkins, 1977).

$$^3He_{trit} = ^3He_{tot} - ^3He_{ex} - ^3He_{ter} \tag{5}$$

2.2.4 Argon-39

Argon-39 (^{39}Ar) is a noble gas isotope with a half-life of $269\,yrs$. Similar to tritium it is mostly formed by cosmic ray interactions in the stratosphere with ^{40}Ar as main precursor. As a noble gas it is highly inert and there are no known sources or sinks in the ocean besides the radioactive decay. ^{39}Ar thus matches all requirements of a transient tracer. However, the measurement of ^{39}Ar is expensive, time-consuming and laborious. In contrast to CFCs, SF_6 and tritium, it is not possible to use the common way of water sampling with Niskin bottles. One of the first measurement systems for environmental samples was based on low level decay counting (LLC) of $0.3 - 1\,L$ of pure argon gas extracted from $1 - 3$ tons of water per sample (Loosli, 1983; Schlitzer and Roether, 1985; Rodriguez, 1993). The concentration of ^{39}Ar is expressed as the isotopic ratio in water in relation to the isotopic ratio in the atmosphere (% modern). In spite of the obviously big stumbling blocks during sampling, and the enormous efforts that had to be put in the measurement facilities, the strong interest in this isotope and its scientific use have never ceded. Recently, a new method was developed to measure ^{39}Ar among other isotopes. The new technique is based on a laser induced atom counting method, the so called Atom Trap Trace Analysis (ATTA) (Jiang et al.,

2011; Lu et al., 2014). This method allows for ^{39}Ar measurements from only $25\,L$ of water down to an isotopic abundance of $8 \cdot 10^{-16}$ (Jiang et al., 2011) which provides a possibility of measuring ^{39}Ar as part of transient tracer surveys in the ocean in the near future, thus significantly enhancing the modest current global dataset.

2.2.5 Carbon-14

Carbon-14 (^{14}C), also known as radiocarbon, is a radioactive isotope with a half-life of $\approx 5730\,yrs$ (Engelkemeir et al., 1949). The radiocarbon dating method, developed by W. F. Libby and co-workers (Libby, 1955), is a commonly used technique for dating carbon containing material. However, this tracer is difficult to apply to the IG-TTD because of its indistinct boundary conditions at $c_0(t_s - t)$, i.e. the condition at the origin of the water parcel. This is caused by an alternating background concentration based on variability in the sun's activity (DeVries-Effect) and the earth's geomagnetic field (Stuiver, 1961). Furthermore, the massive burning of fossil fuels with low radiocarbon content has led to a dilution of the natural atmospheric concentration, i.e. the Suess-Effect (Tans et al., 1979) whilst nuclear bomb-tests in the 1960s and nuclear fuel rods reprocessing have resulted in radiocarbon inputs to the atmosphere. Both effects, the dilution and the input of atmospheric radiocarbon, have their major origin in the northern hemisphere so that a gradient in ^{14}C occurs to the southern hemisphere. The third error source is the equilibration time at the air-sea-boundary of almost 10 years which leads to a permanent disequilibrium at the ocean's surface (Broecker and Peng, 1974). Despite these problems, radiocarbon is a powerful tracer for water masses in the ocean, in particular those that are expected to be very old, e.g. in the deep basins of the northern Pacific.
Radiocarbon concentrations of oceanic measurements are commonly stated as $\Delta^{14}C$ in ‰ (Eq. 6, 7). The zero value of $\Delta^{14}C$ is defined by the used standard (usually A.D. 1950). Measurements are carried out with an accelerator mass spectrometry (AMS). The detection limit of this technique is defined by an isotopic abundance of 10^{-15} (Krane, 1987) (Table 1) with a precision of $2-4.5$‰. The sampling procedure is similar to the one of DIC samples described in Dickson et al. (2007) with a volume of $0.5\,L$ and poisoning to inhibit biological activity during storage.

$$\Delta^{14}C = \delta^{14}C - 2\left(\delta^{13}C + 25\right)\left(1 + \frac{\delta^{14}C}{1000}\right) \tag{6}$$

$$\delta^{14}C = \left[\frac{(^{14}C/C)_{sample} - (^{14}C/C)_{std}}{(^{14}C/C)_{std}}\right] 1000 \tag{7}$$

2.3 Limit of detection

Transient tracer measurements in the ocean can be restricted by the detection limit of the used analytical system which influences the application range of the tracer. The detection limits stated in Table 1 are only representing common mean detection limits, since most measurements are carried out with a variety of custom-made analytical systems, sampling methods and sample volumes which causes different detection limits. Furthermore, detection limits of on board measurements are usually lower than under ideal laboratory conditions and the methods of determining the detection limit also vary between the different working groups. For gas chromatographic systems, the detection limit should be stated as three times the standard deviation of the calibration blank (3σ) which is, for example, described by CLSI (2004). However, data far below the detection limit can be found in published data sets as a result of data calibration routines or offset corrections. The significance and the impact of systematic errors remains questionable and should be well discussed when using such data.

2.4 Tracer age

The tracer age (τ), also known as apparent age, has been used in the past to estimate the age of a water parcel. It is a simple approach which is described by a purely advective flow in the ocean, neglecting any mixing processes. It is also the lower limiting case of the IG-TTD for $\Delta/\Gamma = 0$. Equations 8 and 9 describe the tracer age for chronological transient tracers with $c(t_s)$ as concentration at sampling year t_s and the referred atmospheric concentration $c(t_{hist})$ at year t_{hist}. The tracer age of radioactive transient tracers can be determined by the decay function (Eq. 10) with c_i as the initial concentration, c the measured concentration and the decay rate λ. The tracer age of δ^3H depends on a decay function similar to Eq. 10 except that the equation is rewritten by using the decay product $^3He_{trit}$ instead of initial concentration (Eq. 11).

$$c(t_s) = c_0(t_{hist}) \tag{8}$$

$$\tau = t_s - t_{hist} \tag{9}$$

$$\tau = \frac{1}{\lambda} \cdot ln\left(\frac{c_i}{c}\right) \tag{10}$$

$$\tau = \frac{1}{\lambda} \cdot ln\left(1 + \frac{[^3He_{trit}]}{[^3H]}\right) \tag{11}$$

Although the tracer age only provides approximate time information it is still very useful as a generally applicable tracer unit since all the different concentration units can be directly related to a tracer age (Waugh et al., 2003). Another

possible application is the so called time lag analysis of CFC-12 and SF_6 (Tanhua et al., 2013). The basic principle is the similar growth rate of CFC-12 and SF_6 in the past with a time lag of ≈ 14 years. This means that a water parcel being steadily ventilated has the same tracer age based on SF_6 as it had ≈ 14 years earlier based on CFC-12. Therefore, differences between the SF_6 and CFC-12 tracer age indicate changes in ventilation. A slowing down of ventilation would lead to a higher, modern SF_6 tracer age and an increase in ventilation to a lower age compared to the historic CFC-12 tracer age. This method is clearly restricted by the availability of data sets covering the same region and the required time lag.

2.5 Time ranges

The specific time range of a transient tracer is essential when using field data within a TTD model and is defined by its input function and decay rate. The input functions of chronological transient tracers (CFCs, SF_6) are given by their atmospheric histories and information about surface ocean saturation trends. The input functions should exhibit a monotonic increase in tracer concentrations in the atmosphere for a proper applicability. Figure 1 shows the atmospheric histories of CFC-11/12 and SF_6 in the northern hemisphere. The recently decreasing trends of CFC-11/12 can clearly be seen which cause restrictions of use (see section 2.2). Data of atmospheric trace gas measurements at several locations in the world are provided by, for example, the AGAGE network with monthly updated data (Bullister, 2015). The distributed measurement stations are necessary, because most of the anthropogenic trace gases are released by the industrial nations in the northern hemisphere (see Fig 9 in Bullister, 2015). Although the recent concentration gradient between the northern and southern hemisphere is small, significant differences of earlier years still persist in, e.g. North Atlantic Deep Water (NADW), Antarctic Bottom water (AABW) and many more. Note that the hemisphere of the origin of the water parcel is more important than the hemisphere in which the sample was taken.

Natural radioactive transient tracers, such as ^{39}Ar, are independent of an input function due to a constant concentration level in the atmosphere although deviations from saturation can occur. The formation processes of nuclides are usually radiatively initiated in the stratosphere and counterbalanced by the radioactive decay of the isotopes. Thus, natural isotopes are homogeneously distributed with relatively small variances in surface saturation in large parts of the ocean. An isotope meets the demand of an ideal tracer for the TTD method when there are no sources in the ocean and when a sufficient decay rate exists, serving as the only sink. Isotopes which are or were produced and released in the course of the operation of nuclear power plants or nuclear bomb tests might have a significant local or global input function into the ocean which leads to several problems and restrictions in their use (see ^{14}C and ^{3}H in section 2.2).

2.6 Mean age

For chronological transient tracers, such as CFCs and SF_6, the input function, the year of sampling and to a minor extent, the hemisphere, are the required information for IG-TTD calculations. In contrast, radioactive transient tracer concentrations depend only on the decay rate (^{39}Ar) and some additional factors (^{3}H, ^{14}C, see above). The input function or decay related concentration of a transient tracer is used as boundary condition ($c_0(t_s - t)$ or $c_0\, e^{-\lambda t}$) to calculate theoretical tracer concentrations ($c(t_s, r)$) for a range of Δ/Γ-ratios and a mean age spectrum (see Eq. 1). Figure 2 shows the model output of the different transient tracers. The theoretical tracer concentrations were calculated for Δ/Γ-ratios between $0.1-1.8$ and a mean age spectrum between $1-1500$ years. The theoretical tracer concentrations can then be interpolated to measured concentrations ($c(t_{mes})$), which yields the different mean age results for the different Δ/Γ-ratios. The IG-TTD model results of CFCs and ^{3}H show a sort of twist in lower mean age (Fig. 2d, 2e, 2c), which is based on the declining trends of the atmospheric concentrations. Such a twist leads to a partly decreasing mean age with increasing Δ/Γ-ratio. However, it has no limiting influence on the IG-TTD model since it just describes the effect of a decreasing atmospheric tracer concentration. Note that the use of δ^3H shows no twist since it is independent of the tritium input function.

Related to possible age information, each tracer has a specific time and application range. Accordingly, the area between the Δ/Γ-ratio isolines indicate the application range of the tracer (Fig. 2a-2g). The bigger the difference between the isolines the less sensitive are the results to deviations (errors) in measured concentrations and the more significant are the results. Figure 3 shows the relation between the relative tracer concentration in % and the tracer age which highlights tracer similarities and the tracer order of the specific application ranges. The faster the tracer concentration declines the smaller the time frame of application but the higher the time increment resolution. SF_6 and ^{3}H as well as CFC-11 and CFC-12 provide relatively similar time information. Application ranges of SF_6 and ^{3}H are younger to moderately old water masses, i.e. halocline and strongly ventilated water layers which is indicated by the fast declining trend of both tracers. The application range of CFC-11/12 is restricted in shallower layers due to the atmospheric concentration limit, but provides time information for intermediate and deep water layers with significant ventilation due to deep water formation. Note that the tracer age at 100 % of CFC-11/12 is defined by the atmospheric concentration limit and thus not equal to zero. ^{39}Ar extends the application ranges of CFC-11/12 due to the half-life of 269 years and the resulting slow decline of its concentration. Similar to SF_6 and δ^3H it has

also no restrictions besides the detection limit. The use of ^{14}C is restricted by the knowledge of the boundary conditions. A general TTD based concentration can be calculated by using a boundary condition of $\Delta^{14}C = 0$ so that the measured concentrations (related to a standard) just need to be converted to this scale. ^{14}C is a tracer for very old water masses ($\Gamma >> 300$) and thus can be used in the time range of ^{39}Ar and beyond.

2.7 Constraining the IG-TTD

The shape of the IG-TTD (i.e. the Δ/Γ ratio) and thus the mean age can be constrained under certain assumptions using two transient tracers with sufficiently different time ranges. For example, SF_6/CFC-12 and CFC-12/^{39}Ar show clear differences in time ranges and tracer order (Fig. 3). Waugh et al. (2003) describes the characteristics of a tracer couple by using the relation between Δ and Γ for different tracer age isolines. The more the isolines differ from each other the more useful the tracer couple. There are different methods described in the literature how to constrain the IG-TTD, e.g. Waugh et al. (2002, 2004) and Schneider et al. (2012). Here we describe the method of Stöven and Tanhua (2014), which is based on intersections of mean age functions.

In the first step, the mean age of both tracers is calculated for each discrete water sample and a range of Δ/Γ ratios as described in section 2.6. The mean age results of the corresponding Δ/Γ ratios can be expressed by a polynomial function of 2nd degree, which yields two mean age functions for each discrete water sample. The intersection of the mean age functions then describes the constrained mean age and Δ/Γ ratio, i.e. both tracers specify the same results. The sensitivity of this method to deviations in tracer concentrations is discussed below in section 3.1.

3 The concept of validity areas

The specific characteristics of a tracer couple, such as the time range of application, limiting factors and other features of the IG-TTD, can be described by validity areas (grey shaded areas in Fig. 4a-4i). They are defined by the TTD based tracer age relationship, which means that every distinct point within the area describes a tracer age relationship which belongs to a specific Δ/Γ ratio and mean age, i.e. the tracer age relationship is defined by the IG-TTD. For example, the isoline of $\Delta/\Gamma = 1.0$ (blue line in Fig. 4) is calculated applying the concentration range of one tracer to the IG-TTD of this particular ratio. The determined mean age results are then used to backcalculate the theoretical concentrations of the second tracer (see section 2.6), so that both tracer concentrations describe the same mean age. The tracer age relationship is then determined by recalculating both tracer concentrations to the corresponding tracer age.

The limits are defined by the detections limits of the tracers and the lower and upper limit of the IG-TTD. As stated above, the detection limits can vary within a certain range, so that the indicated limits for CFCs and SF_6 (dash dotted grey lines) only show an example of detection limits by (Bullister and Wisegarver, 2008). Additionally to these upper tracer age limits, the atmospheric concentration limit of the CFCs lead to a lower tracer age limit, reducing the size of the validity area (dotted grey line in Fig. 4b-4h). The lower IG-TTD limit is defined by $\Delta/\Gamma = 0$ where $\tau_1 = \tau_2$ (solid grey line), which describes a purely advective flow. The upper IG-TTD limit depends on the chosen error range. The isolines of the Δ/Γ ratios in Fig. 4 are color coded as in Fig. 2. The red isolines in Fig. 4 clearly show a decreasing distance between each other for an increasing Δ/Γ ratio, with the only exception of the tracer couple $^{14}C/^{39}Ar$. This means, that the higher the Δ/Γ the more sensitive the mean age for deviations in tracer saturation and tracer age. Therefore, we recommend a limit of $\Delta/\Gamma = 1.8$ (solid black line) for tracer couples including CFCs, SF_6 and δ^3H. The different sensitivities are discussed below in section 3.1.

Intersections between the lower IG-TTD limit (bisecting line) with Δ/Γ ratio isolines and between the isolines themselves (black box in Fig. 4g) can be explained by a change in the tracer order (see curve intersections in Fig. 3). This causes an infinite number of indistinct tracer age relationships which are described by several Δ/Γ ratios. Consequently, these areas cannot be used to constrain the IG-TTD and are not part of the validity area.

Figure 4a and 4h show the validity areas for tracer combinations of δ^3H/SF_6 and CFC-11/12, i.e. combinations of tracers with a similar time range of application (see Fig. 3). Both combinations are examples for less adequate tracer couples, which is indicated by the small validity area and the small differences between the Δ/Γ ratio isolines. This causes a high sensitivity to deviations in tracer age and thus high uncertainties in constraining the IG-TTD. In contrast, the remaining tracer couples provide significant information about Δ/Γ ratios in the range of their validity areas. The concept of validity areas can be used to determine the applicability of the IG-TTD by plotting the tracer age relationship of field data together with the validity area. Furthermore, the prevailing Δ/Γ ratios of field data within the validity area can simply be estimated (see section 4.2).

3.1 Tracer saturation and TTD sensitivity

The unknown saturation state of CFCs and SF_6 at the time a water parcel was formed, i.e. when it lost contact with the atmosphere, constitutes the highest uncertainty in tracer applications (Shao et al., 2013). The equilibration time of the tracer, deep convection or subduction of surface waters, entrainment of subsurface water with low tracer concentrations, ice covered areas, wind speed and sea surface temperature and salinity are all factors that influence the saturation state and can result in an under- or supersaturated

water parcel. Compared to systematic or analytical errors in the range of $2-3$ %, the uncertainty of the saturation can be up to 60 % undersaturation (Haine and Richards, 1995; DeGrandpre et al., 2006; Tanhua et al., 2008; Shao et al., 2013). To this end, saturation is corrected with respect to the original approximate surface saturation of the water parcel. Shao et al. (2013) modeled the surface saturation of CFC-12, CFC-11 and SF_6 on a global scale with a monthly resolution up to the year 2010. The model output is provided at *http:\\www.apl.washington.edu/project/project.php?id=cfc_mixed_layer* and allows for various options of saturation corrections. The ideal correction of the saturation would be the specification of all involved source water masses, e.g. via optimum multi parameter (OMP) analysis, which then provides information about the source areas and thus about the different degrees of saturation of the transient tracers. Complex water mass mixtures would probably entail a disproportionately high effort considering the gained reduction of uncertainty and a mean saturation correction would be the more reasonable choice.

The constrained parameters of the IG-TTD, such as the Δ/Γ ratio and mean age, depend on the saturation ratio of the used tracer couple. Figure 5 shows the relative deviation of the Δ/Γ ratio and mean age for different saturation ratios of the tracer couples CFC-12/SF_6 and CFC-12/^{39}Ar. In generating Fig. 5, the SF_6 and ^{39}Ar concentrations were kept constant so that the sensitivity of saturation effects only depended on changes in CFC-12 concentration in the range of 15 % under- and supersaturation. The initial points either vary in the Δ/Γ ratio (0.4, 0.6, 1.0, 1.4 and 1.8) for a constant initial CFC-12 concentration of 100 ppt (Fig. 5a, 5b, 5e, 5f) or vary in the CFC-12 concentration (100, 200, 300 and 400 ppt) for a constant initial $\Delta/\Gamma = 1.0$ (Fig. 5c, 5d, 5g, 5h). The corresponding initial concentrations of SF_6 and ^{39}Ar were determined by backcalculating the theoretical tracer concentration according to the method in section 3. This means that the initial points also correspond to specific points (tracer age relationships) within the validity area in Fig. 4c and 4g. In these figures, a change in the CFC-12 concentration leads to a shift along the CFC-12 tracer age axis. The associated changes in Δ/Γ ratios and mean age are then illustrated by Fig. 5. The error of the Δ/Γ ratios 1.4 and 1.8 is partly not illustrated because the shape of the IG-TTD becomes extremely flat for Δ/Γ ratios > 2.5 and the used numerical integration method produced indistinct results above this limit.

Figure 5a and 5b show an increasing sensitivity of the Δ/Γ ratio and mean age for increasing initial Δ/Γ ratios and constant initial concentrations of SF_6 and CFC-12. This can be explained by the increasing rate of change of the Δ/Γ ratios for an increasing CFC-12 tracer age (see Δ/Γ ratio isolines in Fig. 4c). Given by the tracer couple of CFC-12/SF_6, an undersaturation causes negative and smaller errors compared to a supersaturation, which causes positive and larger errors in the Δ/Γ ratio and mean age. Looking at the initial ratio of $\Delta/\Gamma = 1.0$ in Fig. 5a and 5b, which is a commonly used standard ratio, it can be seen that an undersaturation of 15 % causes a Δ/Γ ratio error of -47.6 % and a mean age error of -55.7 %. The same undersaturation causes an error of -63.8 % and -79.1 %, respectively, for the initial ratio of $\Delta/\Gamma = 1.8$. Such CFC-12 saturation states occur frequently during water mass formation. Supersaturation is assumed to appear rarely in the ocean compared to undersaturation. However, only 5 % supersaturation would lead to an error of 45.2 % in Δ/Γ ratio and 84.9 % in mean age for the standard ratio and can be both expected to be far beyond 100 % for an initial ratio of $\Delta/\Gamma = 1.8$. The differences of sensitivities for changes in the intial CFC-12 concentration are less significant for Δ/Γ ratios with an error range of $50-60$ % and 15 % undersaturation (Fig. 5c). In contrast, Fig. 5d shows a clear trend with an increasing sensitivity of the mean age for decreasing CFC-12 concentrations from -35.9 to -55.7 % at 15 % undersaturation and from 41.8 to 84.9 % at 5 % supersaturation.

The differences in errors between the tracer couples CFC-12/SF_6 and CFC-12/^{39}Ar are due to the position of CFC-12 in the tracer order. SF_6 is ranked below and ^{39}Ar above CFC-12 (see Fig. 3). This generally means that changes in concentration of the lower ranked transient tracer influences the TTD parameters in opposition to changes of the higher ranked transient tracer. Accordingly, the combination of CFC-12 and ^{39}Ar (with a constant ^{39}Ar concentration) leads to a reversal of the error signs and, furthermore, undersaturation now causes a higher sensitivity to both parameters than supersaturation. Figure 5e and 5f indicate that the tracer combination of CFC-12 and ^{39}Ar also leads to an increasing sensitivity of the Δ/Γ ratio and mean age for increasing initial Δ/Γ ratios but yields smaller errors compared to CFC-12 and SF_6. However, low Δ/Γ ratios are less significant. This can be explained by the similar rate of change of Δ/Γ ratios of the different initial points (see $\Delta/\Gamma = 0.4$ in Fig. 5e). A CFC-12 undersaturation of 15 % results in a relatively low positive error of the Δ/Γ ratio between $10-15$ % up to an initial $\Delta/\Gamma = 1.0$. The corresponding error of the mean age is also relatively low for $\Delta/\Gamma = 0.4$ with 0.7 % and $\Delta/\Gamma = 0.6$ with 1.8 % but is significantly higher for higher ratios. Increasing initial CFC-12 concentrations from 100 to 300 ppt lead to increasing Δ/Γ ratio errors from $14-76$ % and mean age errors from $7.4-22.8$ % for an undersaturation of 15 %. Note that an initial CFC-12 concentration of $400\,ppt$ is close to the limit of the validity area of the tracer couple so that the error is partly undefined in the range of supersaturation.

We have demonstrated that the sensitivity of the IG-TTD parameters to changes in tracer concentration can be completely different depending on the tracer couple. Furthermore, the results presented above are based on the limiting case that only one tracer differs in concentration (saturation) while the other remains constant. For the chronological transient tracers it is expected that occurring deviations

from surface saturation applies to all tracers, although the magnitude will differ (Shao et al., 2013). It should be noted that the upper limit of the IG-TTD of $\Delta/\Gamma = 1.8$ is not arbitrary and fixed but with respect to described problems above, an application of higher Δ/Γ ratios appears to be questionable.

4 Field data applications

4.1 Transient tracer data

In the following we focus on data of less problematic transient tracers, namely SF_6, CFC-12, CFC-11 and ^{39}Ar, which have relatively well defined input functions and represent different time ranges, i.e. they can be applied to well and less well ventilated water masses. The data sets were chosen to cover an area in the Southern Ocean but for different years. We present a new data set of CFC-12 and SF_6 which was obtained during the ANT-XXVIII/3 expedition from 7 January to 11 March 2012 from Cape Town, South Africa to Punta Arenas, Chile on the German research vessel *Polarstern* (Wolf-Gladrow, 2013). The red line in Fig. 6 shows the sampling section along 10°E including 28 full depths stations of CFC-12 and SF_6 measurements. The sampling procedure and measurement system (VS1) is identical as described in Stöven and Tanhua (2014). The data was corrected with $0.15\,(\pm 0.02)\,fmol\,kg^{-1}$ for SF_6 and $0.01\,(\pm 0.003) pmol\,kg^{-1}$ for CFC-12 due to a permanent offset of the ampule blank. The blank offset was continuously rechecked as part of the robust quality control routine described in Stöven (2011). Furthermore, the detection limit was sensitive to wave height changes which had direct impact on the baseline noise of the gas chromatograph. With increasing wave height, the baseline started to oscillate and became more noisy. The maximum elevated detection limit of $0.36\,fmol\,kg^{-1}$ for SF_6 was observed during a storm with wind speeds of $20-25\,ms^{-1}$ and a mean wave height of $8-9\,m$. The precision was $\pm 3.6\,\%/0.03\,fmol\,kg^{-1}$ for SF_6 and $\pm 0.8\,\%/0.015\,pmol\,kg^{-1}$ for CFC-12. The data will be available at the Carbon Dioxide Information Analysis Center (CDIAC) data base in October, 2015.

The second data set (expo code:33RO20100308) contains 129 stations with CFC-11, CFC-12 and SF_6 data which were obtained during the CLIVAR A13.5 expedition along the Greenwich Meridian in 2010 (black line in Fig. 6). The expedition took place from 8 March to 14 April from Cape Town, South Africa to Takoradi, Ghana on the American research vessel *Ronald H. Brown* (Bullister and Key, 2010). The measurement procedure can be found in Bullister and Wisegarver (2008). The precision was $\pm 2\,\%/0.02\,fmol\,kg^{-1}$ for SF_6 and $\pm 1\,\%/0.002\,pmol\,kg^{-1}$ for CFC-12 and CFC-11 (Bullister and Key, 2010).

The third data set (expo code:91AA19971204) containing CFC-12 and SF_6 data was collected during the SWEDARP expedition in January-February 1998 on board the South African research vessel *S.A. Agulhas* (Turner et al., 2004). The section along 6°E includes 38 stations with a maximum depth of $3100\,m$ due to the limited wire length on the winch. Two GC-ECD systems were used for on board measurements where the SF_6 measurement system was similar to Law et al. (1994) and the CFC-12 measurement system to Grasshoff et al. (1999). The data, sampling and measurement procedure is discussed by Tanhua et al. (2004). The precision was $\pm 3.1\,\%/0.06\,fmol\,kg^{-1}$ for SF_6 and $\pm 0.7\,\%/0.03\,pmol\,kg^{-1}$ for CFC-12.

The fourth data set (expo code:06AQANTX_4) contains 98 stations with CFC-11 and CFC-12 data which were obtained during the ANT-X/4 expedition from 21 May to 06 August 1992 from Cape Town, South Africa to Puerto Madryn, Argentina on the German research vessel *Polarstern* (Lemke, 1994). The measurement procedure was similar to Bullister and Weiss (1988) and the data is discussed in Klatt et al. (2002) with a stated CFC-11 and CFC-12 precision of $\pm 1.4\,\%/0.006\,pmol\,kg^{-1}$ for CFC-11 and CFC-12.

Ocean data of ^{39}Ar was taken from Rodriguez (1993). The data includes measurements of deep water masses in the eastern Atlantic close to the northern part of the A13.5 expedition and measurements in the whole water column near the south-east end of the Weddell Sea (Table 2) during the 1980s and early 1990s. The sampling for one measurement was based on four $250\,L$ Gerard Ewing samplers distributed over a depth range of $400\,m$ so that every data point describes the corresponding mean value. The measurements were conducted at the University of Bern using the LLC method with a given relative error of $10-14\,\%$ (Schlitzer and Roether, 1985). The sampling and measurement procedure as well as data statistics are discussed by Loosli (1983) and Rodriguez (1993).

4.2 Validity areas

The new method of validity areas, introduced in section 3, allows for rapid determination of the application range of the IG-TTD. Figure 7 shows the application to the field data using the CFC-12/SF_6 and CFC-11/SF_6 tracer couples of three different cruises colored by the latitude of the sample station. The data was used unaltered for this approach, while the application of saturation corrections is discussed in section 4.3 below.

For the SWEDARP data from 1998 about half of the data points are in the range of the IG-TTD (Fig. 7a). The data shows a sort of randomly scattered structure rather than a clear trend which is probably caused by low precisions of early SF_6 data. Nevertheless, it can be seen that most of the northern (red) data points are within the validity area and most of the southern (blue) data points are above the upper limit of the IG-TTD. The transition zone is indicated by the mid latitude (green/yellow) data points, which show the most scattered structure. Data points below the lower limit of the

IG-TTD describe either an unusual relation between the saturation of both tracers or can be explained by measurement uncertainties. Note that the emission rate of CFC-12 was still slightly higher than the atmospheric degradation rate in 1998 and thus, there is no atmospheric concentration limit. Figure 7b and 7c illustrate the validity area of the tracer couples CFC-12/SF_6 and CFC-11/SF_6, respectively, using the CLIVAR A13.5 cruise in 2010. Both tracer couples show the same trend up to a SF_6 tracer age of ≈ 32 years. Beyond that, the data points are shifted towards higher Δ/Γ ratios and then beyond the IG-TTD limit the more southward the sample stations, similar to results obtained for the SWEDARP data. Comparison of the shape of the upper IG-TTD limit with the indicated shape of the scattered data points in Fig. 7c suggests that the tracer age relationship of the field data corresponds approximately to the IG-TTD based tracer age relationship. In contrast, the data points for a tracer age > 32 years show a different structure. Data from the northern part (red data points) are shifted towards lower Δ/Γ ratios and the data from the southern part (blue data points) is diverging in both directions whilst still remaining outside the validity area. Data above the SF_6 tracer age of 47 years corresponds to SF_6 concentrations below the stated detection limit. Similar to the corrections of the ANT-XXVII/3 data, this can be explained by a calibration routine, which included a concentration offset so that negative SF_6 concentrations and concentrations below the detection limit were produced (see data information at CCHDO). Here, too, the application of such data is questionable due to the low significance. The ANT-XXVIII/3 data from 2012 is, except for a few data points in the lower age range, not applicable to the IG-TTD (Fig. 7d). Nevertheless, the same data trend, as determined from the SWEDARP and CLIVAR data, can be identified.

4.3 Saturation effects

The relative saturation state of transient tracer couples can cause large deviations in Δ/Γ ratios and mean age which also influence the applicability of the IG-TTD. For reasons of convenience, only every third element of the CLIVAR data set was used. The degree of tracer saturation was obtained by calculating the mean surface saturation of the tracers using the model output from Shao et al. (2013). Since most of the water mass formations take place during winter, we used a three month mean centered around the month of maximum undersaturation. The area, used for the calculations, was selected to be $50-68°$S and $-30-20°$E, which represents large parts of the Atlantic sector of the Southern Ocean. Figure 8 shows the results of this approach for CFC-11, CFC-12 and SF_6. The black and red star in year 1992 corresponds to the mean surface saturation of CFC-11 and CFC-12, based on the ANT-X/4 data which was obtained during austral winter in this region. This indicates that the model based saturation approach possibly overestimates CFC undersaturations in particular regions, e.g. along the Greenwich Meridian. The yearly related saturation correction was applied to the atmospheric histories (boundary conditions) of the tracers which led to changes in tracer age (Fig. 9). The red dots show the tracer age relationship of the uncorrected and the arrowheads of the saturation corrected data. The tracer age of all tracers is lowered but significant changes, e.g. decreasing Δ/Γ ratios, can only be observed for a SF_6 tracer age < 20 years. This general trend can be explained by the counter balancing effect of the similar undersaturation and on the increasing sensitivity of the tracer age to high CFC concentrations. A relatively improbable correction based on undersaturation of CFCs and supersaturation of SF_6 would be necessary for most of the data to enable an application of the IG-TTD.
Interestingly, supersaturation of CFC-12 and SF_6 was observed during the ANT-XXVIII/3 cruise. Surface measurements a few hours after heavy wind conditions showed significant supersaturation of SF_6 (Fig. 10). The equilibrium values for SF_6 and CFC-12 ($\approx 2.7\, fmol\, kg^{-1}$ and $\approx 2.5\, pmol\, kg^{-1}$) were elevated between $20-50$ and 2 %, respectively, which corresponds to a bubble of modern air (SF_6 $= 7.7\, ppt$ and CFC-12 $= 526\, ppt$) of volume $\approx 1.6-3.9\, cm^3$ and $\approx 2.2\, cm^3$ completely dissolving. This shows that the concentration offset of the supersaturation is in the range of an atmospheric concentration ratio rather than in the range of equilibrated surface water. According to Liang et al. (2013) it can be assumed that bubble effects lead to elevated surface tracer concentrations during heavy wind conditions. The degree of supersaturation depends on the gas solubility, i.e. less soluble gases are more affected than soluble. This would explain the much higher supersaturation of SF_6 compared to CFC-12 in Fig. 10.

4.4 Application range of the IG-TTD

To investigate the different limiting factors of the IG-TTD we used the CLIVAR A13.5 data set which provides transient tracer data from $5°$N to $54°$S along the Greenwich Meridian. The concentrations are shown in Fig. 11. The data was not interpolated to avoid a distortion of results due to the large share of data below the detection limit (indicated by black dots in Fig. 11). CFC-11 and CFC-12 show, as expected, a similar distribution. Concentrations below the detection limit and CFC free water masses are found in the depth range below $\approx 1200\, m$ between $10-30°$S. Elevated CFC concentrations between $2-30\, ppt$ of CFC-12 and $1-16\, ppt$ of CFC-11 characterize the intermediate and deep water below $1200\, m$ in the northern part from $4°$N to $7°$S. In contrast, SF_6 shows only single data points above the detection limit ($\approx 0.07\, ppt$) which seem randomly distributed in the deep water. This underlines that measurements of SF_6 are still very challenging and that SF_6 applications with concentrations close to the detection limit do not provide robust results. South of $30°$S both CFCs can be detected in almost the complete water column. This is a result of the circulation pattern in the Southern Ocean (e.g. Whitworth and Nowlin, 1987), which

transports tracer rich water masses into the ocean's interior. The Antarctic Bottom Water (AABW) plays a major role in deep water ventilation. It is formed at the shelf regions of the Antarctic continent and propagates northwards along the bottom of the ocean. The CFC-12 bottom concentration decreases from $30\,ppt$ at $54°$S to $5\,ppt$ at $30°$S. The CFC-11 bottom concentration decreases from 16 to $2\,ppt$ whereas SF_6 shows no clear trend with a mean bottom concentration of $0.15\,ppt$. The water layer above the AABW consists of Circumpolar Deep Water (CDW), which is split into an upper and lower part (UCDW, LCDW) and mixes with southwards propagating NADW. The CFC concentrations are $4-20\,ppt$ of CFC-12 and $2-8\,ppt$ of CFC-11 between $1500-3000\,m$ and $40-50°$S. Here again, SF_6 is barely detectable. Similar for all three tracers is the decreasing concentration from a nearly saturated surface layer to low tracer concentrations in intermediate layers with concentration gradients corresponding to the shape of the pycnocline.

Applying the IG-TTD model to the tracer couples CFC-12/SF_6 and CFC-11/SF_6 it is shown that the model (i.e. the Δ/Γ ratios) can be constrained for most of the intermediate depths and that both tracer couples yield similar results (Fig. 12). The indicated north-south trend of Fig. 7b and 7c can be seen by the increasing Δ/Γ ratios with increasing southern latitude until they reach the upper limit of the IG-TTD. Based on the theory of the IG-TTD model, these high ratios describe more diffusive water masses. However, according to Holzer and Primeau (2012) it should also be taken into account, that different mixing mechanisms (e.g. diapycnal mixing) change water mass characteristics in a way, which cannot by determined with the IG-TTD and which cause high Δ/Γ ratios in the transition area. Figure 13 shows the salinity of the CLIVAR A13.5 section where black dots indicate tracer data which is within the validity area of the IG-TTD. Similar to the findings of Holzer and Primeau (2012) and Waugh et al. (2013), the southern IG-TTD limit is near the Subantarctic Front (SAF) which is shown by the surface salinity gradient at $\approx 46°$S. Furthermore, the corresponding low salinity layer of the Antarctic Intermediate Water (AAIW) denotes the vertical limiting layer.

Comparing the transition zone of the detection limit of SF_6 between $5°$N and $20°$S in Fig. 7c with the related area in Fig. 12a and 12b, it can be seen that this transition is characterized by very low Δ/Γ ratios (< 0.2). This feature corresponds to the shifted data points towards lower Δ/Γ ratios for a SF_6 tracer age > 32 years in Fig. 7b and 7c. Here again, these low ratios correspond to specific characteristics of low tracer concentrations rather than describing a highly advective behavior of water masses in this area. This effect can also be found south of the SAF, as indicated by the isolated occurring low Δ/Γ ratios. This specific limit can be estimated using the tracer order plot (Fig. 3). The CFCs and SF_6 show relatively linear decreasing trends of the relative tracer concentration which flatten out for higher tracer age. This causes a high tracer age sensitivity on changes in concentration and the transition between the linear trend and the flattening is defined as the tracer age limit. The corresponding tracer concentrations are described as sensitivity limit which replaces the LOD as limit of the validity area (see black dotted lines in Fig. 7b and 7c). The sensitivity limit changes with time, i.e. depends on the atmospheric histories of the tracers. The sensitivity limit in 2010 was ≈ 32 years for SF_6 ($0.6\,ppt/\approx 0.22\,fmol\,kg^{-1}$) and ≈ 50 years for CFC-11 ($10\,ppt/\approx 0.22\,pmol\,kg^{-1}$) and CFC-12 ($30\,ppt/\approx 0.17\,pmol\,kg^{-1}$). Figure 7b and 7c show that the smallest sensitivity limit, defined by SF_6, determines the validity area. The sensitivity limit of radioactive transient tracers cannot be determined in a similar way, since the relative tracer concentrations depend on decay functions instead of atmospheric histories. A tracer couple usually includes a non-radioactive tracer (except ^{39}Ar/^{14}C) and it can be assumed that the sensitivity limit of CFCs or SF_6 is smaller than that of radioactive tracers. Therefore, the sensitivity limits of radioactive transient tracers do not change the validity area.

The non-constrainable data points in Fig. 12a and 12b of the surface layer are related to the atmospheric concentration limits of the CFCs which prohibit any statements about age related results. The remaining constrained data points have Δ/Γ ratios between $0.8-1.2$, i.e. around the standard ratio of 1.0.

4.5 Argon-39 investigations

The tracer couple combinations with SF_6 have shown that deep water cannot be investigated due to the absence of this tracer or the bias of IG-TTD results near the detection limit. Therefore, we interpolated CFC-12 data from the northern part of the CLIVAR cruise and the southern part of the ANT-X/4 cruise to the corresponding isopycnals of the ^{39}Ar data in the eastern Atlantic and the Weddell Sea, respectively (Tab. 2). This data was then applied to the validity area of the CFC-12/^{39}Ar tracer couple of 1992 and 2010 (Fig. 14). It can be seen that the IG-TTD could be constrained in the eastern Atlantic (triangles in the light grey area of 2010) and remains outside of the validity area for the Weddell Sea (dots in the dark grey area of 1992). The error range of ^{39}Ar was assumed to be ± 5 % which is ≈ 20 years in tracer age whereas the error range of CFC-12 is related to the standard deviation of the interpolated concentrations (see error bars in Fig. 14). Similar to the tracer couples including SF_6, the north-south trend of the tracer data can be identified. Furthermore, this approach shows that ^{39}Ar data is a promising alternative for deep water analyses.

5 Conclusions

Transient tracers in combination with the IG-TTD are a powerful tool to investigate ocean ventilation. To analyze well

ventilated water masses, SF_6 and δ^3H should be used due to the young atmospheric history and high decay rate, respectively. CFCs have declined in the atmosphere since the late 1990s, which leads to ambiguous results in tracer age and mean age for values above this atmospheric concentration limit. This restriction only effects surface waters and to a certain extent intermediate waters at present, so that CFC data still plays a major role in the analysis of deep water ventilation. ^{39}Ar has a low decay rate, which provides a larger time range than CFC-12. It is thus a useful tracer for less ventilated water masses, e.g. deep ocean basins in the Pacific Ocean. The recent developments of the ATTA method provide a more adequate sampling and measurement of ^{39}Ar than in the past so that ^{39}Ar will become more focused in future work. The ambiguous or unknown boundary conditions of radiocarbon complicate the application of the IG-TTD model and thus ^{14}C is not recommended for use in combination with the IG-TTD.

The IG-TTD can be empirically constrained by using a transient tracer couple. Each tracer couple has a specific validity area, e.g. CFC-12 and SF_6 for intermediate and CFC-12 and ^{39}Ar for deep water masses. The new concept of validity areas provides information about the application range of a specific tracer couple and the limits of the IG-TTD. Data sets of transient tracer surveys in the ocean can simply be checked against validity areas to ascertain whether the IG-TTD can be applied or not. The radioactive transient tracers have constant validity areas in time which is based on their steady boundary conditions. The chronological transient tracers depend on their atmospheric history and thus a changing boundary condition which has direct impacts on the determination of the validity area. Tracer saturation is an important factor with possible large impact on Δ/Γ ratios and thus also the mean age. Specific corrections for the saturation of CFC-11, CFC-12 and SF_6 can be taken from a surface saturation model provided by Shao et al. (2013).

The field data application of the CLIVAR A13.5 cruise in 2010 indicate that Δ/Γ ratios, which are based on the tracer couples CFC-11/SF_6 and CFC-12/SF_6, do not necessarily correspond to the advective/diffusive behavior of a water parcel but rather describe the transition between the validity area and the different limits of the IG-TTD. The limits of the IG-TTD in the Southern Ocean are defined by the SAF as southern limit and, as a consequence, the AAIW is the limiting water layer. The constrained Δ/Γ ratios are between $0.8 - 1.2$ which is close to the commonly applied ratio of 1.0. The IG-TTD can be applied to large parts in the ocean but reaches its limits where complex ventilation patterns prevail, e.g. in the Southern Ocean. Thus other models are required to analyze such ventilation processes, e.g. the maximum enthropy method by Holzer and Primeau (2012) or the linear combination of two IG-TTDs (Waugh et al., 2003).

Acknowledgements. This work was supported by the Deutsche Forschungsgemeinschaft (DFG) in the framework of the priority programme "Antarctic Research with comparative investigations in Arctic ice areas" by a grant to T. Tanhua and M. Hoppema: Carbon and transient tracers dynamics: A bi-polar view on Southern Ocean eddies and the changing Arctic Ocean (TA $317/5$, HO $4680/1$). Partial support to T. Tanhua and M. Hoppema was received from EU FP7 project CARBOCHANGE "Changes in carbon uptake and emissions by oceans in a changing climate" (European Community's 7th Framework Programme, grant agreement no. 264879). Support for J. Bullister was provided by NOAA's Climate Program Office. This is PMEL Contribution no.4316. We are grateful to the Alfred-Wegener-Institut for participation in Polarstern cruise "Eddy Pump". We are happy to acknowledge the great support by the master and crew of Polarstern, the chief scientist and the scientific party. Special thanks goes to Boie Bogner for his technical support during the ANT-XXVIII/3 cruise and David Wisegarver on the CLIVAR A13.5 cruise.

References

Aeschbach-Hertig, W.: Helium und Tritium als Tracer für physikalische Prozesse in Seen, Ph.D. thesis, ETH Zürich, 1994.

Bolin, B. and Rodhe, H.: A note on the concepts of age distribution and transit time in natural reservoirs, Tellus, 25, 58–62, doi: 10.1111/j.2153-3490.1973.tb01594.x, 1973.

Broecker, W. and Peng, T.: Gas exchange rates between air and sea, Tellus, 26, 21–35, doi: 10.1111/j.2153-3490.1974.tb01948.x, 1974.

Bullister, J.: Atmospheric Histories (1765-2015) for CFC-11, CFC-12, CFC-113, CCl_4, SF_6 and N_2O, Carbon Dioxide Information Analysis Center, http://cdiac.ornl.gov/ftp/oceans/CFC_ATM_Hist/CFC_ATM_Hist_2015, doi: 10.3334/CDIAC/otg.CFC_ATM_Hist_2015, 2015.

Bullister, J. and Key, R.: CLIVAR/Carbon A13.5 Cruise Report, CCHDO, http://cchdo.ucsd.edu/data/b/c34715/a13-5_33RO20100308do.txt, 2010.

Bullister, J. and Weiss, R.: Determination of CCl_3F and CCl_2F_2 in seawater and air, Deep Sea Res. Part A. Oceanographic Research Papers, 35, 839 – 853, doi: 10.1016/0198-0149(88)90033-7, 1988.

Bullister, J. and Wisegarver, D.: The shipboard analysis of trace levels of sulfur hexafluoride, chlorofluorocarbon-11 and chlorofluorocarbon-12 in seawater, Deep Sea Res. Part I, 55, 1063–1074, doi: 10.1016/j.dsr.2008.03.014, 2008.

CLSI: Protocols for Determination of Limits of Detection and Limits of Quantification, Clinical and Laboratory Standards Institute, Wayne, PA USA, approved Guideline, CLSI document EP17, 2004.

CNSC: Investigation of the Environmental Fate of Tritium in the Atmosphere, INFO-0792, Canadian Nuclear Safety Commission, minister of Public Works and Government Services Canada, 2009.

Cossairt, J.: Background Levels of Tritium, Environmental Protection Note, 28, 1–4, 2012.

DeGrandpre, M. D., Körtzinger, A., Send, U., Wallace, D. W. R., and Bellerby, R. G. J.: Uptake and sequestration of atmospheric CO_2 in the Labrador Sea deep convection region, Geophys. Res. Lett., 33, doi:10.1029/2006GL026881, 2006.

Dickson, A., Sabine, C., and Christian, J.: Guide to Best Practices for Ocean CO_2 Measurements, 2007.

Dreisigacker, E. and Roether, W.: Tritium and ^{90}Sr in North Atlantic surface water, Earth Planet. Sci. Lett., 38, 301–312, 1978.

Engelkemeir, A., Hamill, W., Inghram, M., and Libby, W.: The Half-Life of Radiocarbon (^{14}C), Phys. Rev., 75, 1825, 1949.

Grasshoff, K., Kremling, K., and Ehrhardt, M.: Methods of Seawater Analysis, Wiley-VCH, Weinheim, 1999.

Haine, T. W. N. and Richards, K. J.: The influence of the seasonal mixed layer on oceanic uptake of CFCs, J. Geophys. Res. Oceans, 100, 10 727–10 744, doi:10.1029/95JC00629, 1995.

Hall, T. M. and Plumb, R. A.: Age as a diagnostic of stratospheric transport, J. Geophys. Res., 99, 1059–1070, 1994.

Holzer, M. and Primeau, F. W.: Improved constraints on transit time distributions from argon 39: A maximum entropy approach, J. Geophys. Res.: Oceans, 115, doi: 10.1029/2010JC006410, 2012.

Huhn, O., Rhein, M., Hoppema, M., and van Heuven, S.: Decline of deep and bottom water ventilation and slowing down of anthropogenic carbon storage in the Weddell Sea, 1984-2011, Deep Sea Res. Part I, 76, 66–84, doi:10.1016/j.dsr.2013.01.005, 2013.

Jenkins, W. J.: Tritium-Helium Dating in the Sargasso Sea: A Measurement of Oxygen Utilization Rates, Science, 196, 291–292, doi: 10.1126/science.196.4287.291, 1977.

Jiang, W., Williams, W., Bailey, K., Davis, A., Hu, S., Lu, Z., O'Connor, T., Purtschert, R., Sturchio, N., Sun, Y., and Mueller, P.: ^{39}Ar Detection at the 10^{-16} Isotopic Abundance Level with Atom Trap Trace Analysis, Phys. Rev. lett., 106, doi: 10.1103/PhysRevLett.106.103001, 2011.

Klatt, O., Roether, W., Hoppema, M., Bulsiewicz, K., Fleischmann, U., Rodehacke, C., Fahrbach, E., Weiss, R. F., and Bullister, J. L.: Repeated CFC sections at the Greenwich Meridian in the Weddell Sea, J. Geophys. Res. - Oceans, 107, doi: 10.1029/2000JC000731, 2002.

Krane, K.: Introductory Nuclear Physics, Wiley-VCH, 1987.

Krysell, M., Fogelqvist, E., and Tanhua, T.: Apparent removal of the transient tracer carbon tetrachloride from anoxic seawater, Geophys. Res. Lett., 21, 2511–2514, doi: 10.1029/94GL02336, 1994.

Law, C. S., Watson, A. J., and Liddicoat, M. I.: Automated vacuum analysis of sulphur hexafluoride in seawater: derivation of the atmospheric trend (1970-1993) and potential as a transient tracer, Mar. Chem., 48, 57 – 69, 1994.

Lee, B., Bullister, J., and Whitney, F.: Chlorofluorocarbon CFC-11 and carbon tetrachloride removal in Saanich Inlet, an intermittently anoxic basin, Mar. Chem., 66, 171–185, doi: 10.1016/S0304-4203(99)00039-0, 1999.

Lee, B.-S., Bullister, J. L., Murray, J. W., and Sonnerup, R. E.: Anthropogenic chlorofluorocarbons in the Black Sea and the Sea of Marmara, Deep Sea Res. Part I, 49, 895–913, doi: 10.1016/S0967-0637(02)00005-5, 2002.

Lemke, P.: The expedition ANTARKTIS X/4 of RV "Polarstern" in 1992, Reports on polar and marine research, 140, 1994.

Liang, J.-H., Deutsch, C., McWilliams, J. C., Baschek, B., Sullivan, P. P., and Chiba, D.: Parameterizing bubble-mediated air-sea gas exchange and its effect on ocean ventilation, Global Biogeochem. Cycles, 27, 894–905, doi: 10.1002/gbc.20080, 2013.

Libby, W.: Radiocarbon Dating, Univ. of Chicago Press, Chicago, Ill., 1955.

Loosli, H.: A dating method with ^{39}Ar, Earth Planet. Sci. Lett., 63, 51–62, 1983.

Lu, Z., Schlosser, P., Jr., W. S., Sturchio, N., Fischer, T., Kennedy, B., Purtschert, R., Severinghaus, J., Solomon, D., Tanhua, T., and Yokochi, R.: Tracer applications of noble gas radionuclides in the geosciences, Earth Sci. Rev., 138, 196 – 214, doi: 10.1016/j.earscirev.2013.09.002, 2014.

Minschwaner, K., Hoffmann, L., Brown, A., Riese, M., Müller, R., and Bernath, P. F.: Stratospheric loss and atmospheric lifetimes of CFC-11 and CFC-12 derived from satellite observations, Atmos. Chem. Phys., 13, 4253–4263, doi: 10.5194/acp-13-4253-2013, 2013.

Orr, J. C., Fabry, V. J., Aumont, O., Bopp, L., Doney, S. C., Feely, R. A., Gnanadesikan, A., Gruber, N., Ishida, A., Joos, F., Key, R. M., Lindsay, K., Maier-Reimer, E., Matear, R., Monfray, P., Mouchet, A., Najjar, R. G., Plattner, G. K., Rodgers, K. B., Sabine, C. L., Sarmiento, J. L., Schlitzer, R., Slater, R. D., Totterdell, I. J., Weirig, M. F., Yamanaka, Y., and Yool, A.: Anthropogenic ocean acidification over the twenty-first century and its impact on calcifying organisms, Nature, 437, 681–686, doi: 10.1038/nature04095, 2005.

Ravishankara, A., Solomon, S., Turnipseed, A., and Warren, R.: Atmospheric Lifetimes of Long-Lived Halogenated Species, Science, 259, 194–199, doi: 10.1126/science.259.5092.194, 1993.

Rodriguez, J.: Beiträge zur Verteilung von ^{39}Ar im Atlantik, Ph.D. thesis, University of Bern, Switzerland, 1993.

Roether, W.: On Oceanic Boundary Conditions for Tritium, on Tritiugenic ^{3}He, and on the Tritium-^{3}He Age Concept, in: Oceanic Circulation Models: Combining Data and Dynamics, edited by Anderson, D. and Willebrand, J., vol. 284 of *NATO ASI Series*, pp. 377–407, Springer Netherlands, doi: 10.1007/978-94-009-1013-3-12, 1989.

Roether, W., Schlosser, P., Kuntz, R., and Weiss, W.: Transient-tracer studies of the thermohaline circulation of the Mediterranean, Reports in Meteorology and Oceanography, 41, 291–317, 1992.

Roether, W., Jean-Baptiste, P., Fourrè, E., and Sültenfuß, J.: The transient distribution of nuclear weapon-generated tritium and its decay product ^{3}He in the Mediterranean Sea, 1952 - 2011, and their oceanographic potential, Ocean Sci., 9, 837–854, doi:10.5194/os-9-837-2013, 2013.

Sabine, C. and Tanhua, T.: Estimation of Anthropogenic CO_2 Inventories in the Ocean, Annu. Rev. Mar. Sci., 2, 175–198, doi: 10.1146/annurev-marine-120308-080947, 2010.

Schlitzer, R. and Roether, W.: A Meridional ^{14}C and ^{39}Ar Section in Northeast Atlantic Deep Water, J. Geophys. Res., 90, 6945–6952, 1985.

Schlosser, P., Bayer, R., Bönisch, G., Cooper, L. W., Ekwurzel, B., Jenkins, W. J., Khatiwala, S., Pfirman, S., and Smethie, W. M.: Pathways and mean residence times of dissolved pollutants in the ocean derived from transient tracers and stable isotopes, Sci. Total Environ., 237-238, 15 – 30, doi: 10.1016/S0048-9697(99)00121-7, 1999.

Schneider, A., Tanhua, T., Körtzinger, A., and Wallace, D.: High anthropogenic carbon content in the eastern Mediterranean, J. Geophys. Res., 115, doi:10.1029/2010JC006171, 2010.

Schneider, A., Tanhua, T., Körtzinger, A., and Wallace, D.: An evaluation of tracer fields and anthropogenic carbon in the equatorial and the tropical North Atlantic, Deep Sea Res. Part I, 67, 85 –

97, doi:10.1016/j.dsr.2012.05.007, 2012.

Schneider, A., Tanhua, T., Roether, W., and Steinfeldt, R.: Changes in ventilation of the Mediterranean Sea during the past 25 year, Ocean Sci., 10, 1–16, doi: 10.5194/os-10-1-2014, 2014.

Shao, A. E., Mecking, S., Thompson, L., and Sonnerup, R. E.: Mixed layer saturations of CFC-11, CFC-12, and SF6 in a global isopycnal model, J. Geophys. Res.: Oceans, 118, 4978–4988, doi: 10.1002/jgrc.20370, 2013.

Sonnerup, R., Mecking, S., and Bullister, J.: Transit time distributions and oxygen utilization rates in the Northeast Pacific Ocean from chlorofluorocarbons and sulfur hexafluoride, Deep Sea Res. Part I, 72, 61 – 71, doi: 10.1016/j.dsr.2012.10.013, 2013.

Stöven, T.: Ventilation processes of the Mediterranean Sea based on CFC-12 and SF_6 measurements, GEOMAR OceanRep, http://oceanrep.geomar.de/id/eprint/13936, diploma thesis, Christian-Albrechts-Universität zu Kiel, 2011.

Stöven, T. and Tanhua, T.: Ventilation of the Mediterranean Sea constrained by multiple transient tracer measurements, Ocean Sci., 10, 439–457, doi: 10.5194/os-10-439-2014, 2014.

Stuiver, M.: Variations in radiocarbon concentration and sunspot activity, J. Geophy. Res., 66, 273–276, doi: 10.1029/JZ066i001p00273, 1961.

Tanhua, T., Olsson, K., and Fogelqvist, E.: A first study of SF_6 as a transient tracer in the Southern Ocean, Deep Sea Res. Part II, 51, 2683–2699, doi: 10.1016/j.dsr2.2001.02.001, 2004.

Tanhua, T., Olsson, K. A., and Jeansson, E.: Formation of Denmark Strait overflow water and its hydro-chemical composition, J. Mar. Syst., 57, 264–288, doi: 10.1016/j.jmarsys.2005.05.003, 2005.

Tanhua, T., Waugh, D., and Wallace, D.: Use of SF_6 to estimate anthropogenic CO_2 in the upper ocean, J. Geophys. Res., 113, 2156–2202, doi:10.1029/2007JC004416, 2008.

Tanhua, T., Waugh, D., and Bullister, J.: Estimating changes in ocean ventilation from the early 1990s CFC-12 and late SF_6 measurements, Geophys. Res. Lett., 40, 927–932, doi:10.1002/grl.50251, 2013.

Tans, P. P., de Jong, A. F. M., and Mook, W. G.: Natural atmospheric ^{14}C variations and the Suess effect, Nature, 280, 826–828, doi: 10.1038/280826a0, 1979.

Turner, D. R., Bertilsson, S., Fransson, A., and Pakhomov, E.: The SWEDARP 1997/98 marine expedition: overview, Deep Sea Res. Part II, 51, 2543–2556, doi: 10.1016/j.dsr2.2003.08.006, 2004.

Waugh, D., Primeau, F., DeVries, T., and Holzer, M.: Recent Changes in the Ventilation of the Southern Oceans, Science, 339, 568–570, doi: 10.1126/science.1225411, 2013.

Waugh, D. W., Vollmer, M. K., Weiss, R. F., Haine, T. W. N., and Hall, T. M.: Transit time distributions in Lake Issyk-Kul, Geophys. Res. Lett., 29, 84–1–84–4, doi:10.1029/2002GL016201, 2002.

Waugh, D. W., Hall, T. M., and Haine, T. W. N.: Relationships among tracer ages, J. Geophys. Res., 108, doi:10.1029/2002JC001325, 2003.

Waugh, D. W., Haine, T. W. N., and Hall, T. M.: Transport times and anthropogenic carbon in the subpolar North Atlantic Ocean, Deep Sea Res. Part I, 51, 1475 – 1491, 2004.

Waugh, D. W., Hall, T. M., McNeil, B. I., Key, R., and Matear, R. J.: Anthropogenic CO_2 in the oceans estimated using transit time distributions, Tellus Ser. B, 58, 376 – 389, 2006.

Whitworth, T. and Nowlin, W.: Water masses and currents of the Southern Ocean at the Greenwich Meridian, J. Geophys. Res. Oceans, 92, 6462–6476, doi: 10.1029/JC092iC06p06462, 1987.

Wolf-Gladrow, D.: The expedition of the research vessel" Polarstern" to the Antarctic in 2012 (ANT-XXVIII/3), Reports on polar and marine research, 661, 2013.

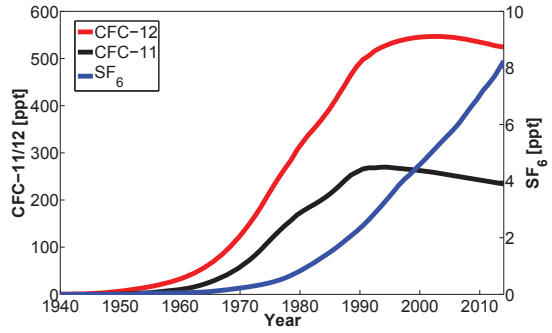

Fig. 1: Atmospheric histories of CFC-12, CFC-11 and SF_6 of the northern hemisphere. The data was taken from Bullister (2015).

Table 1: Detection limits of transient tracers. The presented values are approximate values which can deviate between different systems and the measurement conditions, e.g. lab or on board measurements.

Tracer	**LOD**	**Unit**
CFC-12	$0.01 - 0.001$	$pmol\,kg^{-1}$
CFC-11	$0.01 - 0.001$	$pmol\,kg^{-1}$
SF_6	$0.1 - 0.01$	$fmol\,kg^{-1}$
^{3}H	0.02	TU
^{3}He	$4.0 \cdot 10^{-9}$	$^{3}He/^{4}He$
^{39}Ar	$8 \cdot 10^{-16}$	$^{39}Ar/Ar$
^{14}C	$1 \cdot 10^{-15}$	$^{14}C/C$

Table 2: ^{39}Ar data of the eastern Atlantic and south eastern Weddell Sea from the 1980s and early 1990s. The data is taken from Rodriguez (1993).

	LAT [°N]	**LON [°E]**	**^{39}Ar [% modern]**	**pressure [dBar]**
Eastern Atlantic				
	-17	1.1	45	4440
	-10.5	1.1	55	820
	-1.2	-4.1	42	4480
	-0.1	-4.1	67	1800
	-0.5	-4.4	53	2810
	2.4	-3.6	57	750
Eastern Weddell Sea				
	-65.2	-2	46	245
	-65.2	-2	52	3055
	-62.7	3	41	240
	-66.7	5	34	1245
	-67.3	-0.5	38	1990
	-61.5	-6.5	37	445
	-61.5	-6.5	44	675
	-61.5	-6.5	52	4070

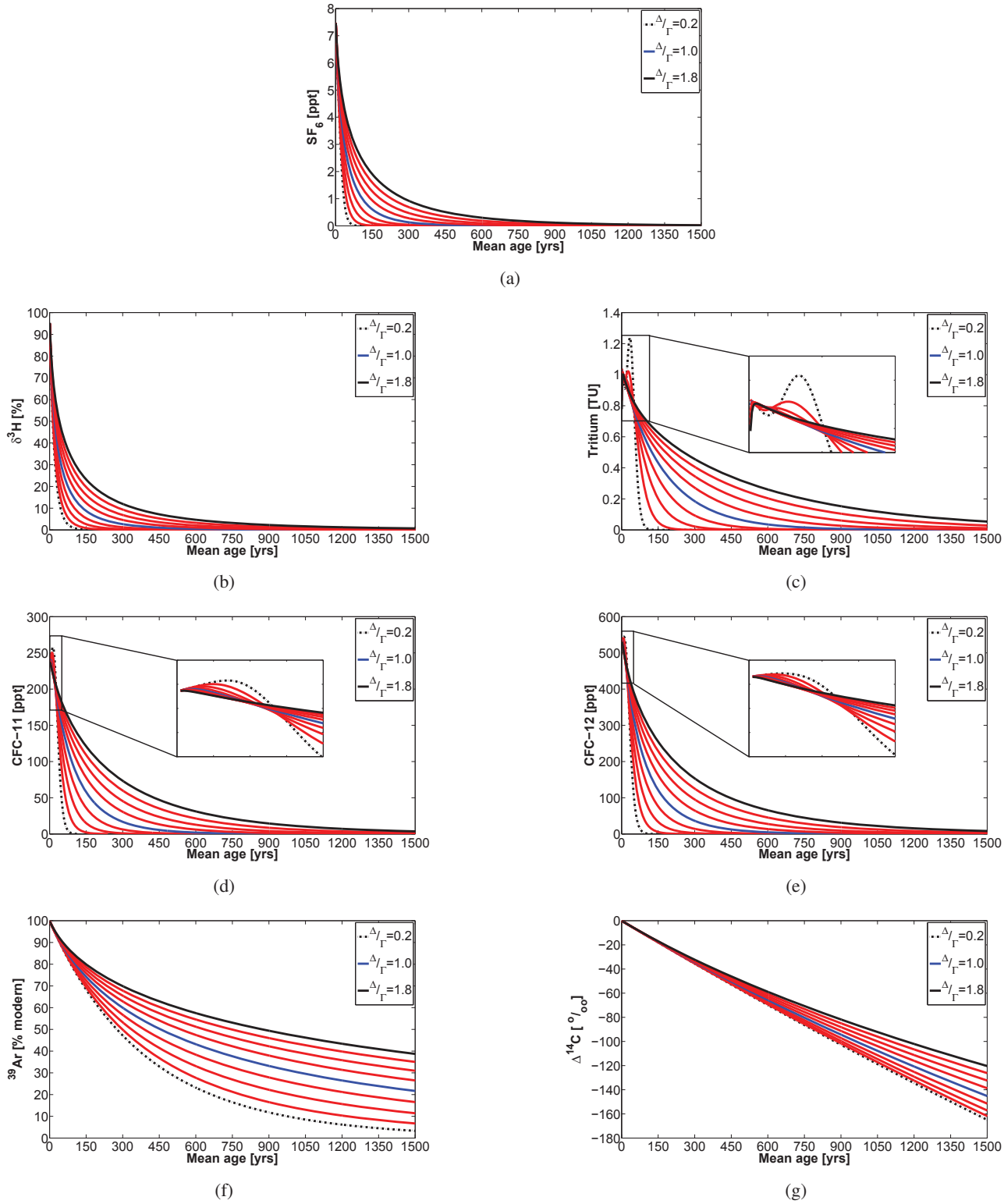

Fig. 2: Transient tracer concentration of (**a**) SF_6, (**b**) δ^3H , (**c**) Tritium, (**d**) CFC-11, (**e**) CFC-12, (**f**) ^{39}Ar, (**g**) $\Delta^{14}C$ vs. mean age for different Δ/Γ ratios. The standard ratio of 1.0 is shown as a blue line and the lower and upper limit as dashed and solid black line, respectively. The CFCs and tritium show a distribution anomaly which is caused by the decreasing atmospheric concentration of the tracers.

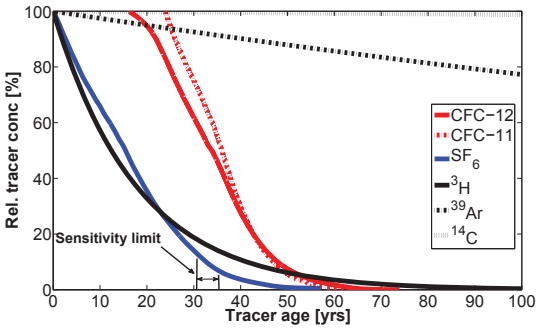

Fig. 3: Tracer order based on the relation between the relative tracer concentration and the corresponding tracer age of 2012. SF_6 and ^3H as well as CFC-11 and CFC-12 show a similar behavior and cannot be used as tracer couples to constrain the IG-TTD. The sensitivity limit is explained in section 4.4.

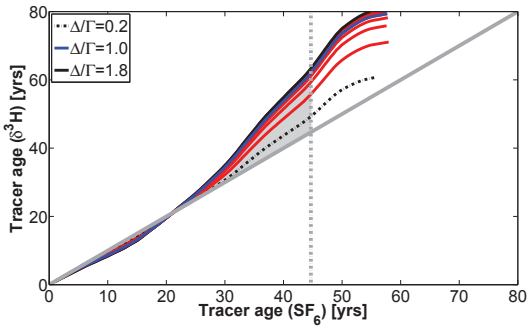
Δ/Γ=0.2
Δ/Γ=1.0
Δ/Γ=1.8
Tracer age (δ3H) [yrs]
Tracer age (SF6) [yrs]

(a)

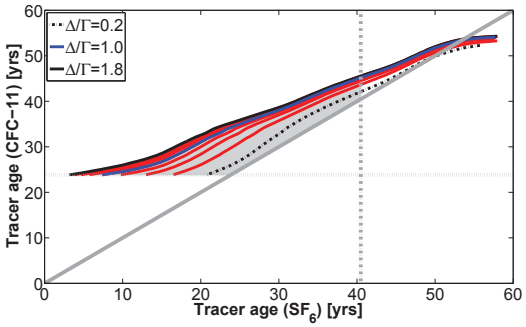
Δ/Γ=0.2
Δ/Γ=1.0
Δ/Γ=1.8
Tracer age (CFC−11) [yrs]
Tracer age (SF6) [yrs]

(b)

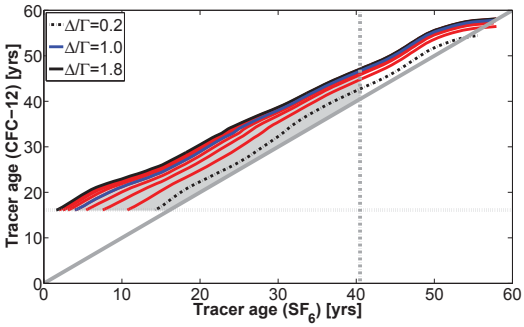
Δ/Γ=0.2
Δ/Γ=1.0
Δ/Γ=1.8
Tracer age (CFC−12) [yrs]
Tracer age (SF6) [yrs]

(c)

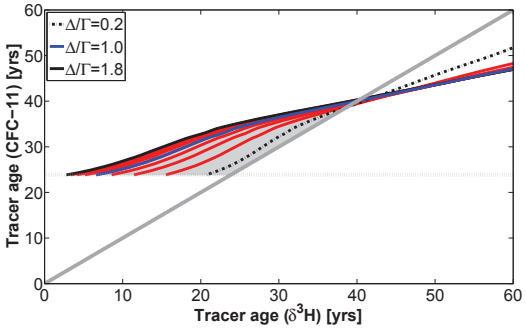
Δ/Γ=0.2
Δ/Γ=1.0
Δ/Γ=1.8
Tracer age (CFC−11) [yrs]
Tracer age (δ3H) [yrs]

(d)

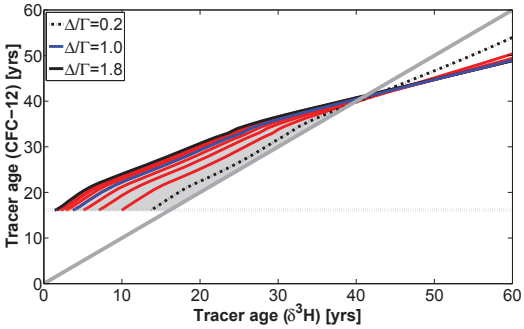
Δ/Γ=0.2
Δ/Γ=1.0
Δ/Γ=1.8
Tracer age (CFC−12) [yrs]
Tracer age (δ3H) [yrs]

(e)

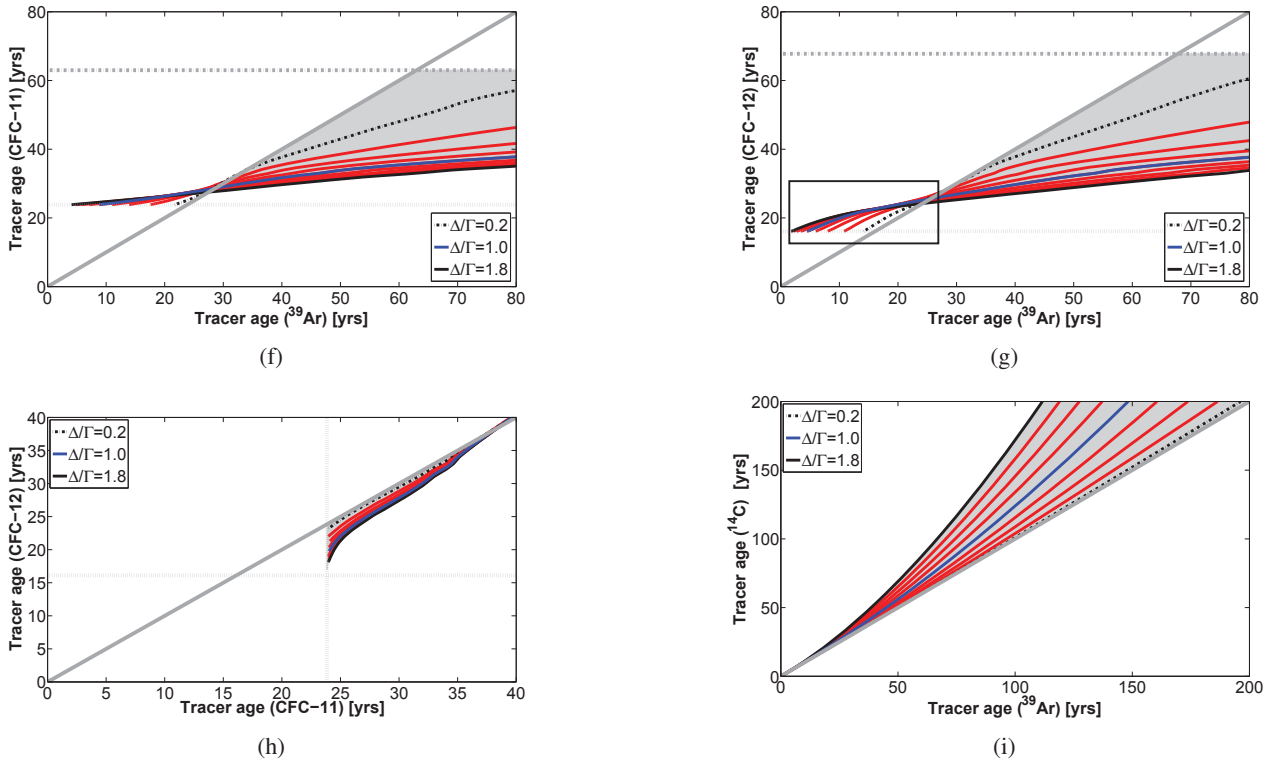

Fig. 4: IG-TTD validity areas of the transient tracer couples using the tracer age relationship. The grey area describes the IG-TTD based tracer age relationship for Δ/Γ-ratios between $0-1.8$ (see section 3 for explanation). Consequently, the boundaries are the bisecting line (grey solid line) with $\Delta/\Gamma = 0$, i.e. where both tracer age are equal, the detection and atmospheric concentration limit of the tracer (dashed and dash dotted grey line, respectively) and the IG-TTD based tracer age relationship of $\Delta/\Gamma = 1.8$ (black solid line). The red solid lines indicate a Δ/Γ-ratio increment of 0.2. The tracer couples are (**a**) δ^3H/SF_6, (**b**) CFC-11/SF_6, (**c**) CFC-12/SF_6, (**d**) CFC-11/δ^3H, (**e**) CFC-12/δ^3H, (**f**) CFC-11/^{39}Ar, (**g**) CFC-12/^{39}Ar, (**h**) CFC-12/CFC-11 and (**i**) ^{39}Ar/Δ^{14}C. Areas with intercepting Δ/Γ isolines (black box in **g**) are indistinct in tracer age and thus non-constrainable.

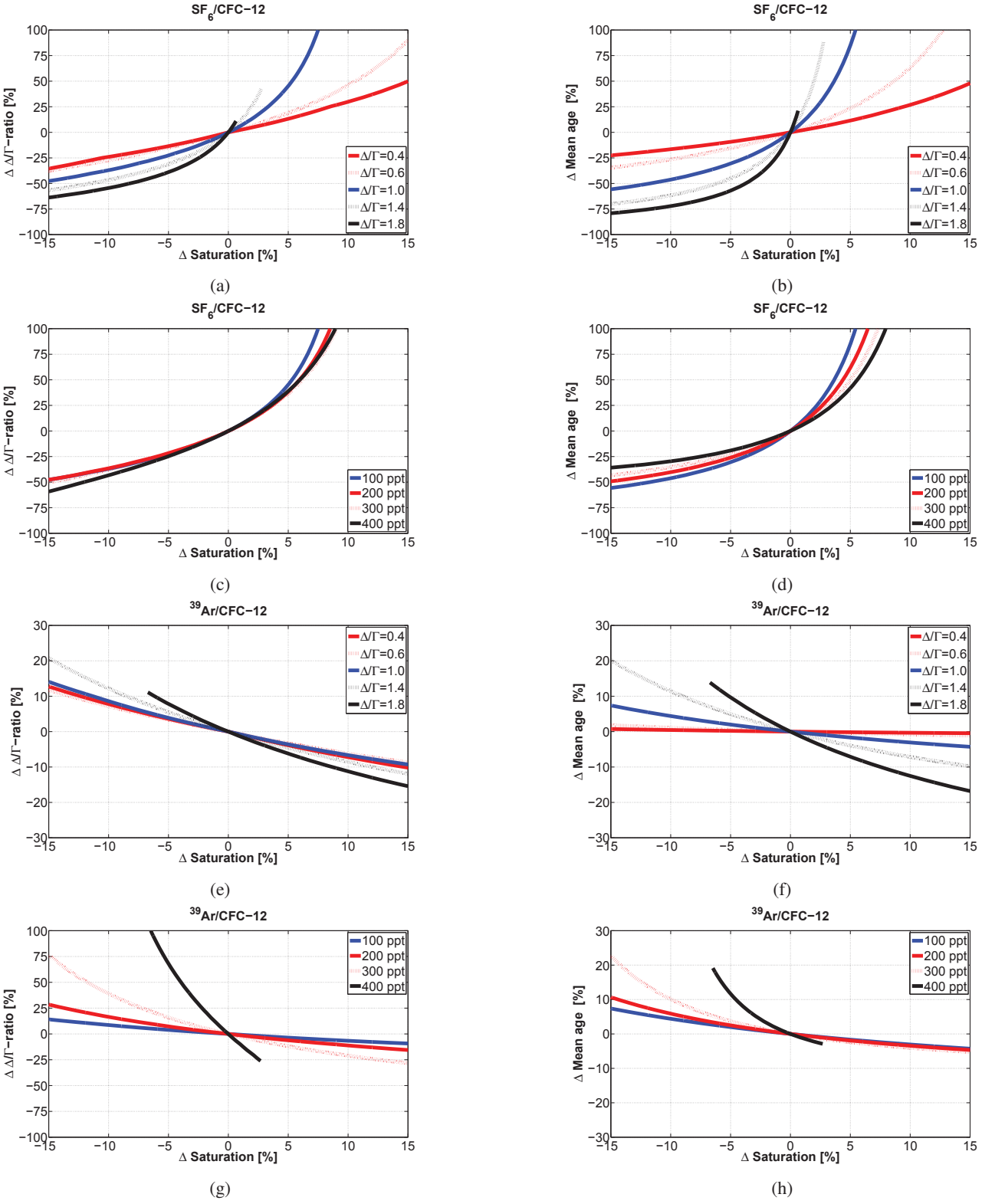

Fig. 5: Δ/Γ ratio and mean age sensitivities to deviations in CFC-12 saturation based on the combination with (**a**-**d**) SF_6 and (**e**-**h**) ^{39}Ar. The sensitivities are shown for either a constant initial CFC-12 concentration of $100\,ppt$ and a changing initial Δ/Γ ratio (**a**, **b**, **e** and **f**) or a changing initial CFC-12 concentration and a constant initial Δ/Γ ratio of 1.0 (**c**, **d**, **g** and **h**). The related tracer concentrations of SF_6 and ^{39}Ar are backcalculated by using the IG-TTD.

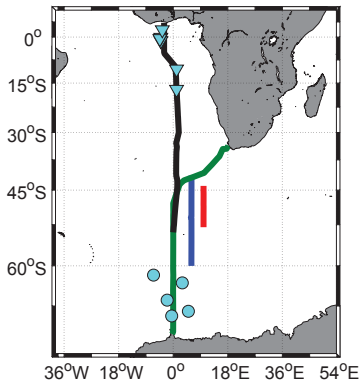

Fig. 6: Sections of transient tracer surveys. The section of the ANT-XXVIII/3 cruise of 2012 is highlighted as red line, the CLIVAR A13.5 cruise of 2010 as black line, the SWEDARP cruise of 1997/98 as blue line, the ANT-X/4 cruise as green line and the ^{39}Ar data as cyan dots and triangles.

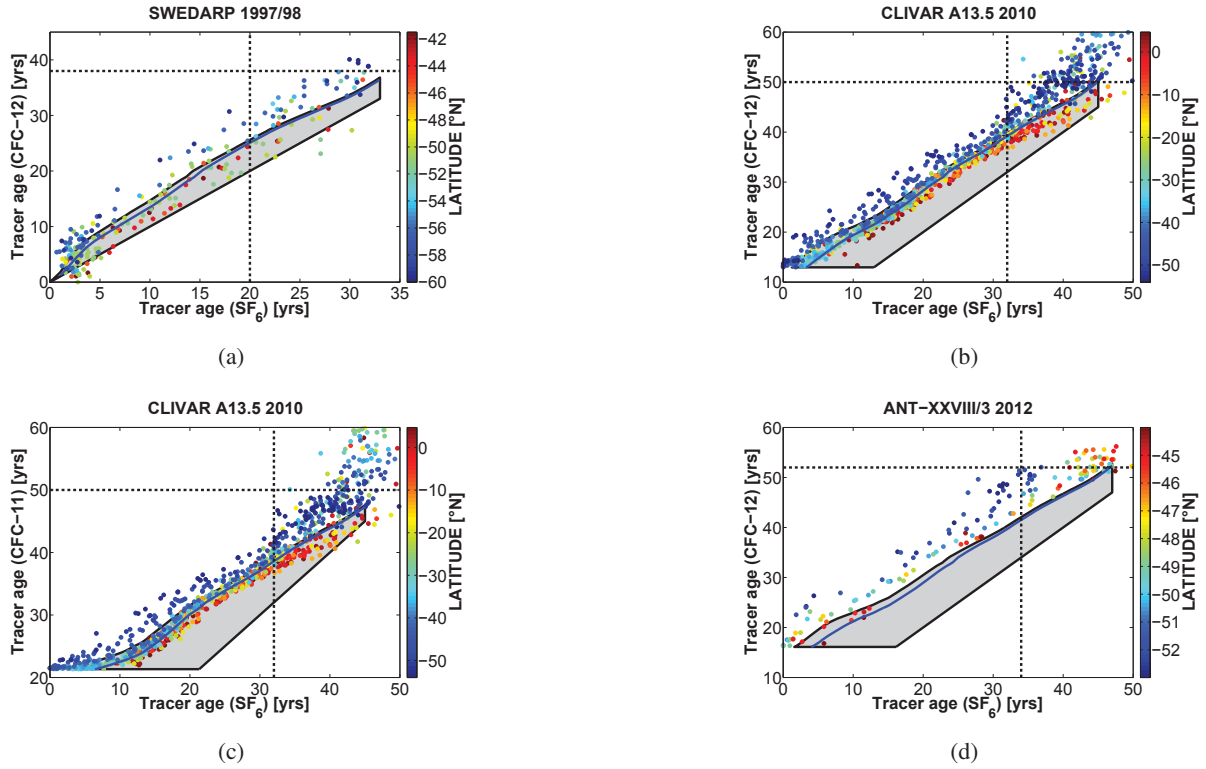

Fig. 7: Tracer age relationship and validity areas of (**a**) CFC-12/SF_6 of the SWEDARP cruise of 1998, (**b**, **c**) CFC-12/SF_6 and CFC-11/SF_6 of the CLIVAR A13.5 cruise of 2010 and (**d**) CFC-12/SF_6 of the ANT-XXVIII/3 cruise of 2012. The data is colored by latitude from red (north) to blue (south). The north-south trend of Δ/Γ ratios being shifted towards the upper limit of the IG-TTD can be seen for all data sets. The CLIVAR A13.5 data show that the northern data is in the application range of the IG-TTD whereas ANT-XXVIII/3 data cannot be applied to the model. The SWEDARP data shows a scattered and indistinct structure with no clear trend. The dashed black lines indictae the sensitivity limit which is explained in section 4.4.

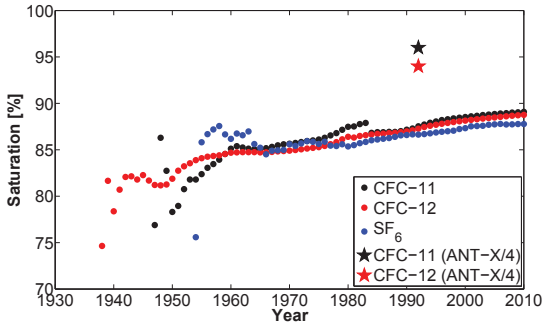

Fig. 8: Yearly maximum surface undersaturation of CFC-12, CFC-11 and SF_6 between $50-68°S$ and $30°W-20°E$ in the Southern Ocean. The surface saturation was relatively similar for all three transient tracers over the last 30 years. The black and red star indicate the CFC-12 and CFC-11 mean surface saturations which were obtained during the ANT-X/4 cruise in 1992.

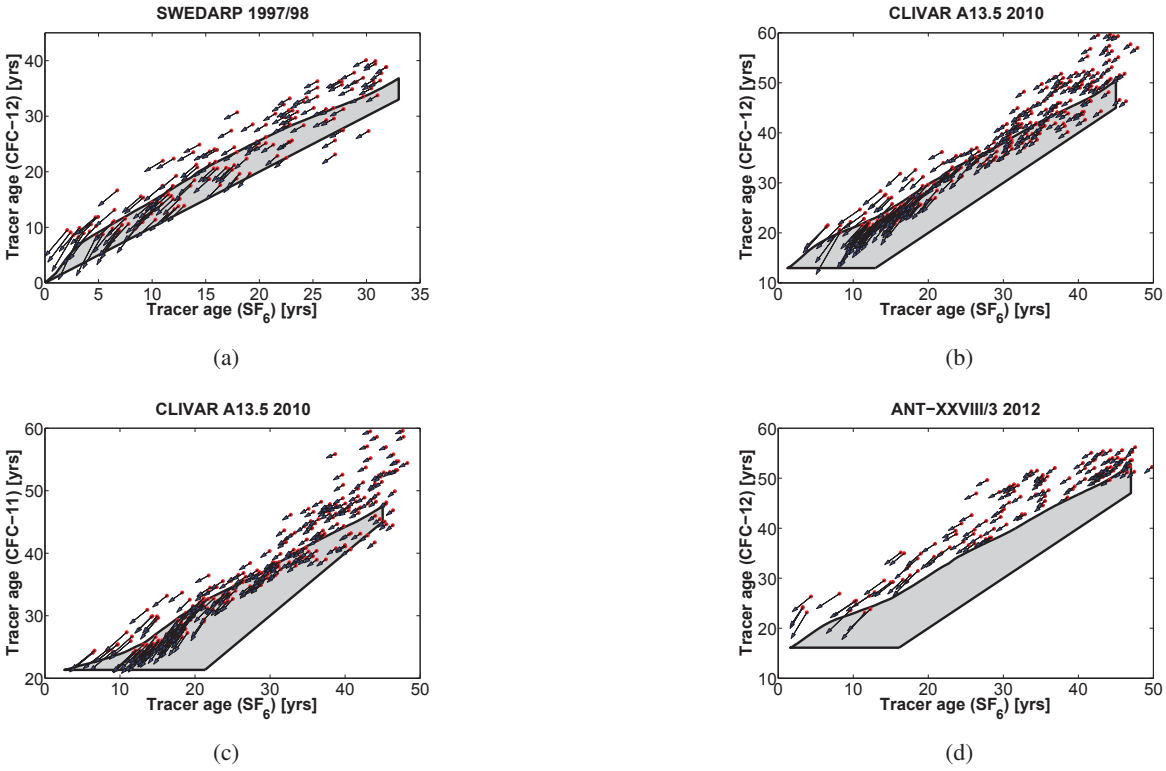

Fig. 9: Changes in the tracer age relationships based on saturation corrections. The red dots indicate the relationship of the original and the arrowheads of the saturation corrected data. The data sets are similar to Fig. 7 of (**a**) SWEDARP, (**b**, **c**) CLIVAR A13.5 and (**d**) ANT-XXVIII/3. The saturation correction affects the Δ/Γ ratios only to minor extent for a SF_6 tracer age > 20 years but shows a shift towards lower Δ/Γ ratios below this limit.

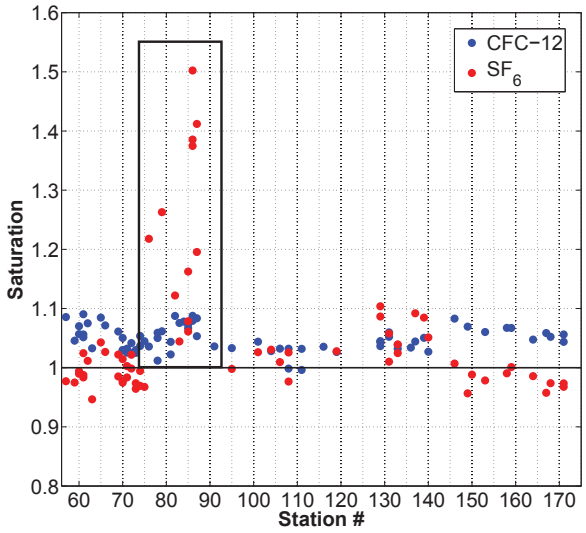

Fig. 10: Surface saturation of CFC-12 and SF_6 during the ANT-XXVIII/3 cruise in 2012. SF_6 shows significant supersaturation one day after heavy weather conditions with wind speeds between $20 - 25\,ms^{-1}$ (black box).

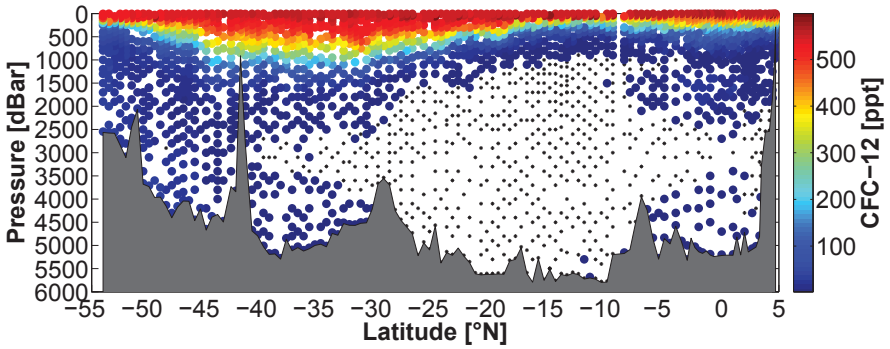

(a)

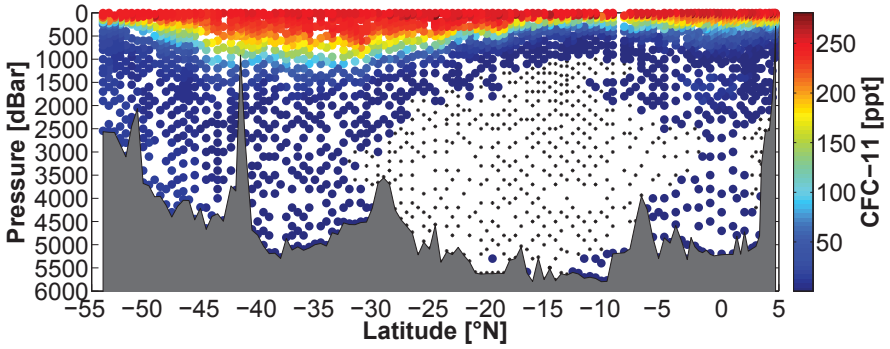

(b)

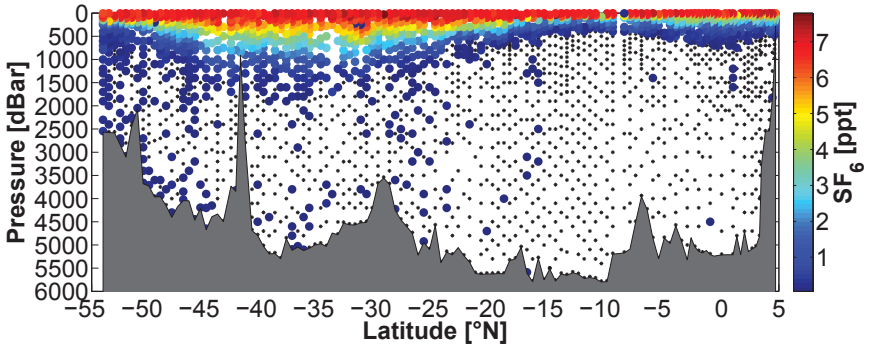

(c)

Fig. 11: Transient tracer concentrations of the CLIVAR A13.5 section along the Greenwich Meridian in 2010 of (**a**) CFC-12, (**b**) CFC-11 and (**c**) SF_6 in ppt. The black dots indicate measurements with concentrations below the detection limit.

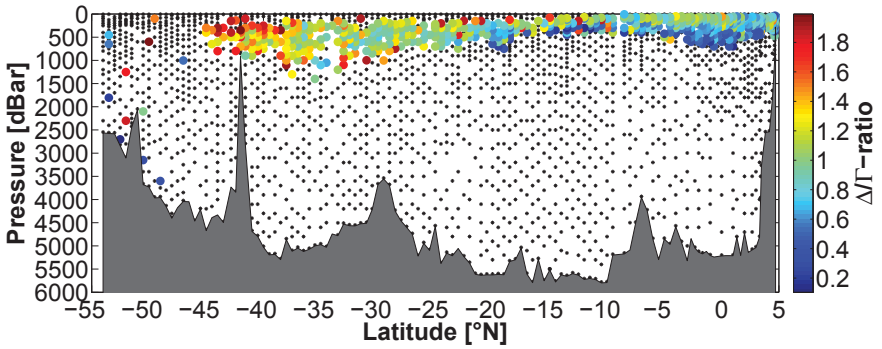

(a)

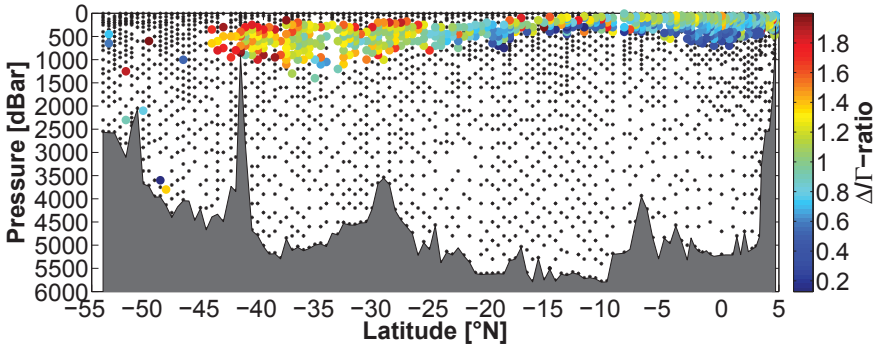

(b)

Fig. 12: Constrained Δ/Γ ratios of the CLIVAR A13.5 section along the Greenwich Meridian in 2010 using the tracer couples (**a**) CFC-12/SF_6 and (**b**) CFC-11/SF_6. The black dots indicate data below the detection limit and data outside the application range of the IG-TTD.

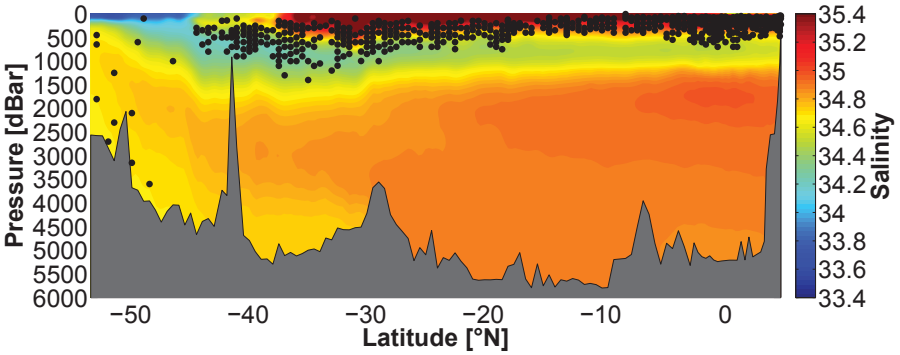

Fig. 13: Salinity section of the CLIVAR A13.5 section along the Greenwich Meridian in 2010. The black dots indicate data within the application range of the IG-TTD (i.e. constrainable data points). The IG-TTD limiting SAF can be identified by the salinity drop at $\approx 46°$S and the AAIW by the low salinity layer originating south of the SAF.

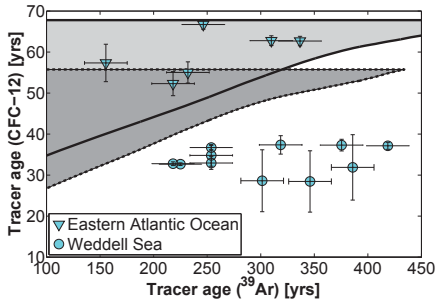

Fig. 14: Tracer age relationship of CFC-12 and ^{39}Ar. The CFC-12 data of the CLIVAR A13.5 cruise (validity area of 2010, light grey area) was interpolated to the isopycnals of the ^{39}Ar data of the eastern Atlantic Ocean (cyan triangles). Accordingly, the CFC-12 data of the ANT-X/4 cruise (validity area of 1992, dark grey area) was interpolated to the ^{39}Ar data of the Weddell Sea (cyan dots). The validity areas of 1992 (dark grey area) and 2010 (light grey area) correspond to the year of sampling of CFC-12. Data from the eastern Atlantic Ocean (triangles) can be found within the application range of the IG-TTD whereas most of the data from the Weddell Sea remains outside.

Manuscript III

Manuscript prepared for Ocean Sci.
with version 5.0 of the LaTeX class copernicus.cls.
Date: 3 June 2015

Recent transient tracer distributions in the Fram Strait: Estimation of anthropogenic carbon content and transport

T. Stöven[1], **T. Tanhua**[1], **M. Hoppema**[2], **and W.-J. von Appen**[2]

[1]Helmholtz Centre for Ocean Research Kiel, GEOMAR, Germany
[2]Alfred Wegener Institute Helmholtz Centre for Polar and Marine Research, Bremerhaven, Germany

Correspondence to: T. Stöven
(tstoeven@geomar.de)

Abstract. The storage of anthropogenic carbon in the ocean's interior is an important process which modulates the increasing carbon dioxide concentrations in the atmosphere. The polar regions are expected to be net sinks for anthropogenic carbon. Transport estimates of dissolved inorganic carbon and the anthropogenic offset can thus provide information about the magnitude of the corresponding storage processes.

Here we present a transient tracer, dissolved inorganic carbon (DIC) and total alkalinity (TA) data set along $78°50'$N sampled in the Fram Strait in 2012. A theory on tracer relationships is introduced which allows for an application of the Inverse Gaussian - Transit Time Distribution (IG-TTD) at high latitudes and the estimation of anthropogenic carbon concentrations. Current velocity measurements along the same section were used to estimate the net flux of DIC and anthropogenic carbon through the Fram Strait.

The new theory explains the differences between the theoretical (IG-TTD based) tracer age relationship and the specific tracer age relationship of the field data by saturation effects during water mass formation and / or the deliberate release experiment of SF_6 in the Greenland Sea in 1996 rather than by different mixing or ventilation processes. Based on this assumption, a maximum SF_6 excess of $0.5 - 0.8\, fmol\, kg^{-1}$ was determined in the Fram Strait at intermediate depths ($500\,m$ - $1600\,m$). The anthropogenic carbon concentrations are $50 - 55\, \mu mol\, kg^{-1}$ in the Atlantic Water / Recirculating Atlantic Water, $40 - 45\, \mu mol\, kg^{-1}$ in the Polar Surface Water / warm Polar Surface Water and between $10 - 35\, \mu mol\, kg^{-1}$ in the deeper water layers, with lowest concentrations in the bottom layer. The net DIC and anthropogenic carbon fluxes through the Fram Strait indicate a balanced exchange between the Arctic Ocean and the North Atlantic, although with high uncertainties.

1 Introduction

Changes in the Arctic during the last decades stand in mutual relationship with changes in the adjacent ocean areas such as the Nordic Seas, the Atlantic and the Pacific Ocean. The elevated heat flux of warm Atlantic Water into the Arctic Ocean has, for example, significant influence on the perennial sea ice thickness and volume and thus on the fresh water input (Polyakov et al., 2005; Stroeve et al., 2008; Kwok et al., 2009; Kurtz et al., 2011). The exchange and transport of heat, salt and fresh water through the major gateways like Fram Strait, Barents Sea Opening, Canadian Archipelago and Bering Strait are also directly connected to changes in ventilation of the adjacent ocean areas (Wadley and Bigg, 2002; Vellinga et al., 2008; Rudels et al., 2012). The ventilation processes of the Arctic Ocean have a major impact on the anthropogenic carbon storage in the world ocean (Tanhua et al., 2008). Studying the fluxes of anthropogenic carbon through the major gateways contributes to the estimate of the integrated magnitude of such ocean-atmosphere interactions. It additionally provides information of a changing environment in the Arctic Mediterranean. The required flux data of the prevailing water masses, i.e. current velocity fields, are obtained by time series of long-term maintained mooring arrays in the different gateways. The Fram Strait is the deepest gateway to the Arctic Ocean with highest volume fluxes equatorwards and polewards. One of the well-established cross-section mooring arrays is located at $\approx 78°50'$N in the Fram Strait (Fahrbach et al., 2001; Schauer et al., 2008) which provided the basis for heat transport estimates in the past (Fahrbach et al., 2001; Schauer et al.,

2004, 2008; Beszczynska-Möller et al., 2012). However, it turned out that the current data interpretation and analysis of this mooring array is complicated due to a recirculation pattern and mesoscale eddy structures in this area (Schauer and Beszczynska-Möller, 2009; Rudels et al., 2008; Marnela et al., 2013; de Steur et al., 2014). The spatial and temporal volume flux variability and the insufficient instrument coverage in the deeper water layers, i.e. below the West Spitsbergen Current (WSC) and East Greenland Current (EGC), lead to high uncertainties of the net flux through Fram Strait. Hence, it is the most relevant but also the most challenging gateway with respect to transport budgets in the Arctic Mediterranean.

Estimating an anthropogenic carbon budget presupposes the knowledge of the concentration ratio between the natural dissolved inorganic carbon (DIC) and the anthropogenic part (C_{ant}) in the water column. An estimate of DIC transport across the Arctic Ocean boundaries is provided by MacGilchrist et al. (2014) who used velocity fields by Tsubouchi et al. (2012) and available DIC data. That work provides a proper estimate of DIC fluxes, although it does not separate the specfic share of anthropogenic carbon and the uncertainties are relatively high. Here we present anthropogenic carbon column inventories in Fram Strait using a new data set of SF_6 and CFC-12 along the cross-section of the mooring array at $78°50'$N and a short meridional section along the fast ice edge in 2012. The anthropogenic carbon column inventories were estimated using the transient tracers and the Inverse Gaussian transit time distribution (IG-TTD) model. Flux estimates of DIC and anthropogenic carbon with the Atlantic Water, Recirculating / Return Atlantic Water and Polar Water water masses through Fram Strait are provided based on current velocities measured with moorings. Common error sources and specific aspects using these tracers and method in Fram Strait are highlighted.

2 Material and Methods

2.1 Tracer and carbon data

A data set of CFC-12, SF_6, DIC and TA was obtained during the ARK-XXVII/1 expedition from 14 June to 15 July 2012 from Bremerhaven, Germany to Longyearbyen, Svalbard on the German research vessel *Polarstern* (Beszczynska-Möller, 2013). Figure 1 shows the stations of the zonal section along $78°50'$N, where measurements of CFC-12, SF_6, DIC, and TA were conducted. The meridional section along the fast ice edge was only sampled for CFC-12 and SF_6.

Water samples of the transient tracers CFC-12 and SF_6 were taken with $250\,ml$ glass syringes and directly measured on board, using a purge and trap GC-ECD system similar to Law et al. (1994) and Bullister and Wisegarver (2008). The measurement system is identical to the "PT3" system described in Stöven and Tanhua (2014) except the cooling system and column composition. The trap consisted of a 1/16" column packed with 70 cm *Heysep D* and cooled to $-70°$C during the purge process using a Dewar filled with a thin layer of liquid nitrogen. The 1/8" precolumn was packed with 30 cm *Porasil C* and 60 cm *Molsieve 5 Å* and the 1/8" main column with 180 cm *Carbograph 1AC*. Due to malfunctioning of the Electron Capture Detector (ECD) of the measurement system, the samples between station 15 and 53 were taken with $300\,ml$ glass ampules and flame sealed for later onshore measurements at GEOMAR. The onshore measurement procedure is described in Stöven and Tanhua (2014). The precision for the onshore measurements is $\pm 4.4\,\%/0.09\,fmol\,kg^{-1}$ for SF_6 and $\pm 1.9\,\%/0.09\,pmol\,kg^{-1}$ for CFC-12. The precision for onboard measurements is $\pm 0.5\,\%/0.02\,fmol\,kg^{-1}$ for SF_6 and $\pm 0.6\,\%/0.02\,pmol\,kg^{-1}$ for CFC-12.

The DIC and total alkalinity (TA) samples were taken with $500\,ml$ glass bottles and poisened with $100\,\mu l$ of a saturated mercuric chloride solution to prevent biological activities during storage time. The sampling procedure was carried out according to Dickson et al. (2007). The measurements of DIC and TA were performed onshore at the GEOMAR, using a coulometric measurement system (SOMMA) for DIC (Johnson et al., 1993, 1998) and a potentiometric titration (VINDTA) for TA (Mintrop et al., 2000). The precision is $\pm 0.05\,\%/1.1\,\mu mol\,kg^{-1}$ for DIC and $\pm 0.08\,\%/1.7\,\mu mol\,kg^{-1}$ for TA. The data of all obtained chemical parameters will be avaiable at CDIAC by the end of 2015. The physical oceanographic data (temperature, salinity, and pressure) from the cruise where the tracers were measured can be found at Beszczynska-Möller and Wisotzki (2012).

2.2 Water transport data

An array of moorings across the deep Fram Strait from $9°$E to $7°$W has been maintained since 1997 by the Alfred Wegener Institute and the Norwegian Polar Institute. Since 2002, it has contained 17 moorings at $78°50'$N. Here we use the gridded data from the array from summer 2002 to summer 2010 as described in Beszczynska-Möller et al. (2012). The more recent data has either not been recovered yet or the processing is still in progress. The moorings contained temperature and velocity sensors at five standard depths: $75\,m$, $250\,m$, $750\,m$, $1500\,m$, and $10\,m$ above the bottom. These hourly measurements were averaged to monthly values and then gridded onto a regular $5\,m$ vertical by $1000\,m$ horizontal grid using optimal interpolation. Since interannual trends are small (Beszczynska-Möller et al., 2012), we consider the long term average volume flux of the following water masses: Atlantic Water advected in the West Spitsbergen Current defined as longitude $\geq 5°$E and depth $\leq 750\,m$; Recirculating and Return Atlantic Water which is both due to the recirculation of Atlantic Water in Fram Strait (de Steur et al., 2014) and the long loop of Atlantic Water through the Arctic Ocean (Karcher et al., 2012), defined as longitude $\leq 5°$E, mean

temperature $\geq 1°C$, and depth $\leq 750\,m$; and finally Polar Water flowing southward in the East Greenland Current defined as mean temperature $\leq 1°C$ and depth $\leq 750\,m$. The estimate of the volume transport across Fram Strait below $750\,m$ from the moorings is more complicated. The method of Beszczynska-Möller et al. (2012) which was developed to study the fluxes in the West Spitsbergen Current predicts a net southward transport of $3.2\,Sv$ below $750\,m$. This is unrealistic given that there are no connections between the Nordic Seas and the Arctic Ocean below the sill depth of the Greenland-Scotland Ridge ($750\,m$) other than Fram Strait. No vertical displacements of isopycnals in these two basins are observed that would suggest a non-zero net transport across Fram Strait below $750\,m$ (von Appen et al., 2015, in review). The large net transport inferred by Beszczynska-Möller et al. (2012) is due to errors and will be discussed in section 3.6. For these reasons we assume a net flux of $0\,Sv$ across Fram Strait for the deep waters below $750\,m$.

2.3 TTD method

A transit time distribution (TTD) model (Eq. 1) describes the propagation of a boundary condition into the interior of the ocean and is based on the Green's function (Hall and Plumb, 1994).

$$c(t_s,r) = \int_0^\infty c_0(t_s-t)e^{-\lambda t}\cdot G(t,r)dt \tag{1}$$

Here, $c(t_s,r)$ is the specific tracer concentration at year t_s and location r, $c_0(t_s-t)$ the boundary condition described by the tracer concentration at source year t_s-t and $G(t)$ the Green's function of the age spectra t of the tracer. The exponential term corrects for the decay rate of radioactive transient tracers. Equation 2 provides a possible solution of the TTD model, based on a steady and one-dimensional advective velocity and diffusion gradient (Waugh et al., 2003).

$$G(t) = \sqrt{\frac{\Gamma^3}{4\pi\Delta^2 t^3}}\cdot exp\left(\frac{-\Gamma(t-\Gamma)^2}{4\Delta^2 t}\right) \tag{2}$$

It is known as the Inverse-Gaussian transit time distribution (IG-TTD) where $G(t)$ is defined by the width of the distribution (Δ), the mean age (Γ) and the age spectra of the tracer (t). One can define a Δ/Γ ratio of the IG-TTD which represents the proportion between the advective and diffusive properties of the mixing processes as included in the TTD. The lower the Δ/Γ ratio, the higher is the advective share. A Δ/Γ ratio of 1.0 is the commonly applied ratio at several tracer surveys (e.g. Waugh et al., 2004, 2006; Tanhua et al., 2008; Schneider et al., 2010; Huhn et al., 2013; Schneider et al., 2014). Here we also applied this unity ratio to the ARK-XXVII/1 data set.

The application of chlorofluorocarbons (CFCs) is restricted due to partly indistinct input functions to the ocean since the early 1990s. This is related to the recently decreasing atmospheric concentrations of CFCs. To this end, dichlorodifluoromethane (CFC-12) data above the atmospheric concentration limit of $528\,ppt$ in 2012 (Bullister, 2015) have no clear time information and are thus not applicable.

2.4 Anthropogenic carbon and the TTD

The IG-TTD model can be used to estimate the total amount of anthropogenic carbon in the water column (Waugh et al., 2004). For this purpose it is assumed that the anthropogenic carbon behaves like an inert passive tracer, i.e. similar to a transient tracer. Then applying equation 1, the concentration of anthropogenic carbon in the interior ocean ($C_{ant}(t_s)$) is given by equation 3.

$$C_{ant}(t_s) = \int_\infty^0 C_{ant,0}(t_s-t)\cdot G(r,t)dt \tag{3}$$

$C_{ant,0}$ is the boundary condition of anthropogenic carbon at year t_s-t and $G(r,t)$ the distribution function (see equation 1). The historic boundary conditions are described by the differences between the preindustrial and modern DIC concentrations at the ocean surface. These anthropogenic offsets can be calculated by applying the modern (elevated) partial pressures of CO_2 and then subtracting the corresponding value of the preindustrial partial pressure. In each case, the preformed alkalinity was used as second parameter to determine the specific DIC concentrations (calculated using the Matlab version of the CO2SYS (van Heuven et al., 2011)). Here we assumed a constant $pCO_{2,water}$ saturation in the surface. Since exact saturations are not well constrained, we present sensitivity calculations of different saturation states / disequilibria (see section 3.6 below). The atmospheric history of $pCO_{2,atm}$ is taken from Tans and Keeling (2015). The preformed alkalinity was determined by using the alkalinity / salinity relationship of MacGilchrist et al. (2014). This relationship is based on surface alkalinity and salinity measurements in Fram Strait which were corrected for sea-ice melt and formation processes.

The time dependent boundary conditions ($C_{ant,0}$) and Eq. 3 can then be used to calculate anthropogenic carbon concentrations ($C_{ant}(t_s)$) and the corresponding mean age. Finally, the mean age of Eq. 3 can be set in relation to the transient tracer based mean age of the water and allows for back-calculating $C_{ant}(t_s)$, i.e. it provides the link between the tracer concentration and the anthropogenic carbon concentration.

3 Results and Discussion

3.1 Water masses in Fram Strait

To highlight the different transient tracer characteristics we defined the water mass type of each sample by using the water mass properties suggested by Rudels et al. (2000, 2005) and the salinity and temperature data of this cruise from Beszcynska-Möller and Wisotzki (2012). Note that this water mass classification is not based on an optimum multiparameter analysis and only serves as an indication for this specific purpose.

Water masses of the Arctic Ocean are the Polar Surface Water (PSW) which is the cold and less saline surface and halocline water; the warm Polar Surface Water, defined by a potential temperature (Θ) > 0, which comprises sea ice melt water due to interaction with warm Atlantic Water; the Arctic Atlantic Water / Return Atlantic Water which derives from sinking Atlantic Water due to cooling in the Arctic Ocean; the deep water masses are upper Polar Deep Water (uPDW), Canadian Basin Deep Water (CBDW) and Eurasian Basin Deep Water (EBDW). Deep water formation, e.g. on the Arctic shelves, usually involves densification from brine rejection. The Eurasian Basin Deep Water mixes with Greenland Sea Deep Water so that this layer corresponds to two sources in the Fram Strait (von Appen et al., 2015, in review).

Water masses of the Atlantic Ocean / Nordic Seas are the warm and saline Atlantic Water (AW) and the corresponding Recirculating Atlantic Water (RAW); the Arctic Intermediate Water which is mainly formed in the Greenland Sea; the Nordic Seas Deep Water which comprises Greenland Sea Deep Water (GSDW), Iceland Sea Deep Water (ISDW) and Norwegian Sea Deep Water (NSDW) and is formed by deep convection during winter time.

Figure 2 shows the zonal water mass distribution in Fram Strait, which also includes the data from the fast-ice section. The surface layer is dominated by Atlantic Water and Recirculating Atlantic Water in the east and by Polar Surface Water in the west with a transition between 6°W and 4°E where Polar Surface Water overlays the Atlantic Water. Warm Polar Surface Water can be found within the Atlantic Water between $4-8$°E. The Atlantic Water layer extends down to $\approx 600\,m$. Arctic Atlantic Water / Return Atlantic Water (AAW/RAAW) can be found at the upper continental slope of Greenland between $300-700\,m$. The intermediate layer between $500-1600\,m$ consists mainly of Arctic Intermediate Water and, at the Greenland slope, partly of Upper Polar Deep Water. Canadian Basin Deep Water can be found between $1600-2400\,m$ west of 4°E. Nordic Seas Deep Water is the prevailing water mass along the continental slope of Svalbard between $700-2400\,m$ but can be also observed in the range of the Canadian Basin Deep Water layer. The Eurasian Basin Deep Water / Greenland Sea Deep Water forms the bottom layer below $2400\,m$.

3.2 Transient tracer and DIC distributions

Figure 3 shows the partial pressure of CFC-12 and SF_6 along the zonal section. Both tracers have significant concentrations through the entire water column and show a similar distribution pattern. The Atlantic Water shows a relatively homogeneous distribution of both tracers with CFC-12 partial pressures $> 450\,ppt$ and SF_6 partial pressures $> 6\,ppt$. The Polar Surface Water at the shelf region shows a more distinct structure with partial pressures between $4-8\,ppt$ of SF_6 and $410-560\,ppt$ of CFC-12. The smaller concentration gradient of CFC-12 is related to the recently decreasing atmospheric concentration of CFC-12, which causes only slightly varying boundary conditions at the air-sea interface (see section 2.3). The high-tracer concentration layer of the Polar Surface Water extends further eastwards as overlaying tongue of the Atlantic Water between $2-6$°W. The intermediate layer between $500-1600\,m$ is characterized by a clear tracer minimum along the continental slope of Greenland with partial pressures between $1.8-4.0\,ppt$ of SF_6 and $150-350\,ppt$ of CFC-12 and mainly comprises Arctic Atlantic Water / Return Atlantic Water. East of this minimum, a remarkable tracer maximum can be observed at $1-3$°W with partial pressures between $3-6\,ppt$ of SF_6 and $250-450\,ppt$ of CFC-12. A smaller maximum can be observed between $5-6$°E at $\approx 1000\,m$ with partial pressures of $\approx 5\,ppt$ of SF_6 and $\approx 330\,ppt$ of CFC-12. Both tracer maxima probably correspond to extensive ventilation events which mainly affected the Arctic Intermediate Water and partly the Atlantic Water in the transition zone of both water masses. The Arctic Intermediate Water in the Fram Strait thus consists of recently ventilated areas and less ventilated areas which is also indicated by the large range of transient tracer concentrations. The remaining intermediate layer above $1700\,m$ is characterized by lower partial pressures between $2-3\,ppt$ of SF_6 and $150-300\,ppt$ of CFC-12 with decreasing concentrations with depth. This gradient extends throughout the deep water layers down to the bottom with partial pressures from $2\,ppt$ down to $0.2\,ppt$ of SF_6 and from $150\,ppt$ down to $34\,ppt$ of CFC-12. The fast-ice section is not presented here since it does not show any differences compared to the same longitude range of the zonal section.

Figure 4 shows the DIC concentrations along the zonal section separated into an upper and lower panel to highlight the different concentration ranges of the shallow and deep water layers. The Greenland shelf region shows concentrations between $1970\,\mu mol\,kg^{-1}$ in the surface and $2145\,\mu mol\,kg^{-1}$ at $\approx 200\,m$. The upper $200\,m$ between $4-8$°E shows increasing concentrations with depth between $2070\,\mu mol\,kg^{-1}$ and $2155\,\mu mol\,kg^{-1}$. There are three significant DIC maxima below $200\,m$. Two are located at the continental slope of Svalbard at $300-800\,m$ and at $1400-2100\,m$ with concentrations $> 2158\,\mu mol\,kg^{-1}$ and a maximum concentration of $2167\,\mu mol\,kg^{-1}$. The third maximum corresponds to the transient tracer maximum at $1-3$°W but extends fur-

ther eastwards with concentrations between $2158\,\mu mol\,kg^{-1}$ and $2162\,\mu mol\,kg^{-1}$. The area of the East Greenland Current at $3-8°$W is characterized by concentrations between $2118\,\mu mol\,kg^{-1}$ and $2152\,\mu mol\,kg^{-1}$. The deep water below $1700\,m$ shows concentrations between $2150\,\mu mol\,kg^{-1}$ and $2158\,\mu mol\,kg^{-1}$.

3.3 Transient tracers and the IG-TTD

The IG-TTD can be numerically constrained using transient tracer couples, CFC-12 and SF_6 in our case, which provides information about the mean age and the parameters of the IG-TTD (Waugh et al., 2002; Sonnerup et al., 2013; Stöven and Tanhua, 2014). The method of validity areas, introduced in Stöven et al. (2014), is used to determine the applicability of the tracer couple. For this purpose, the tracer age is calculated from the transient tracer concentrations (Waugh et al., 2003) which provides the tracer age relationship of the tracer couple. Figure 5 shows the tracer age relationship of our field data (colored by water mass) in relation to the range of theoretical tracer age relationships of the IG-TTD, i.e. for Δ/Γ ratios between $0.1-1.8$, which describe the range from advectively dominated to diffusively dominated water masses (grey shaded area). The black line in Fig. 5 denotes the tracer age relationship based on the unity ratio of $\Delta/\Gamma = 1.0$. Field data which corresponds to this unity ratio would be centered around the black line. The Fram Strait data can be separated into two branches of tracer age relationships. The upper branch consists of Atlantic Water / Recirculating Atlantic Water, Arctic Intermediate Water, Nordic Seas Deep Water, Eurasian Basin Deep Water / Greenland Sea Deep Water and Canadian Basin Deep Water whereas the lower branch consists of Polar Surface Water, warm Polar Surface Water, Arctic Atlantic Water / Return Atlantic Water and upper Polar Deep Water. The Polar Surface Water and warm Polar Surface Water can also partly be found in the upper branch for a SF_6 tracer age < 10 years. Note that the Arctic Atlantic Water / Return Atlantic Water and upper Polar Deep Water show a transition to the upper branch for a SF_6 tracer age larger than about 20 years. The data shows a more scattered and indistinct structure between 10 and 20 years of the SF_6 tracer age. However, the upper branch does not correspond to the unity ratio and, moreover, it is outside the validity area of the IG-TTD. Water masses related to the lower branch can be applied to the IG-TTD with tendencies towards higher Δ/Γ ratios (> 1.0) since the data is clearly above the black line indicating a dominance of diffusive processes.

Based on the raw field data, and on assumptions implemented in the IG-TTD (like 100 % saturation of the gases at the surface before entering deeper layers), the IG-TTD cannot describe the ventilation pattern of the different water masses in Fram Strait. Nevertheless, by comparing the shape of the two field data branches with the shape of the black line in Fig. 5, it is noted that both branches show similar characteristics as the unity ratio or, generally, as IG-TTD based tracer age relationships. This opens up the possibility to use the IG-TTD the other way around, i.e. to assume a fixed Δ/Γ ratio to determine the deviation of transient tracer concentrations rather than using the transient tracer concentration to determine the Δ/Γ ratio. Since several publications found the unity ratio of $\Delta/\Gamma = 1.0$ to be valid in large parts of the ocean, we assumed that this is also true for water masses in Fram Strait. Figure 6 shows the mean tracer age relationship of the upper branch (red line) and the tracer age relationship of the unity ratio (black line / same as in Fig. 5). The offset of the field data related to the unity ratio suggests an undersaturation of CFC-12 and / or a supersaturation of SF_6 (see black box in Fig. 6). This uncommon coexistence of under- and supersaturated transient tracers is discussed in the following section.

3.4 Saturations and excess SF_6

The surface saturations of transient tracers are influenced by sea surface temperature and salinity, ice coverage, wind speed, bubble effects, atmospheric growth rate of the tracer and the boundary dwell time of the water parcel (i.e. the time the water parcel is in contact with the atmosphere). However, the saturation state of transient tracers at the air-sea interface before, during and after water mass formation is rarely known, since water mass formation generally occurs in winter at high latitudes, which renders it almost impossible to obtain measurements. Shao et al. (2013) provide modelled data of monthly surface saturations of CFC-11, CFC-12 and SF_6 from 1936 to 2010 on a global scale. This model output can be used to estimate the tracer saturation ratio of different water masses by using the surface saturation of the specific formation area and yearly formation period. The formation types and areas are notably different for water masses that occur in Fram Strait. The model output shows high variabilities in surface saturations at different formation sites, namely the Greenland Sea, the Arctic shelf regions and the Arctic open water (Fig. 7 and 8). In contrast, the tracer age relationships of the two branches in Fig. 5 indicate relatively similar deviations in saturation. The complex boundary conditions in the Arctic, e.g. possible gas exchange through ice cover, might bias the results of the saturation model. Therefore, we only used the surface saturation of the Greenland Sea (Area 1 in Fig. 7 and 8) which agrees with the findings of Tanhua et al. (2008) who used available field data to investigate historic tracer saturations. The IG-TTD based mean age provides the link between the observed tracer concentrations and the corresponding time-dependent saturation factors. Therefore, the saturation factors were applied to the atmospheric history (boundary conditions) of each tracer. These new boundary conditions are then applied to the measured tracer concentrations and the IG-TTD which then yields a saturation-corrected mean age. This mean age in turn can then be used to back-calculate the saturation-corrected tracer concentrations using the originally (uncorrected) boundary conditions. We expect that undersaturation effects also hold for SF_6 but

are counterbalanced by effects of supersaturation in this survey area.

The SF_6 excess is estimated using the corrected CFC-12 concentrations and the IG-TTD ($\Delta/\Gamma = 1.0$) to calculate theoretical SF_6 concentrations of the water parcel, i.e. back-calculated SF_6 concentrations. The difference between the theoretical SF_6 concentration and the measured SF_6 concentration denotes the SF_6 excess in the water. Note that this SF_6 excess is based on the assumption that the IG-TTD and unity ratio describe the prevailing ventilation pattern of the water masses. Figure 9 shows the SF_6 excess in $fmol\,kg^{-1}$ and ppt for depths below $200\,m$. This upper depth limit is invoked by the fact that CFC-12 concentrations above the current atmospheric concentration limit cannot be applied to the IG-TTD. The SF_6 excess is much higher ($0.5-0.8\,fmol\,kg^{-1}$ / $1.0-1.6\,ppt$) for northwards propagating water masses compared to water masses of Arctic origin ($0-0.4\,fmol\,kg^{-1}$ / $0-0.8\,ppt$). There are at least two possible effects which can cause such significant supersaturations of SF_6.

One possibility refers to the deliberate tracer release experiment in 1996 where $320\,kg$ ($\approx 2190\,mol$) of SF_6 were introduced into the central Greenland Sea (Watson et al., 1999). The patch was redistributed by mixing processes and entered the Arctic Ocean via the Fram Strait and Barents Sea Opening and the North Atlantic via Denmark Strait and the Faroe Bank Channel (Olsson et al., 2005; Tanhua et al., 2005). Assuming that $50-80$ % of the deliberatly released SF_6 still remains in the northern North Atlantic and the Arctic Ocean ($1095-1752\,mol$) and that $10-50$ % of the corresponding total volume of $1.875\cdot10^{18}-9.375\cdot10^{18}\,l$ (Eakins and Sharman, 2010) is affected, a mean offset of $0.12-0.93\,fmol\,l^{-1}$ is estimated. This mean offset is thus in the range of the observed SF_6 excess concentrations. However, CFC-12 and SF_6 data of the Southern Ocean (Stöven et al., 2014) shows similar tracer age relationships compared to the Fram Strait data but with no influence of deliberately released SF_6. This indicates that probably an additional source of excess SF_6 exists.

Liang et al. (2013) introduced a model which estimates supersaturations of dissolved gases by bubble effects in the ocean. This model predicted an increasing supersaturation for increasing wind speed and decreasing temperature, i.e. the bubble effect becomes more significant at high latitudes. Furthermore, Liang et al. (2013) show that the magnitude of supersaturation depends on the solubility of the gas. The less soluble a gas, the more supersaturation can be expected. Supporting this, Stöven et al. (2014) describe surface measurements of SF_6 and CFC-12 directly after heavy wind conditions in the Southern Ocean where SF_6 supersaturations between $20-50$ % could be observed. The CFC-12 concentrations were only affected to a minor extent which indeed seems to be explained by the differences in solubility. This bubble induced supersaturation can also be expected to apply during the process of water mass formation in the Greenland Sea which usually occurs during late winter, i.e. during a period with low surface temperatures and heavy wind conditions. Furthermore, looking at the maximum SF_6 excess in the Arctic Intermediate Water layer in Fig. 9 and the generally elevated tracer concentrations of CFC-12 and SF_6 in the same area (see Fig. 3) reaffirms the assumption of bubble induced supersaturation of SF_6. However, this hypothesis stands in opposition to the current assumption that trace gases are generally undersaturated during water mass formation (Tanhua et al., 2008; Shao et al., 2013).

Future investigations are necessary to determine the different impact of under- and supersaturation effects on soluble gases at the air-sea interface. It can be expected that possible scenarios are not restricted to distinct saturation states anymore but rather comprise mixtures of equilibrated, under- and supersaturated states of the different gases.

3.5 Anthropogenic carbon and mean age

Since CFC-12 is not affected by tracer release experiments and possibly only to minor extent by bubble effects we used this tracer to calculate the mean age of the water and the corresponding anthropogenic carbon content. SF_6 was only used in the surface and upper halocline, i.e. where CFC-12 exceeds the atmospheric concentration limit of $528\,ppt$ and where effects of SF_6 supersaturation are comparatively small. Saturation-corrected tracer data was applied for subsurface data below $100\,m$ whereas surface data was found to be near equilibrium state with the atmosphere. Figure 10 shows the anthropogenic carbon distribution in $\mu mol\,kg^{-1}$ and Fig. 11 shows the mean age of the water masses. According to the relation between transient tracers, mean age and anthopogenic carbon, the distribution patterns are similar as for the transient tracers. The highest anthropogenic carbon concentrations of $50-55\,\mu mol\,kg^{-1}$ can be found in the upper $600\,m$ of the Atlantic Water / Recirculating Atlantic Water and a little lower concentrations of $40-45\,\mu mol\,kg^{-1}$ in the Polar Surface Water / warm Polar Surface Water layer. The mean age of these water masses is between $0-20$ years. Note that these water layers show the highest mean current velocities in Fram Strait (see section 3.7 below). The area of the tracer maximum at $1-3$°W shows elevated concentrations of $35-40\,\mu mol\,kg^{-1}$ and a mean age of $20-40$ years. The remaining water layers below $600\,m$ show anthropogenic carbon concentrations lower than $35\,\mu mol\,kg^{-1}$ with decreasing concentrations with increasing depth and is comparatively low ($<10\,\mu mol\,kg^{-1}$) in deep water masses such as Canadian Basin Deep Water and Eurasian Basin Deep Water / Greenland Sea Deep Water. Accordingly, the mean age increases with increasing depth from 30 years to 280 years and shows a maximum mean age of 286 years in the bottom layer at the prime meridian. Table 1 shows the mean values and standard deviation of each specific water layer.

The determined values correspond to the findings of Jutterström and Jeansson (2008) who used a similar method to de-

termine anthropogenic carbon of the East Greenland Current in 2002. The Fram Strait section of their data set shows a similar distribution pattern of anthropogenic carbon but with lower concentration levels compared to our data from 2012. The concentration differences indicate an increase of the anthropogenic carbon content between $25-35$ % in the entire water column during the elapsed ten years. This corresponds to an increase of $2\,\mu mol\,kg^{-1}\,yr^{-1}$ in the Atlantic Water, $1\,\mu mol\,kg^{-1}\,yr^{-1}$ in the Polar Water and between $0.5-1\,\mu mol\,kg^{-1}\,yr^{-1}$ in the deeper water layers. Based on these current rates of increase it can be assumed that the import of anthropogenic carbon by Atlantic Water becomes more dominant compared to the export by Polar Water.

3.6 Sensitivities on anthropogenic carbon

The calculations presented above are based on the ideal case of $pCO_{2,atm}$=$pCO_{2,water}$ at the sea surface before entering the ocean interior, and the assumption that the saturation correction of the tracers and the unity ratio of the IG-TTD are true for water masses in the Fram Strait. Since the three parameters involved cannot be directly determined it is very likely that deviations from the ideal case exist. Therefore we present the corresponding sensitivities in the following. The sensitivities are determined by changing only one parameter and keeping the others constant at ideal conditions.

Figure 12a and 12b show the sensitivities of changes in tracer saturation using the example of CFC-12 since most of the anthropogenic carbon calculations are based on this tracer. Small deviations of ±5 % in CFC-12 saturations cause only small deviations of anthropogenic carbon concentrations of $\pm1\,\mu mol\,kg^{-1}$ / $\pm2-4$ %. Furthermore, the sensitivity depends on the partial pressure range of CFC-12. The lower the partial pressure the less sensitive is the anthropogenic carbon concentrations to changes in CFC-12 saturation. The maximum deviations are $\pm6\,\mu mol\,kg^{-1}$ / $\pm11-16$ % for partial pressure $> 400\,ppt$. The white patches in Fig. 12a and 12b correspond to supersaturations which exceed the atmospheric concentration limit of CFC-12.

Figure 12c and 12d show the sensitivities due to changes in the Δ/Γ-ratio of the IG-TTD. The sensitivity is very low ($< 1\,\mu mol\,kg^{-1}$ / < 5 %) for most of the ratio and concentration range. Partial pressures below $100\,ppt$ and $\Delta/\Gamma < 0.4$ show the highest sensitivty with deviations between $5-10\,\mu mol\,kg^{-1}$ / $50-200$ %. The unusual sensitivity distribution is related to the indistinct boundary condition of CFC-12 in recent years and the distribution function of the TTD. For more information see Stöven et al. (2014).

The sensitivities of deviations in pCO_2 saturations are shown in Fig. 12e and 12f. The absolute error is characterized by a relatively steady change with changing saturation states. The absolute error is more or less independent of the partial pressure of CFC-12 and leads to maximum deviations of $\pm20-25\,\mu mol\,kg^{-1}$. The relative error ($0-200$ %) shows an increasing sensitivity of anthropogenic carbon concentrations to changes in pCO_2 saturations and decreasing CFC-12 partial pressures. Note that a negative deviation of 100 % corresponds to a anthropogenic carbon concentration of $0\,\mu mol\,kg^{-1}$ which is also indicated by the turning-points where the contour lines continue parallel to the x-axis in Fig. 12e. This indicates that small uncertainties in pCO_2 saturations can cause large errors in anthropogenic carbon estimates for low tracer concentrations, i.e. for a high mean age of the water. The uncertainty of the pCO_2 saturation remains as the largest error source although the saturation of pCO_2 and CFC-12 counteract each other.

3.7 Carbon transport estimates

Table 2 shows the transport estimates of DIC and anthropogenic carbon separated into northwards propagating (positive values) and southwards propagating (negative values) water masses. The northwards flux comprises the Atlantic Water of the West Spitsbergen Current, the southwards flux comprises the Recirculating / Return Atlantic Water and the Polar Water of the East Greenland Current. The mean flux of deep water layers below $750\,m$ was taken to be $0\,Sv$ and therefore not considered for this estimate. The water masses were defined as described in section 2.2.

The northwards flux transports $3420 \pm 2497\,Tg\,C\,yr^{-1}$ (mean $\pm$ standard deviation) of DIC and $82 \pm 59\,Tg\,C\,yr^{-1}$ of anthropogenic carbon into the Arctic Ocean. This input is counterbalanced by an export of $2274 \pm 5080\,Tg\,C\,yr^{-1}$ / $54 \pm 120\,Tg\,C\,yr^{-1}$ by Recirculating and Return Atlantic Water and $1117 \pm 660\,Tg\,C\,yr^{-1}$ / $23 \pm 13\,Tg\,C\,yr^{-1}$ by Polar Water. The carbon transport uncertainties are relatively high, especially with respect to the error range of the Recirculating / Return water masses of the Atlantic Water. Furthermore, there is a lack of water transport data on the Greenland shelf region, e.g. Belgica Bank, and thus we cannot with great confidence decide whether more anthropogenic carbon is transported into or out of the Arctic region through the Fram Strait.

3.8 Uncertainties

The applicability of IG-TTD model at high latitudes, like in the Fram Strait or the Southern Ocean, is supposed to be limited by complex water mass mixing and ventilation patterns. They should rather be described by more refined models like the maximum entropy method by Holzer and Primeau (2012). The main uncertainty factor is related to the assumption that different saturation states of the transient tracers are responsible for the tracer age relationships rather than specific mixing processes and that thereby the IG-TTD model is valid for all water masses in the Fram Strait. The uncertainties of the IG-TTD model depend on the shape of the IG-TTD, i.e. the Δ/Γ-ratio, and the uncertainties of the boundary conditions and the measurement precision of the transient

tracers and apparent transient tracers (see section 3.6 above). The flux estimates are based on transient tracer and DIC data of the ARK-XXVII/1 cruise which only show the specific distribution pattern during June / July 2012 and thus neglect any interannual variabilities of the parameters. The determination of the preformed alkalinity highly depends on the used method. Here we used the linear relationship between surface alkalinity and salinity which is a commonly used method. However, other authors recommend the use of data from the subsurface layer (Vazquez-Rodriguez et al., 2012) or the surface temperature and salinity dependencies (Lee et al., 2006). The transport estimates are complicated by the fact that the flow field in Fram Strait is dominated by many small scale features. The Rossby radius is $4-6\,km$ which means that the mooring spacing is only able to fully resolve the mesoscale near the shelfbreak in the West Spitsbergen Current. Otherwise, eddies may be aliased between the moorings. The velocities in the recirculation area in the center of Fram Strait are actually mostly westward (Beszczynska-Möller et al., 2012) and thus along the mooring array line. Therefore, the meridional velocities in the center of Fram Strait are only the small residuals of much larger zonal velocities. As a result the finite accuracy and precision of the current direction measurements has a big impact on the meridional exchanges. Additionally, at depth the flow is topographically steered, but the topographic features are also not fully resolved. Interannual variations are also neglected here, but they are small (Beszczynska-Möller et al., 2012). The exchange flow across Fram Strait below $750\,m$ (sill depth of Greenland-Scotland ridge and depth horizon of the third instruments on the moorings) is assumed to be $0\,Sv$ for the present purpose.

4 Conclusions

Measurements of the transient tracers CFC-12 and SF_6 along $78°50'$N in the Fram Strait in 2012 show specific characteristics of the different water masses. The tracer age relationship between both tracers can be separated into two major branches. One branch describes the tracer age relationship of water masses of Atlantic origin as well as deep water masses, the other describes water masses of Arctic origin. We assumed that the different tracer age relationships are due to different saturation effects on the tracers during water mass formation and still existing offsets of the SF_6 concentrations caused by the deliberate tracer release experiment in the Greenland Sea in 1996. The CFC-12 data was saturation corrected by applying the model output of Shao et al. (2013). The corrected data was used to back-calculate theoretical SF_6 data based on the IG-TTD which then provides the excess concentrations of SF_6. The largest excess concentrations of $0.5-0.8\,fmol\,kg^{-1}$ were found for the intermediate layer between $500\,m$ and $1600\,m$.

The anthropogenic carbon content was estimated using the IG-TTD and saturation-corrected CFC-12 data in the ocean interior (depths below $100\,m$) and SF_6 in the surface layer. The Atlantic Water and Recirculating Atlantic Water is characterized by anthropogenic carbon concentrations of $50-55\,\mu mol\,kg^{-1}$ and the Polar Surface Water by concentrations of $40-45\,\mu mol\,kg^{-1}$. Maximum concentrations of $35-40\,\mu mol\,kg^{-1}$ in the intermediate layer can be found at $1-3°$W. Deep water layers show decreasing concentrations with increasing depth from $35\,\mu mol\,kg^{-1}$ down to $\approx 10\,\mu mol\,kg^{-1}$.

The mean current velocity data obtained by a mooring-array at $78°50'$N between 2002 and 2010 suggests a mean northwards flux of $4.2\,(\pm 3.0)\,Sv$ of Atlantic Water (West Spitsbergen Current) and a mean southward flux of $2.8\,(\pm 6.2)\,Sv$ of Recirculating / Return Atlantic Water and $1.4\,(\pm 0.8)\,Sv$ of Polar Water (East Greenland Current). The net flux of water masses below $750\,m$ was taken to be $0\,Sv$. The high uncertainties of the flux data in the Fram Strait inhibit any statements about dominating shares of DIC and anthropogenic exports or imports to the Arctic Ocean. However, the flux estimates indicate a balanced transport budget with a northward flux of $3420\,(\pm 2497)\,Tg\,C\,yr^{-1}$ of DIC and $82\,(\pm 59)\,Tg\,C\,yr^{-1}$ of anthropogenic carbon by Atlantic Water and a southward flux of $2274\,(\pm 5080)\,Tg\,C\,yr^{-1}$ / $54\,(\pm 120)\,Tg\,C\,yr^{-1}$ by Recirculating and Return Atlantic Water and $1117\,(\pm 660)\,Tg\,C\,yr^{-1}$ / $23\,(\pm 13)\,Tg\,C\,yr^{-1}$ by Polar Water.

Acknowledgements. This work was supported by the Deutsche Forschungsgemeinschaft (DFG) in the framework of the priority programme "Antarctic Research with comparative investigations in Arctic ice areas" by a grant to T. Tanhua and M. Hoppema: Carbon and transient tracers dynamics: A bi-polar view on Southern Ocean eddies and the changing Arctic Ocean (TA 317/5, HO 4680/1). Partial support to T. Tanhua and M. Hoppema was received from EU FP7 project CARBOCHANGE "Changes in carbon uptake and emissions by oceans in a changing climate" (European Community's 7th Framework Programme, grant agreement no. 264879). We are grateful to the Alfred-Wegener-Institut for participation in Polarstern cruise ARK-XXVII/1. We are happy to acknowledge the great support by the master and crew of Polarstern, the chief scientist and the scientific party. Special thanks goes to Boie Bogner for his technical support during the ARK-XXVII/1 cruise.

References

Beszcynska-Möller, A. and Wisotzki, A.: Physical oceanography during POLARSTERN cruise ARK-XXVII/1, Alfred Wegener Institute, Helmholtz Center for Polar and Marine Research, Bremerhaven, doi: 10.1594/PANGAEA.801791, 2012.

Beszczynska-Möller, A.: The expedition of the research vessel Polarstern to the Arctic in 2012 (ARK-XXVII/1), Reports on polar and marine research, 660, 1–78, doi: 10.2312/BzPM_0660_2013, 2013.

Beszczynska-Möller, A., Fahrbach, E., Schauer, U., and Hansen, E.: Variability in Atlantic water temperature and transport at the en-

trance to the Arctic Ocean, 1997-2010, ICES Journal of Marine Science: Journal du Conseil, 69, 852–863, 2012.

Bullister, J.: Atmospheric Histories (1765-2015) for CFC-11, CFC-12, CFC-113, CCl_4, SF_6 and N_2O, Carbon Dioxide Information Analysis Center, http://cdiac.ornl.gov/ftp/oceans/CFC_ATM_Hist/CFC_ATM_Hist_2015, doi: 10.3334/CDIAC/otg.CFC_ATM_Hist_2015, 2015.

Bullister, J. L. and Wisegarver, D.: The shipboard analysis of trace levels of sulfur hexafluoride, chlorofluorocarbon-11 and chlorofluorocarbon-12 in seawater, Deep Sea Res. Part I, 55, 1063 – 1074, 2008.

de Steur, L., Hansen, E., Mauritzen, C., Beszczynska-Möller, A., and Fahrbach, E.: Impact of recirculation on the East Greenland Current in Fram Strait: Results from moored current meter measurements between 1997 and 2009, Deep Sea Res., 92, 26–40, 2014.

Dickson, A., Sabine, C., and Chrisitan, J.: Guide to Best Practices for Ocean CO_2 Measurements, 2007.

Eakins, B. and Sharman, G.: Volumes of the World's Ocean from ETOPO1, NOAA National Geophysical Data Center, http://ngdc.noaa.gov/mgg/global/etopo1_ocean_volumes.html, 2010.

Fahrbach, E., Meincke, J., Østerhus, S., Rohardt, G., Schauer, U., Tverberg, V., and Verduin, J.: Direct measurements of volume transports through Fram Strait, Polar Research, 20, 217–224, doi: 10.1111/j.1751-8369.2001.tb00059.x, 2001.

Hall, T. M. and Plumb, R. A.: Age as a diagnostic of stratospheric transport, J. Geophys. Res., 99, 1059–1070, 1994.

Holzer, M. and Primeau, F. W.: Improved constraints on transit time distributions from argon 39: A maximum entropy approach, J. Geophys. Res.: Oceans, 115, doi: 10.1029/2010JC006410, 2012.

Huhn, O., Rhein, M., Hoppema, M., and van Heuven, S.: Decline of deep and bottom water ventilation and slowing down of anthropogenic carbon storage in the Weddell Sea, 1984-2011, Deep Sea Res. Part I, 76, 66–84, doi:10.1016/j.dsr.2013.01.005, 2013.

Johnson, K., Wills, K., Butler, D., Johnson, W., and Wong, C.: Coulometric total carbon dioxide analysis for marine studies: maximizing the performance of an automated gas extraction system and coulometric detector, Marine Chemistry, 44, 167–187, doi: 10.1016/0304-4203(93)90201-X, 1993.

Johnson, K. M., Dickson, A. G., Eischeid, G., Goyet, C., Guenther, P., Key, R. M., Millero, F. J., Purkerson, D., Sabine, C. L., Schottle, R. G., Wallace, D. W., Wilke, R. J., and Winn, C. D.: Coulometric total carbon dioxide analysis for marine studies: assessment of the quality of total inorganic carbon measurements made during the US Indian Ocean CO_2 Survey 1994-1996, Marine Chemistry, 63, 21–37, doi: 10.1016/S0304-4203(98)00048-6, 1998.

Jutterström, S. and Jeansson, E.: Anthropogenic carbon in the East Greenland Current, Prog. Oceanogr., 78, 29–36, doi: 10.1016/j.pocean.2008.04.001, 2008.

Karcher, M., Smith, J. N., Kauker, F., Gerdes, R., and Smethie, W. M.: Recent changes in Arctic Ocean circulation revealed by iodine-129 observations and modeling, J. Geophys. Res.: Oceans (1978–2012), 117, 2012.

Kurtz, N., Markus, T., Farrell, S., Worthen, D., and Boisvert, L.: Observations of recent Arctic sea ice volume loss and its impact on ocean-atmosphere energy exchange and ice production, Journal of Geophysical Research: Oceans, 116, doi: 10.1029/2010JC006235, 2011.

Kwok, R., Cunningham, G., Wensnahan, M., Rigor, I., Zwally, H., and Yi, D.: Thinning and volume loss of the Arctic Ocean sea ice cover: 2003-2008, Journal of Geophysical Research: Oceans, 114, doi: 10.1029/2009JC005312, 2009.

Law, C. S., Watson, A. J., and Liddicoat, M. I.: Automated vacuum analysis of sulphur hexafluoride in seawater: derivation of the atmospheric trend (1970-1993) and potential as a transient tracer, Mar. Chem., 48, 57 – 69, 1994.

Lee, K., Tong, L., Millero, F., Sabine, C., Dickson, A., Goyet, C., Park, G., Wanninkhof, R., Feely, R., and Key, R.: Global relationships of total alkalinity with salinity and temperature in surface waters of the worlds oceans, Geophys. Res. Lett., 33, doi: 10.1029/2006GL027207, 2006.

Liang, J.-H., Deutsch, C., McWilliams, J. C., Baschek, B., Sullivan, P. P., and Chiba, D.: Parameterizing bubble-mediated air-sea gas exchange and its effect on ocean ventilation, Global Biogeochem. Cycles, 27, 894–905, doi: 10.1002/gbc.20080, 2013.

MacGilchrist, G., Naveira Garabato, A., Tsubouchi, T., Bacon, S., Torres-Valdes, S., and Azetsu-Scott, K.: The Arctic Ocean carbon sink, Deep Sea Res. Part I: Oceanographic Research Papers, 86, 39 – 55, doi: 10.1016/j.dsr.2014.01.002, 2014.

Marnela, M., Rudels, B., Houssais, M., Beszczynska-Möller, A., and Eriksson, P.: Recirculation in the Fram Strait and transports of water in and north of the Fram Strait derived from CTD data, Ocean Sci., 9, 499–519, 2013.

Mintrop, L., Pérez, F. F., González-Dávila, M., Santana-Casiano, J. M., Körtzinger, A., et al.: Alkalinity determination by potentiometry: Intercalibration using three different methods, Ciencias Marinas, 26, 23–37, 2000.

Olsson, K. A., Jeansson, E., Tanhua, T., and Gascard, J.-C.: The East Greenland Current studied with CFCs and released sulphur hexafluoride, J. Mar. Sys., 55, 77–95, doi: 10.1016/j.jmarsys.2004.07.019, 2005.

Polyakov, I., Beszczynska, A., Carmack, E., Dmitrenko, I., Fahrbach, E., Frolov, I., Gerdes, R., Hansen, E., Holfort, J., Ivanov, V., Johnson, M., Karcher, M., Kauker, F., Morison, J., Orvik, K. A., Schauer, U., Simmons, H., Skagseth, Ø., Sokolov, V., Steele, M., Timokhov, L., Walsh, D., and Walsh, J.: One more step toward a warmer Arctic, Geophysical Research Letters, 32, doi: 10.1029/2005GL023740, 2005.

Rudels, B., Meyer, R., Fahrbach, E., Ivanov, V., Österhus, S., Quadfasel, D., Schauer, U., Tverberg, V., and Woodgate, R.: Water mass distribution in Fram Strait and over the Yermak Plateau in summer 1997, Annales Geophysicae, 18, 687–705, doi: 10.1007/s00585-000-0687-5, 2000.

Rudels, B., Björk, G., Nilsson, J., Winsor, P., Lake, I., and Nohr, C.: The interaction between waters from the Arctic Ocean and the Nordic Seas north of Fram Strait and along the East Greenland Current: results from the Arctic Ocean-02 Oden expedition, Journal of Marine Systems, 55, 1 – 30, doi: 10.1016/j.jmarsys.2004.06.008, 2005.

Rudels, B., Marnela, M., and Eriksson, P.: Constraints on Estimating Mass, Heat and Freshwater Transports in the Arctic Ocean: An Exercise, in: Arctic-Subarctic Ocean Fluxes, edited by Dickson, R., Meincke, J., and Rhines, P., pp. 315–341, Springer Netherlands, doi: 10.1007/978-1-4020-6774-7_14, 2008.

Rudels, B., Korhonen, M., Budéus, G., Beszczynska-Möller, A., Schauer, U., Nummelin, A., Quadfasel, D., and Valdimarsson, H.: The East Greenland Current and its impacts on the

Nordic Seas: observed trends in the past decade, ICES Journal of Marine Science: Journal du Conseil, 69, 841–851, doi: 10.1093/icesjms/fss079, 2012.

Schauer, U. and Beszczynska-Möller, A.: Problems with estimation and interpretation of oceanic heat transport - conceptual remarks for the case of Fram Strait in the Arctic Ocean, Ocean Science, 5, 487–494, doi: 10.5194/os-5-487-2009, 2009.

Schauer, U., Fahrbach, E., Østerhus, S., and Rohardt, G.: Arctic warming through the Fram Strait: Oceanic heat transport from 3 years of measurements, Journal of Geophysical Research: Oceans, 109, doi: 10.1029/2003JC001823, 2004.

Schauer, U., Beszczynska-Möller, A., Walczowski, W., Fahrbach, E., Piechura, J., and Hansen, E.: Variation of Measured Heat Flow Through the Fram Strait Between 1997 and 2006, in: Arctic-Subarctic Ocean Fluxes, edited by Dickson, R., Meincke, J., and Rhines, P., pp. 65–85, Springer Netherlands, doi: 10.1007/978-1-4020-6774-7_4, 2008.

Schneider, A., Tanhua, T., Koertzinger, A., and Wallace, D.: High anthropogenic carbon content in the eastern Mediterranean, J. Geophys. Res., 115, doi:10.1029/2010JC006171, 2010.

Schneider, A., Tanhua, T., Roether, W., and Steinfeldt, R.: Changes in ventilation of the Mediterranean Sea during the past 25 year, Ocean Sci., 10, 1–16, doi: 10.5194/os-10-1-2014, 2014.

Shao, A. E., Mecking, S., Thompson, L., and Sonnerup, R. E.: Mixed layer saturations of CFC-11, CFC-12, and SF6 in a global isopycnal model, J. Geophys. Res.: Oceans, 118, 4978–4988, doi: 10.1002/jgrc.20370, 2013.

Sonnerup, R., Mecking, S., and Bullister, J.: Transit time distributions and oxygen utilization rates in the Northeast Pacific Ocean from chlorofluorocarbons and sulfur hexafluoride, Deep Sea Res. Part I, 72, 61 – 71, doi: 10.1016/j.dsr.2012.10.013, 2013.

Stöven, T. and Tanhua, T.: Ventilation of the Mediterranean Sea constrained by multiple transient tracer measurements, Ocean Sci., 10, 439–457, doi: 10.5194/os-10-439-2014, 2014.

Stöven, T., Tanhua, T., Hoppema, M., and Bullister, J.: Transient tracer applications in the Southern Ocean, Ocean Sci. Discuss., 11, 2289–2335, doi: 10.5194/osd-11-2289-2014, 2014.

Stroeve, J., Serreze, M., Drobot, S., Gearheard, S., Holland, M., Maslanik, J., Meier, W., and Scambos, T.: Arctic Sea Ice Extent Plummets in 2007, Eos, Transactions American Geophysical Union, 89, 13–14, doi: 10.1029/2008EO020001, 2008.

Tanhua, T., Bulsiewicz, K., and Rhein, M.: Spreading of Overflow Water from the Greenland to the Labrador Sea, Geophys. Res. Lett., 32, doi: 10.1029/2002GL0227700, 2005.

Tanhua, T., Waugh, D. W., and Wallace, D. W. R.: Use of SF_6 to estimate anthropogenic CO_2 in the upper ocean, J. Geophys. Res., 113, 2156–2202, doi:10.1029/2007JC004416, 2008.

Tans, P. and Keeling, R.: Full Mauna Loa CO_2 record, NOAA/ESRL, www.esrl.noaa.gov/gmd/ccgg/trends/, 2015.

Tsubouchi, T., Bacon, S., Naveira Garabato, A. C., Aksenov, Y., Laxon, S. W., Fahrbach, E., Beszczynska-Möller, A., Hansen, E., Lee, C. M., and Ingvaldsen, R. B.: The Arctic Ocean in summer: A quasi-synoptic inverse estimate of boundary fluxes and water mass transformation, Journal of Geophysical Research: Oceans, 117, doi: 10.1029/2011JC007174, 2012.

van Heuven, S., Pierrot, D., Rae, J., Lewis, E., and Wallace, D.: MATLAB Program Developed for CO2 System Calculations, Carbon Dioxide Information Analysis Center, doi: 10.3334/CDIAC/otg.CO2SYS_MATLAB_v1.1, 2011.

Vazquez-Rodriguez, M., Padin, X., Pardo, P., Rios, A., and Perez, F.: The subsurface layer reference to calculate preformed alkalinity and air-sea CO_2 disequilibrium in the Atlantic Ocean, J. Mar. Sys., 94, 52–63, 2012.

Vellinga, M., Dickson, B., and Curry, R.: The Changing View on How Freshwater Impacts the Atlantic Meridional Overturning Circulation, in: Arctic-Subarctic Ocean Fluxes, edited by Dickson, R., Meincke, J., and Rhines, P., pp. 289–313, Springer Netherlands, doi: 10.1007/978-1-4020-6774-7_13, 2008.

von Appen, W.-J., Schauer, U., Cabrillo, R. S., Bauerfeind, E., and Beszczynska-Möller, A.: Exchange of warming deep waters across Fram Strait, Deep Sea Res., 2015, in review.

Wadley, M. and Bigg, G.: Impact of flow through the Canadian Archipelago and Bering Strait on the North Atlantic and Arctic circulation: An ocean modelling study, Quarterly Journal of the Royal Meteorological Society, 128, 2187–2203, doi: 10.1256/qj.00.35, 2002.

Watson, A., Messias, M., Fogelqvist, E., Scoy, K. V., Johannessen, T., Oliver, K., Stevens, D., Rey, F., Tanhua, T., Olsson, K., Carse, F., Simonsen, K., Ledwell, J., Jansen, E., Cooper, D., Kruepke, J., and Guilyardi, E.: Mixing and convection in the Greenland Sea from a tracer-release experiment, Nature, 401, 902–904, doi: 10.1038/44807, 1999.

Waugh, D. W., Vollmer, M. K., Weiss, R. F., Haine, T. W. N., and Hall, T. M.: Transit time distributions in Lake Issyk-Kul, Geophys. Res. Lett., 29, 84–1–84–4, doi:10.1029/2002GL016201, 2002.

Waugh, D. W., Hall, T. M., and Haine, T. W. N.: Relationships among tracer ages, J. Geophys. Res., 108, doi:10.1029/2002JC001325, 2003.

Waugh, D. W., Haine, T. W. N., and Hall, T. M.: Transport times and anthropogenic carbon in the subpolar North Atlantic Ocean, Deep Sea Res. Part I, 51, 1475 – 1491, 2004.

Waugh, D. W., Hall, T. M., McNeil, B. I., Key, R., and Matear, R. J.: Anthropogenic CO_2 in the oceans estimated using transit time distributions, Tellus Ser. B, 58, 376 – 389, 2006.

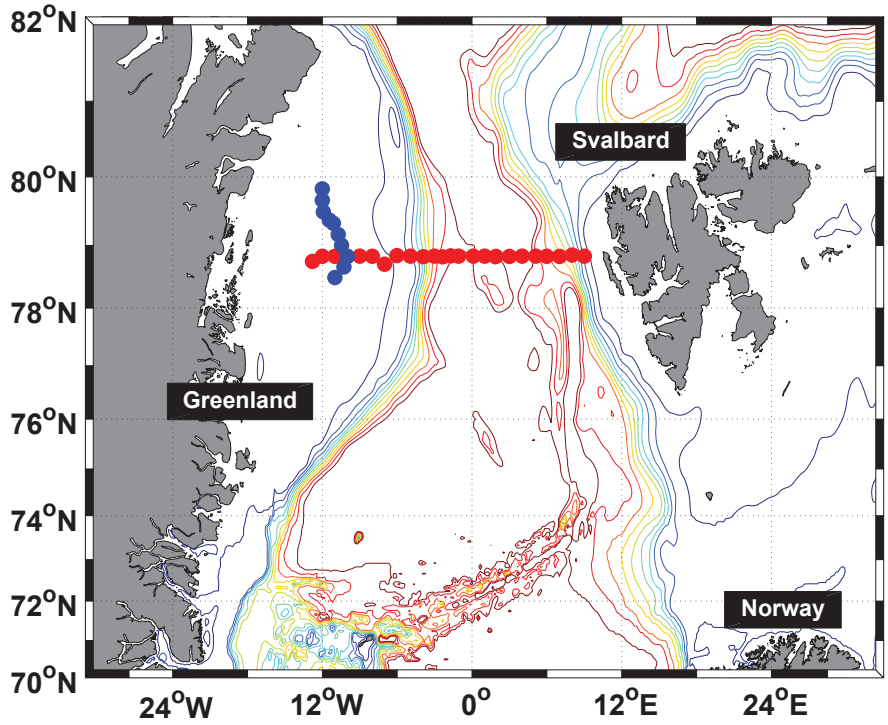

Fig. 1: Sample stations of the ARK-XXVII/1 cruise in 2012. The zonal stations are highlighted as red dots and the meridional stations along the fast ice edge as blue dots. The depth contours are 250:250:2500.

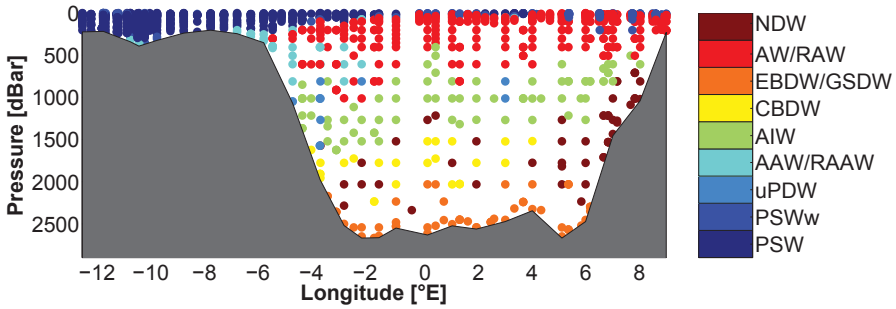

Fig. 2: Water masses in Fram Strait: Nordic Seas Deep Water (NDW), Atlantic Water / Recirculating Atlantic Water (AW / RAW), Eurasian Basin Deep Water (EBDW) / Greenland Sea Deep Water (GSDW), Canadian Basin Deep Water (CBDW), Arctic Intermediate Water (AIW), Arctic Atlantic Water (AAW) / Return Atlantic Water (RAAW), Upper Polar Deep Water (uPDW), Polar Surface Water warm (PSWw) and Polar Surface Water (PSW).

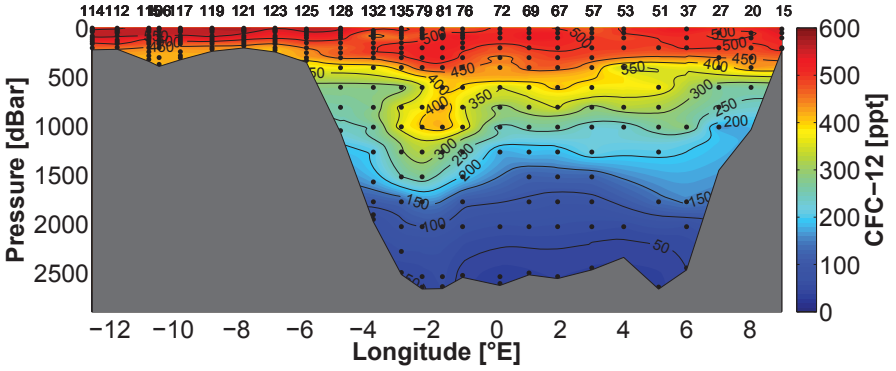

(a)

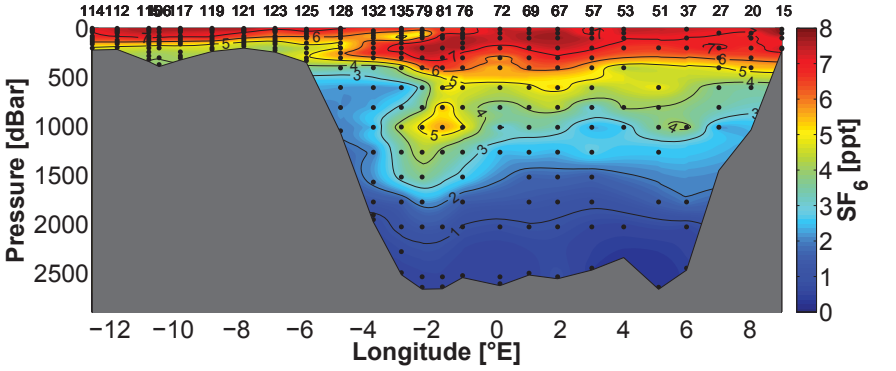

(b)

Fig. 3: (**a**) CFC-12 and (**b**) SF_6 partial pressure in ppt.

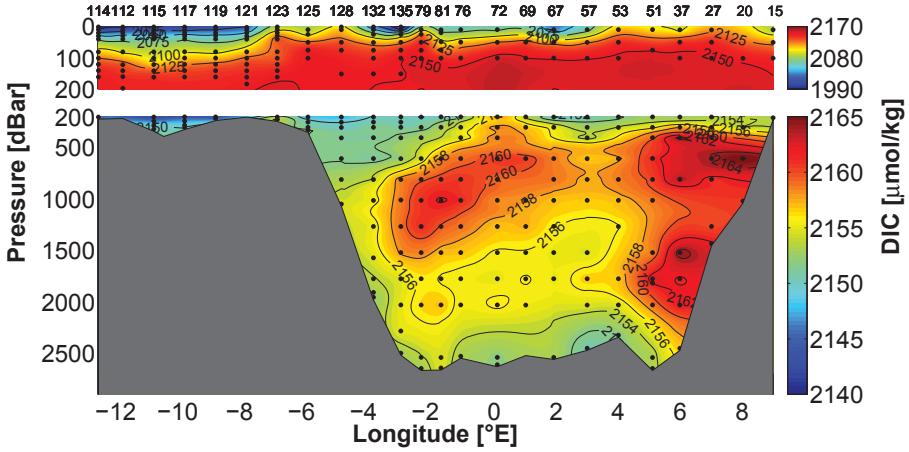

Fig. 4: Dissolved inorganic carbon (DIC) in $\mu mol\, kg^{-1}$.

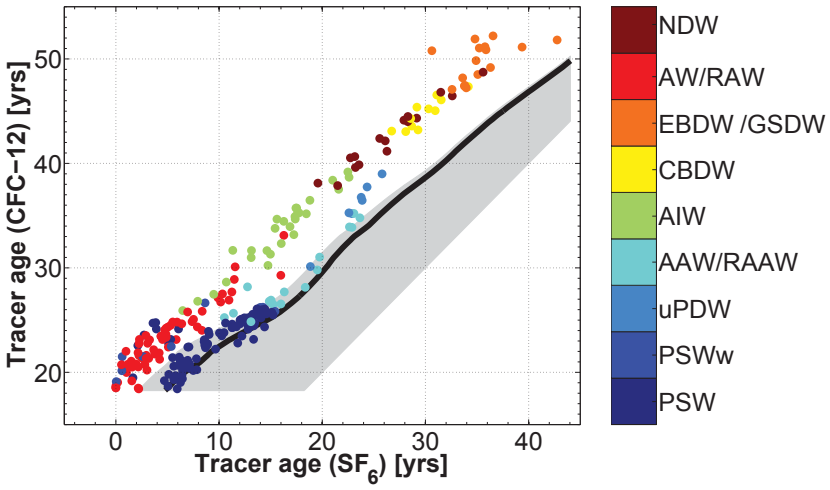

Fig. 5: Validity area of the IG-TTD defined by the tracer couple CFC-12 and SF_6 (grey shaded area). The black line indicates the IG-TTD based tracer age relationship using the unity ratio of $\Delta/\Gamma = 1.0$. The field data is colored by the type of water mass. The lower branch (blue dots) describes surface and intermediate water of Arctic origin whereas the upper branch includes water of Atlantic origin and deep water masses.

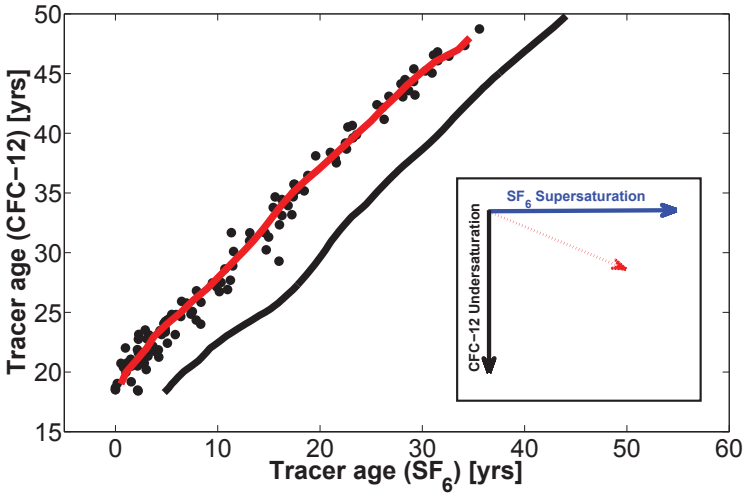

Fig. 6: Relation between the IG-TTD based tracer age relationship of the unity ratio (black line) and the mean tracer age relationship of the upper branch of the field data (red line). The shape of both curves indicates similarities between the modelled and field data. The difference can be explained by undersaturation of CFC-12 and / or supersaturation of SF_6 (see inset).

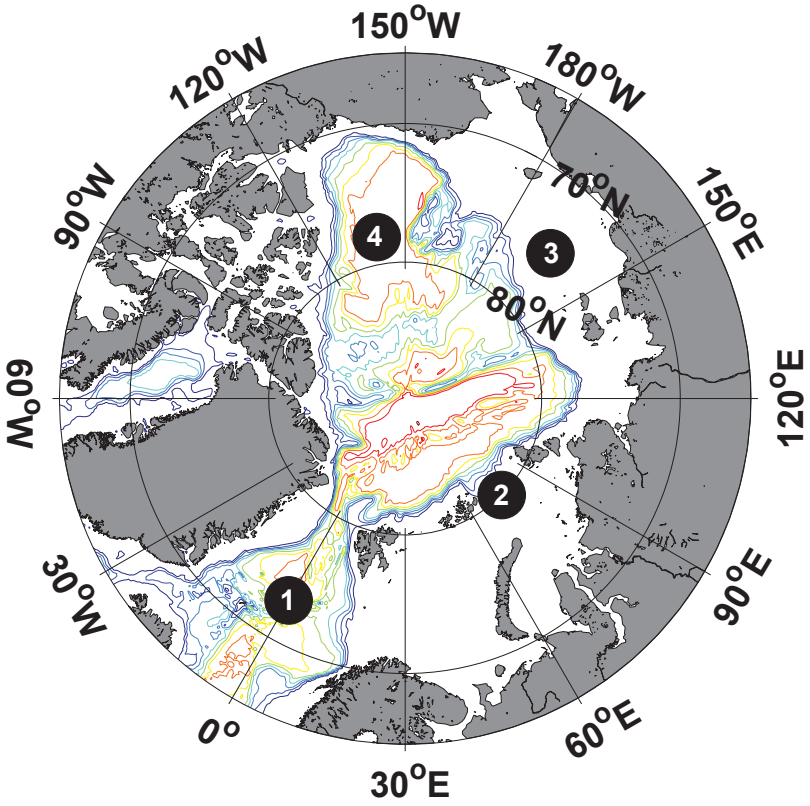

Fig. 7: Typical source regions of different water mass types. (**1**) the Greenland Sea, (**2-3**) Arctic shelf regions and (**4**) Arctic open water / fast-ice region.

Table 1: Mean (± standard deviation) concentrations of anthropogenic carbon (C_{ant}) and mean age in Fram Strait separated in water mass types.

Water mass	C_{ant} [$\mu mol\, kg^{-1}$]	**Mean age** [$years$]
AW/RAW	50 (±6)	9 (±10)
PSWw	46 (±5)	9 (±10)
PSW	43 (±2)	7 (±6)
AAW/RAAW	38 (±5)	32 (±15)
AIW	31 (±5)	54 (±20)
uPDW	28 (±4)	69 (±19)
NDW	18 (±4)	143 (±44)
CBDW	15 (±2)	173 (±23)
EBDW/GSDW	11 (±1)	254 (±32)

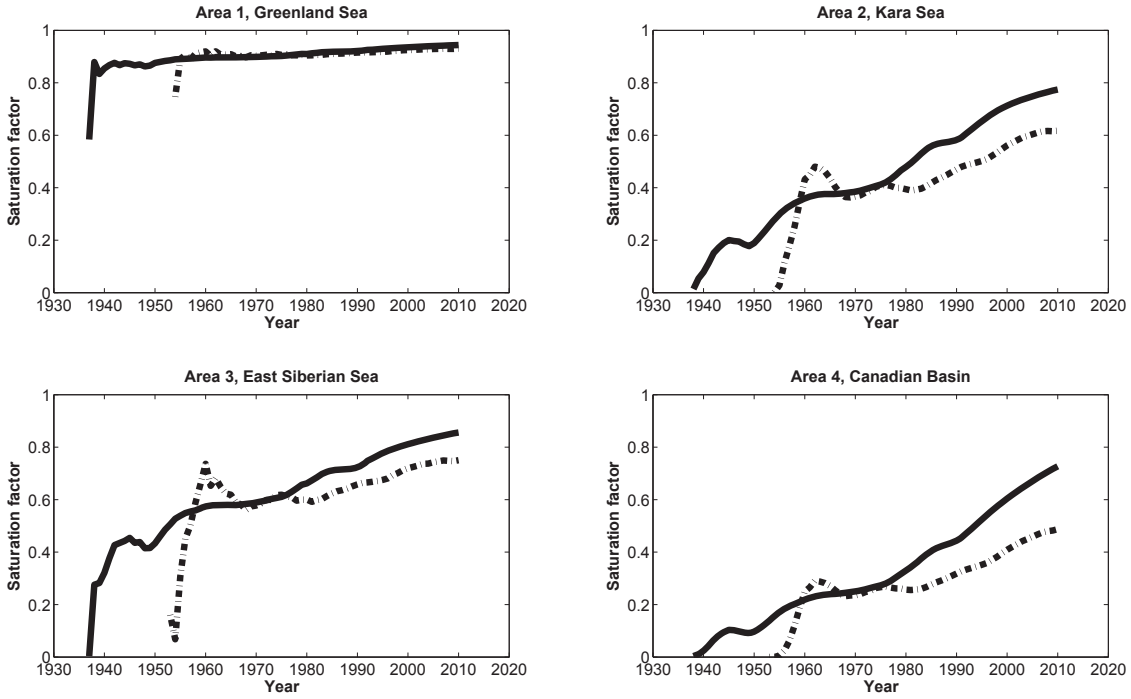

Fig. 8: Surface saturation of CFC-12 (black solid line) and SF_6 (black dash-dotted line) of different source regions (see Fig. 7) based on the model output of Shao et al. (2013). The data shows mean values of the corresponding grids with a dimension of $300x300\,nm$.

Table 2: Flux estimates of DIC and anthropogenic carbon in Fram Strait in 2012.

	Volume [Sv]	**Transport [Tg C yr^{-1}]**	
		DIC	**Anthropogenic carbon**
AW	4.2 ($\pm$3.0)	3420 ($\pm$2497)	82 ($\pm$59)
RAW/RAAW	-2.8 ($\pm$6.2)	-2274 ($\pm$5080)	-54 ($\pm$120)
PW	-1.4 ($\pm$0.8)	-1117 ($\pm$660)	-23 ($\pm$13)
Σ	0	29	5

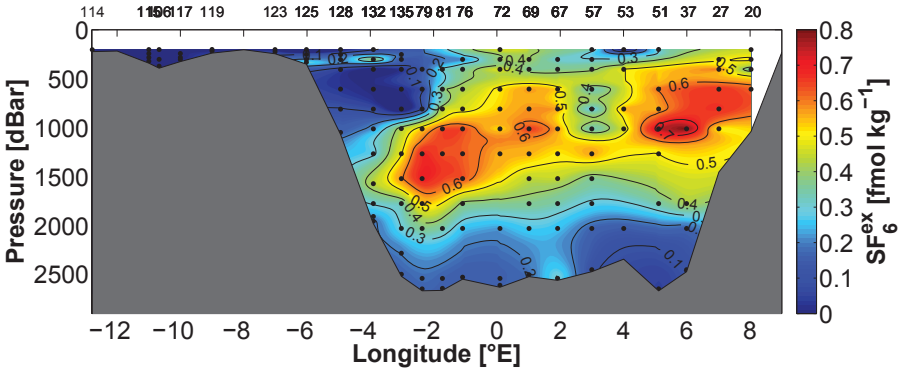

(a)

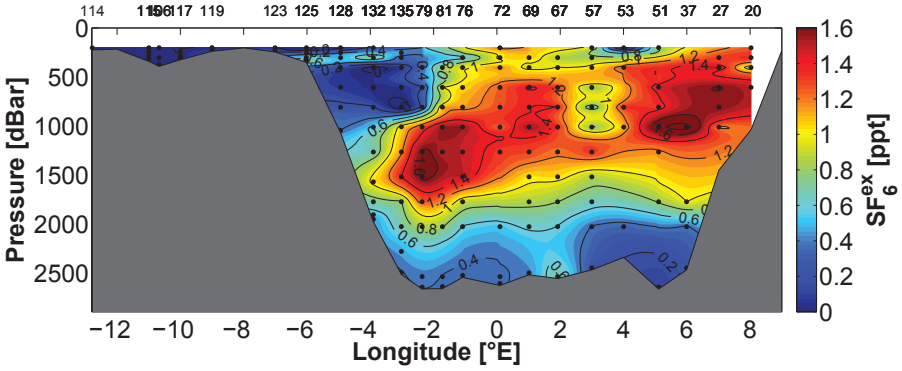

(b)

Fig. 9: SF_6 excess (**a**) concentrations in $fmol\,kg^{-1}$ and (**b**) partial pressures in ppt. The upper $200\,m$ and station #15 cannot be calculated due to the atmospheric concentration limit of CFC-12 which inhibits an application of the IG-TTD.

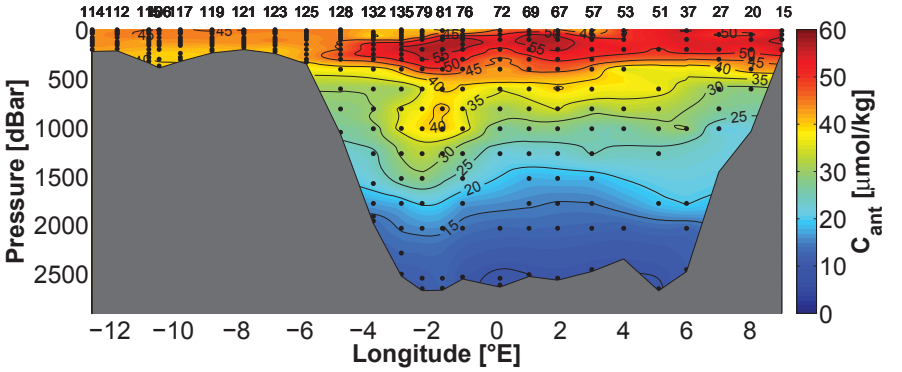

Fig. 10: Anthropogenic carbon in $\mu mol\,kg^{-1}$.

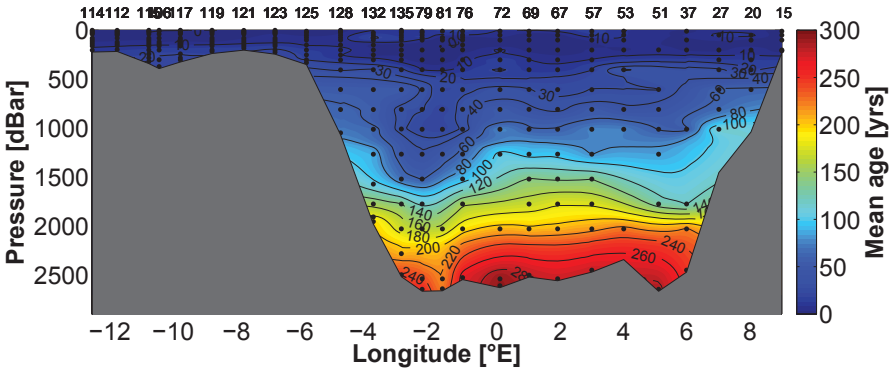

Fig. 11: Mean age based on saturation corrected CFC-12 data below $100\,m$ and SF_6 data in shallower depths.

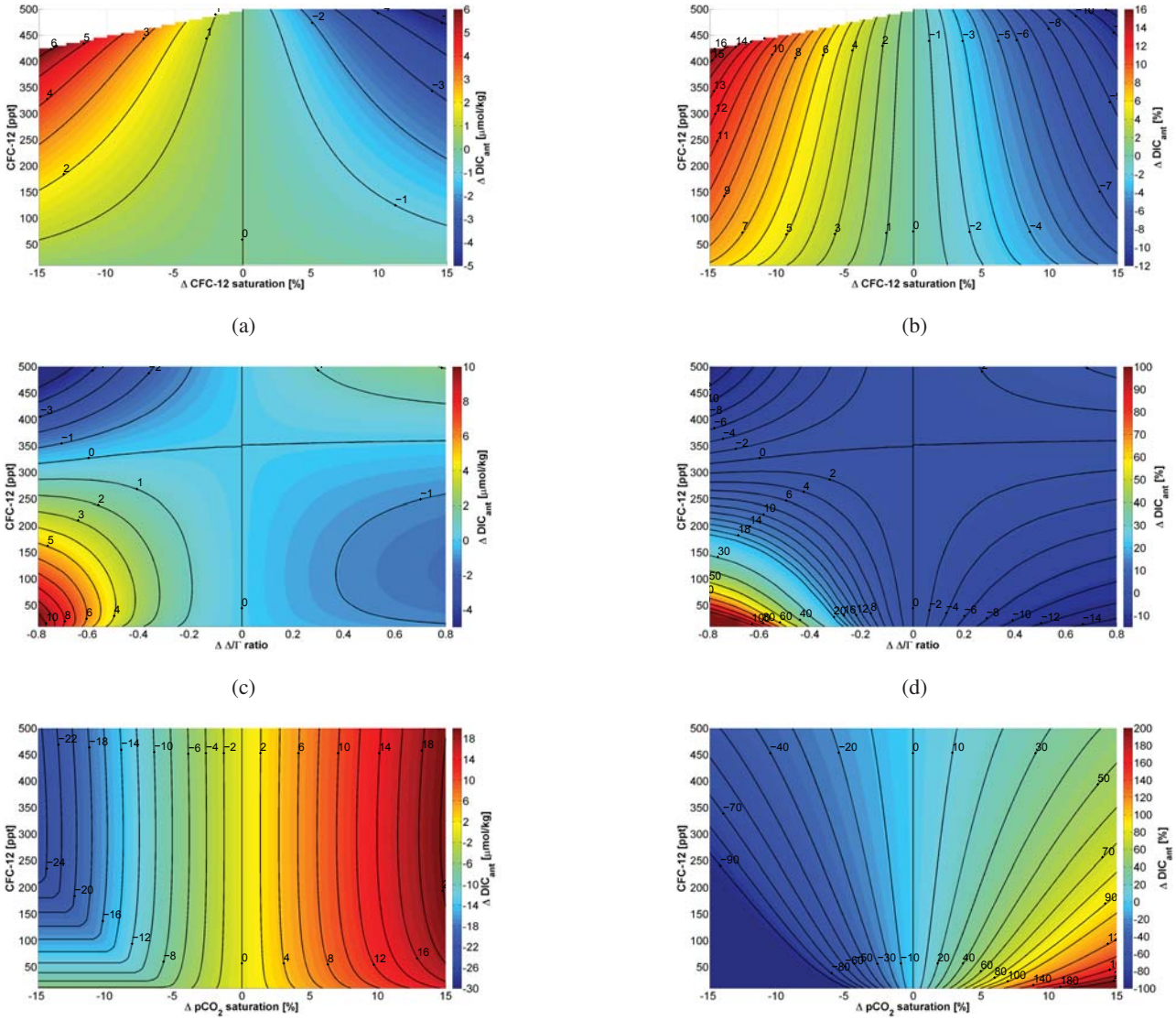

Fig. 12: Anthropogenic carbon concentration sensitivities to changes in (**a**, **b**) CFC-12 saturation, (**c**, **d**) Δ/Γ-ratio and (**e**, **f**) pCO_2 saturation. Deviations are stated in absolute (left panels) and relative (right panels) values. The reference points are defined by 100 % saturation of CFC-12 and pCO_2 and a ratio of $\Delta/\Gamma = 1.0$.

Conclusion and outlook

The evaluations of the transient tracer and IG-TTD applications showed that an improved analogy between the theoretical approach and actually observed ventilation can provide significant information about water mass characteristics such as the mean age, the different types of formation processes and the extent of ventilation events. However, the analysis of singular tracer surveys only provides information about the current state of an ocean area. The information content is improved by the use of transient tracer time series, e.g. additional information about changes in ventilation on decadal time scales [e.g. Huhn et al., 2013, Schneider et al., 2014]. The potential benefit from interconnecting already existing data of singular tracer surveys of similar ocean areas is far from being exhausted, especially for those data sets which are not part of repeat hydrography projects but are publically available.

The development of the new sampling and measurement technique of the argon-39 isotope is already at an advanced state and it can be expected that this tracer becomes more utilized during future tracer surveys. This is a great opportunity since argon-39 allows for investigations of less ventilated water masses where the detection limit of other transient tracers, e.g chlorofluorocarbons (CFCs), is reached. In contrast, investigations of water masses which have recently been in contact with the atmosphere become more difficult due to the loss of the CFC time information (atmospheric concentration limit). SF_6 is typically the only tracer which can be applied to such young water masses. Thus it is highly recommended to conduct multiple transient tracer measurements during an expedition which cover the different requirements and characteristics of the water column.

Another challenge is the surface saturation of transient tracers, which has a large impact on the specific time information and TTD model constraints. High uncertainties in tracer saturations inhibit significant constraints on the IG-TTD and in this case it appears to more reasonable to use mean constraints as, for example, suggested by Waugh et al. [2002] and Schneider et al. [2012]. The application of the method used to constrain the IG-TTD in the Mediterranean Sea is thus restricted

to ocean areas where less deviation in tracer saturation is expected. Furthermore, the general impact of saturation effects on TTD applications is rarely considered in the literature. The model approach of Shao et al. [2013] seems to be a useful approach for deviation in saturation which depend on changes in sea surface temperature and salinity as well as the solubility and atmospheric emission rate of the tracer. However, this model completely neglects possible supersaturations due to bubble injections during heavy wind conditions. Such bubble mediated gas transfer has a large influence on tracer saturations as indicated by the observed surface concentrations of SF_6 during the ANT-XXVIII/3 cruise and the findings by Liang et al. [2013]. Since most water mass formation takes place during winter time, i.e. when most of the surface water cooling and heavy wind conditions occur, it can be assumed that the effect of supersaturation applies for many water masses in the ocean. Based on this assumption it appears to be questionable if currently existing TTD limits correspond to complex mixing processes or rather refer to different degrees of supersaturation of the different tracers. Additional information about saturation states could also provide further information about the historic surface saturation of carbon dioxide which is a key parameter for estimates of anthropogenic carbon contents. The uncertainties of the carbon dioxide surface saturation could be lowered and the anthropogenic carbon estimates improved. Such improved estimates would then also apply for carbon transport into the ocean's interior, i.e. the storage of carbon dioxide in the ocean. To this end, the different aspects of saturation will be the main focus of future work.

Acknowledgements

Dankbarkeit kann sehr facettenreich in Erscheinung treten und es würde einige Seiten in Anspruch nehmen, all diejenigen zu bedenken, denen an dieser Stelle Dankbarkeit gebührt. Hervorheben möchte ich allerdings die Hauptakteure beziehungsweise Dramaturgen, die dieses Stück erst ermöglicht haben. Allen voran Boie Bogner, der maßgeblich dazu beigetragen hat, dass ich überhaupt mit Daten von den Expeditionen heimkehren konnte. Im Hinblick auf all die Geschehnisse an Bord möchte man meinen, dass dies eigentlich ein Ding der Unmöglichkeit war. Meinen beiden Chefs, Toste Tanhua und Mario Hoppema, möchte ich für die hervorragende Betreuung und den mir gewährten umfangreichen Gestaltungsfreiraum danken. Summa summarum war es eine sehr produktive und erfolgreiche Zeit auf die ich gerne zurückblicke. Viel mehr ist an dieser Stelle auch nicht zusagen, denn:

> **"Leider läßt sich eine wahrhafte Dankbarkeit mit Worten nicht ausdrücken."**
>
> Johann Wolfgang von Goethe

Bibliography

A. Beszczynska-Möller. The expedition of the research vessel Polarstern to the Arctic in 2012 (ARK-XXVII/1). *Reports on polar and marine research*, 660: 1–78, 2013. ISSN 1866-3192. doi: 10.2312/BzPM_0660_2013.

P. Brandt, V. Hormann, A. Körtzinger, M. Visbeck, G. Krahmann, L. Stramma, R. Lumpkin, and C. Schmid. Changes in the ventilation of the oxygen minimum zone of the tropical North Atlantic. *J. Phys. Oceanogr.*, 40:1784–1801, 2010. doi: 10.1175/2010JPO4301.1.

T. M. Hall and R. A. Plumb. Age as a diagnostic of stratospheric transport. *J. Geophys. Res.*, 99(D1):1059–1070, 1994.

O. Huhn, M. Rhein, M. Hoppema, and S. van Heuven. Decline of deep and bottom water ventilation and slowing down of anthropogenic carbon storage in the Weddell Sea, 1984-2011. *Deep Sea Res. Part I*, 76:66–84, 2013. ISSN 0967-0637. doi:10.1016/j.dsr.2013.01.005.

O. Klatt, W. Roether, M. Hoppema, K. Bulsiewicz, U. Fleischmann, C. Rodehacke, E. Fahrbach, R. F. Weiss, and J. L. Bullister. Repeated CFC sections at the Greenwich Meridian in the Weddell Sea. *J. Geophys. Res. - Oceans*, 107, 2002. ISSN 0148-0227. doi: 10.1029/2000JC000731.

J.-H. Liang, C. Deutsch, J. C. McWilliams, B. Baschek, P. P. Sullivan, and D. Chiba. Parameterizing bubble-mediated air-sea gas exchange and its effect on ocean ventilation. *Global Biogeochem. Cycles*, 27(3):894–905, 2013. ISSN 1944-9224. doi: 10.1002/gbc.20080.

A. Schneider, T. Tanhua, A. Körtzinger, and D.W.R. Wallace. An evaluation of tracer fields and anthropogenic carbon in the equatorial and the tropical North Atlantic. *Deep Sea Res. Part I*, 67(0):85 – 97, 2012. ISSN 0967-0637. doi:10.1016/j.dsr.2012.05.007.

A. Schneider, T. Tanhua, W. Roether, and R. Steinfeldt. Changes in ventilation of the Mediterranean Sea during the past 25 year. *Ocean Sci.*, 10:1–16, 2014. doi: 10.5194/os-10-1-2014.

A. E. Shao, S. Mecking, L. Thompson, and R. E. Sonnerup. Mixed layer saturations of CFC-11, CFC-12, and SF_6 in a global isopycnal model. *J. Geophys. Res.: Oceans*, 118(10):4978–4988, 2013. ISSN 2169-9291. doi: 10.1002/jgrc.20370.

S. Solomon, G.-K. Plattner, R. Knutti, and P. Friedlingstein. Irreversible climate change due to carbon dioxide emissions. *Proceedings of the National Academy of Sciences*, 106(6):1704–1709, 2009. doi: 10.1073/pnas.0812721106.

T. Stöven. Ventilation processes of the Mediterranean Sea based on CFC-12 and SF_6 measurements. *GEOMAR OceanRep*, 2011. URL `http://oceanrep.geomar.de/id/eprint/13936`. diploma thesis, Christian-Albrechts-Universität zu Kiel.

T. Tanhua, D. Hainbucher, V. Cardin, M. Alvarez, and G. Civitarese. Repeat hydrography in the Mediterranean Sea, data from the Meteor cruise 84/3 in 2011. *Earth Syst. Sci. Data*, 5:289–294, 2013. doi:10.5194/essd-5-289-2013.

D. W. Waugh, M. K. Vollmer, R. F. Weiss, T. W. N. Haine, and T. M. Hall. Transit time distributions in Lake Issyk-Kul. *Geophys. Res. Lett.*, 29(24):84–1–84–4, 2002. doi:10.1029/2002GL016201.

D. W. Waugh, T. M. Hall, and T. W. N. Haine. Relationships among tracer ages. *J. Geophys. Res.*, 108(C5), 2003. doi:10.1029/2002JC001325.

D. W. Waugh, T. M. Hall, B. I. McNeil, R. Key, and R. J. Matear. Anthropogenic CO_2 in the oceans estimated using transit time distributions. *Tellus Ser. B*, 58 (5):376 – 389, 2006.

D. Wolf-Gladrow. The expedition of the research vessel" Polarstern" to the Antarctic in 2012 (ANT-XXVIII/3). *Reports on polar and marine research*, 661, 2013.

Contributions to the manuscripts

Manuscript I: T. Stöven and T. Tanhua, *Ventilation of the Mediterranean Sea constrained by multiple transient tracer measurements*
Tim Stöven conducted the transient tracer measurements during the M84/3 expedition, performed the data processing / method evaluation and wrote the paper. T. Tanhua supported the writing process by certain annotations and revisions.

Manuscript II: T. Stöven, T. Tanhua, M. Hoppema and J.L. Bullister, *Perspectives of transient tracer applications and limiting cases*
Tim Stöven conducted the transient tracer measurements during the ANT-XXVIII/3 expedition, performed the data processing / method evaluation and wrote the paper. T. Tanhua, M. Hoppema and J.L. Bullister supported the writing process by certain annotations and revisions.

Manuscript III: T. Stöven, T. Tanhua, M. Hoppema and J.-W. von Appen, *Recent transient tracer distributions in the Fram Strait: Estimation of anthropogenic carbon content and transport*
Tim Stöven conducted the transient tracer measurements during the ARK-XXVII/1 expedition, performed the data processing and wrote most of the paper. J.-W. von Appen provided the water transport data and wrote the text of the corresponding sections. T. Tanhua and M. Hoppema supported the writing process by certain annotations and revisions.

Eidesstattliche Erklärung

Hiermit erkläre ich an Eides Statt, dass ich die vorliegende Arbeit selbstständig verfasst und keine anderen als die angegebenen Quellen und Hilfsmittel benutzt habe, dass alle Stellen der Arbeit, die wörtlich oder sinngemäß aus anderen Quellen übernommen wurden, als solche kenntlich gemacht sind, dass die Arbeit unter Einhaltung der Regeln guter wissenschaftlicher Praxis der Deutschen Forschungsgemeinschaft entstanden ist und dass die Arbeit in gleicher oder ähnlicher Form noch keiner Prüfungsbehörde vorgelegt wurde.

Kiel, den 01.06.2015